

https://dspace.org/

Finite Element Analysis of Dinocephalian Skulls to Address Head-Butting Behaviour in Early Therapsids

Bolton, Andrew

2024-08

University of the Witwatersrand, Johannesburg

https://hdl.handle.net/10539/45189

Bolton, Andrew. (2024). Finite Element Analysis of Dinocephalian Skulls to Address Head-Butting Behaviour in Early Therapsids. [Master's dissertation, University of the Witwatersrand, Johannesburg]. WIReDSpace. https://hdl.handle.net/10539/45189

Downloaded from a DSpace repository. https://dspace.org/



WITS
UNIVERSITY

Finite Element Analysis of Dinocephalian Skulls to Address Head-Butting Behaviour in Early Therapsids

By

Andrew Bolton

(1444408)

Evolutionary Studies Institute

Research project submitted in fulfilment of the Bachelor of Science with Masters in the field of Palaeontology in the Faculty of Science, in the University of the Witwatersrand, Johannesburg, South Africa.

Supervisors: Dr Julien Benoit & Taahirah Mangera

ORCID: 0000-0003-1059-3228

Master of Science (Dissertation) in the Field of Palaeontology

Johannesburg, 2024





GENUS
DSI-NRF CoE Palaeo

PAST
ALL FROM ONE

I declare that this dissertation is my own, unaided work. It is being submitted for the Degree of Master of Science (Dissertation) in the field of Palaeontology at the University of the Witwatersrand, Johannesburg. It has not been submitted before for any degree or examination at any other University.



Andrew Bolton

27th day of August 2024, Johannesburg, South Africa

Table of contents:

Abstract 1

Introduction 1

Aims and Objectives 11

Hypotheses 11

Materials and methods 12

- **Sampling of models** 12
- **Construction of models** 14
- **Finite element analysis** 18
- **Institutional abbreviations** 26
- **Pathological analysis** 27

Results 27

- **Finite element analysis** 27
- **Palaeopathologies** 47

Discussion 53

- **FEA validation** 53
- **FEA performances** 54
- **Pachyostosis and biting force in *Anteosaurus*** 57
- **Effect of absolute cranial size** 57
- **Implications for social behaviour** 60
- **Remarks on hypotheses** 68

Conclusion 69

Acknowledgements 70

References 71

- **Appendix 1:** 77
- **Appendix 2:** 77
- **Appendix 3:** 78
- **Appendix 4:** 78
- **Appendix 5:** 79

Table of figures:

Figure 1: Dinocephalian phylogenies. 2
Figure 2: Adaptations for head-butting in the Dinocephalia..... 5
Figure 3: Left Lateral view of the skull models. 15
Figure 4: Dorsal view of the skull models. 16
Figure 5: Anterior view of the original and modified *Stegoceras* skull models. 17
Figure 6: *Estemmenosuchus* 3D printed models used to infer the most likely points of impact. 20
Figure 7: *Estemmenosuchus* skull model with force application points and constraints.. 20
Figure 8: *Struthiocephalus* skull model with force application points and constraints. ... 21
Figure 9: *Stegoceras* skull model with force application points and constraints. 21
Figure 10: *Anteosaurus* skull model with force application points and constraints. 22
Figure 11: *Moschops* skull model with force application points and constraints. 22
Figure 12: *Jonkeria* skull model with force application points and constraints. 23
Figure 13: SAM-PK-11693 skull and pathology. 26
Figure 14: Force application point stresses of selected skull models in all tested load magnitude and force protocols. 28
Figure 15: Minimum safety factor values according to the Mohr-Coulomb failure criterion. 29
Figure 16: Minimum safety factor values according to the maximum equivalent stress (von Mises) failure criterion. 30
Figure 17: Graph showing the average of all minimum safety factor values per model in protocols and failure criteria. 31
Figure 18: Comparison of sagittal sections of stress distributions in the 1000 N head-butting protocol. 32
Figure 19: Comparison of sagittal sections of stress distributions in the 3400 N head-butting protocol. 34
Figure 20: Comparison of transverse sections of stress distributions in the 1000 N flank-butting protocol taken at greatest extent of strain from force application points. 35
Figure 21: Comparison of transverse sections of stress distributions in the 3400 N flank-butting protocol. 37
Figure 22: External cranial pathologies and their distributions (A and C adapted from illustrations by Anne Westoby (Rubidge and Day, 2020)). 48
Figure 23: Internal pathology in the skull of *Moshognathus whaitsi* (AM4950). 52
Figure 24*:* Observed evidence for head-butting mapped onto Benoit *et al.'s* (2021a) phylogeny. 62
Figure 25*:* Hypothetical combat interaction between two *Estemmenosuchus.* 65

Abstract

The origin of complex social behaviour in the mammalian lineage has been a long-standing enigma. Behaviours do not leave a rich fossil record; however, adaptations to highly specialised complex behaviour can be traced back in some lineages, such as the dinocephalians. Dinocephalians dominated carnivorous and herbivorous niches of terrestrial ecosystems in the Middle Permian (~273-259 million years ago). Species within this clade often have skulls with considerable pachyostosis (overly thickened bones) and cranial ornamentation (horns and bosses). This morphology has been interpreted as evidence for head-butting, but the evidence is circumstantial at best. For this project, I used three-dimensional models of the skulls of four dinocephalians and two outgroups to simulate and investigate the capabilities of these skulls to withstand different magnitudes of head-butting and flank-butting impacts with finite element analyses. Palaeopathological analyses vindicated the accuracy of FEA data, which indicates that dinocephalian skulls modelled here arguably reflect biological truth. As head-butting is a complex social behaviour, this would strongly suggest the presence of dominance hierarchies, territoriality, and gregariousness. This represents the earliest robust evidence of complex social behaviour in tetrapods, preceding all known examples of social interactions in dinosaurs and mammals by hundreds of millions of years.

Introduction

The Dinocephalia were therapsids that exerted a considerable degree of ecological influence as the dominant carnivores and herbivores in middle Permian terrestrial ecosystems. Furthermore, they hold the titles of the largest therapsids known from the Guadalupian epoch and the oldest large-bodied synapsid known from Gondwana (Romano and Rubidge, 2021).

Dinocephalians are subdivided into the mostly herbivorous Tapinocephalia (which contains the Tapinocephalidae), and the completely carnivorous Anteosauria (Fraser-King *et al.*, 2019; Benoit *et al.*, 2021b). The Tapinocephalia are subdivided into four groups: the Styracocephalidae, Estemmenosuchidae, Titanosuchidae, and Tapinocephalidae (Fig. 1A, B) (Fraser-King *et al.*, 2019).

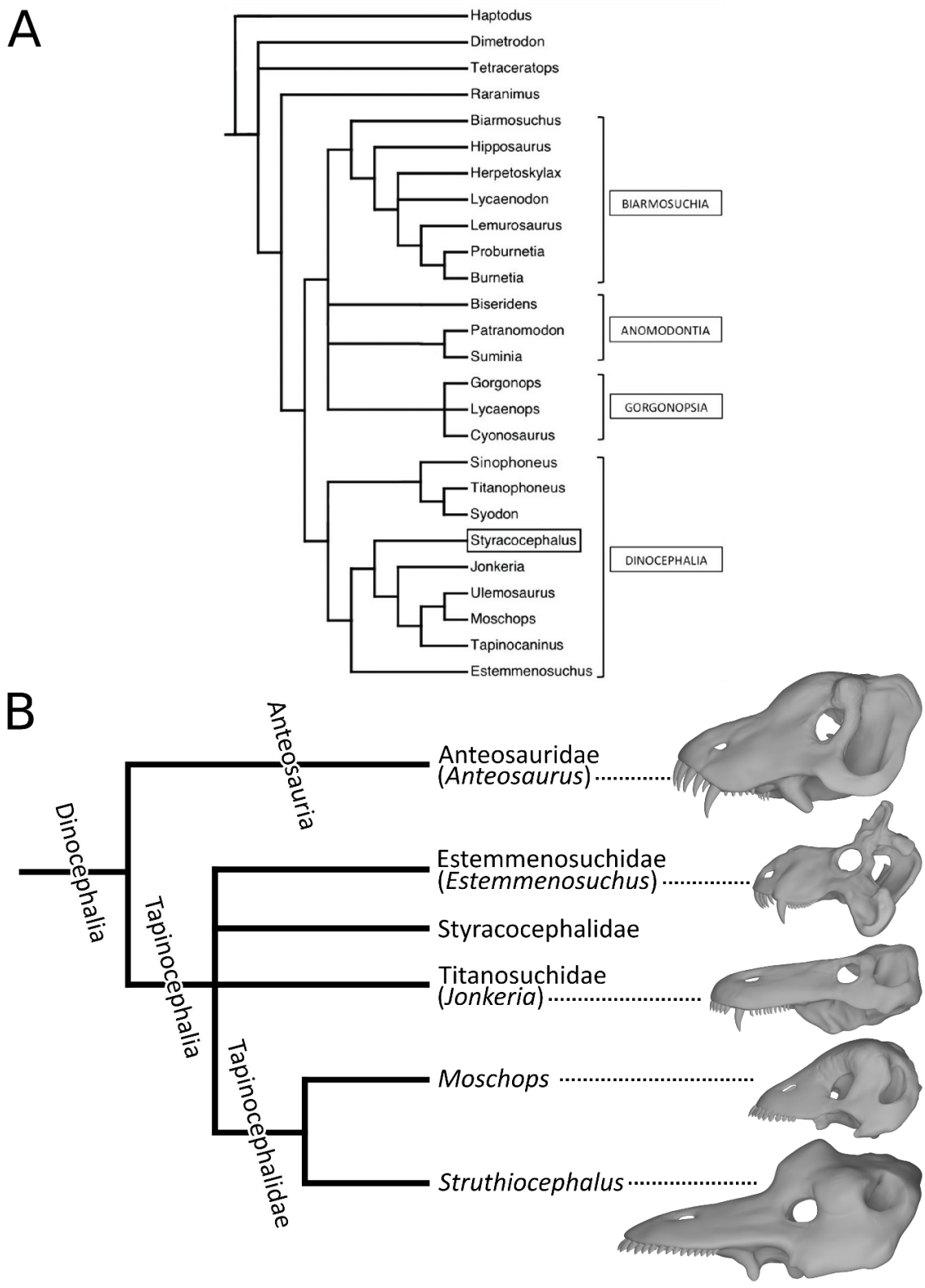

Figure 1: Dinocephalian phylogenies.

A: Dinocephalian phylogenetic position among basal therapsids (from Fraser-King *et al.*, 2019), B: Phylogenetic interrelationships within the Dinocephalia with representative models (Modified from Benoit *et al.* 2021b, models from Adam Midzuk).

In spite of their close phylogenetic affinities with other tapinocephalians, the Tapinocephalidae are identified by several apomorphic traits, such as the anterior-ventral relocation of the occiput, a less robust jaw mechanism, cranial pachyostosis, the loss of a distinguishable canine, and heeled teeth (Boonstra, 1963; Rubidge and Sidor, 2001; Neumann *et al.*, 2009). However, *Tapinocaninus pamelae*, a more basal tapinocephalid, still retains a vestigial canine (Rubidge, 1991; Neumann *et al.*, 2009; Rubidge *et al.*, 2019; Midzuk, 2020).

The Titanosuchidae are a group of long-snouted, herbivorous, and derived dinocephalians with large canines (Jirah, 2022). Jirah's (2022) revision of the group finds it to consist of two valid taxa, *Jonkeria truculenta* and *Titanosuchus ferox*.

The Styracocephalidae is a group consisting of one species, *Styracocephalus platyrhynchus* (Fraser-King *et al.*, 2019). The group is distinguished by the combination of weak-heeled postcanines and incisors, conspicuous posteriorly projecting squamosal and postorbital crests, a thick median nasal boss, moderately sized canines in the upper and lower jaws, a long postcanine tooth row of 8-10 teeth in line with the canine, and specialised supra- and postorbital pachyostosis (Fraser-King *et al.*, 2019).

The Estemmenosuchidae are a group of Russian dinocephalians known for their conspicuous tubercles and antler-like horns, paired with large canines (Barghusen, 1975; Ivakhnenko, 2008).

The carnivorous Anteosauria, as Kammerer (2011) states, is comprised of one family, the Anteosauridae, and two subfamilies, the relatively small Syodontinae, and the larger, more heavily pachyostosed Anteosaurinae.

Dinocephalians are known to display various degrees of cranial pachyostosis (i.e., excessively thickened bones in their skulls) and have various forms of cranial ornamentation such as horns and bosses (Barghusen, 1975; Benoit *et al.*, 2021b). These traits, and a whole host of other adaptations are hypothesised to serve as supporting structures for some sort of head-butting behaviour (Barghusen, 1975; Benoit *et al.*, 2021b). Although great variety exists in terms of the extent of cranial pachyostosis and the shape of the skull among the tapinocephalians, theories regarding head-butting in dinocephalians are typically concerned with skulls that have broad and blunt

pachyostosed domes, exemplified by *Moschops*, with similar structures seen in similarly adapted tapinocephalids, including *Ulemosaurus* and *Tapinocaninus* (Barghusen, 1975; Rubidge, 1991; Midzuk, 2020).

The tapinocephalids are commonly thought to be the most plausible candidates for head-butting within the dinocephalians (Barghusen, 1975; Benoit *et al.*, 2016, 2017b; Midzuk, 2020). This group of robustly constructed genera exhibit a collection of traits that are not found in the closely related Titanosuchidae, and are theorised to have been used in head-butting (Barghusen, 1975).

The parietal and frontal of the tapinocephalid *Moschops* are laterally broadened and constitute a wide and blunt frontoparietal shield (FPS) (Fig. 2A, B) (Boonstra, 1936, 1957; Barghusen, 1975; Benoit *et al.*, 2017b; Midzuk, 2020). This shield is buttressed by relatively thick post-orbital and post-temporal bars that are thought to have behaved like arches, serving as conduits for impact forces to be transmitted through to the occipital condyles and vertebral column (Barghusen, 1975; Benoit *et al.*, 2017b; Midzuk, 2020). Tapinocephalids also exhibit temporal fenestrae that are greatly diminished in size due to pachyostosis of the postorbital bar which would decrease the strength of the musculature of the jaw (Fig. 2A) (Barghusen, 1975; Rubidge and Sidor, 2001; Kemp, 2005; Midzuk, 2020).

Another major adaptation within the tapinocephalids is the reorientation of the skull to a relatively vertical inclination, which is achieved with the aid of several key traits (Barghusen, 1975; Midzuk, 2020). These traits include the relocation of the pineal foramen and canal posteriorly, a reoriented endocranial cavity, and the occiput and occipital condyle moving anteroventrally (Fig. 2B-D) (Boonstra, 1936; Brink, 1958; Boonstra, 1968; Barghusen, 1975; Benoit *et al.*, 2017b; Midzuk, 2020). The orientation of the braincase perpendicular to the impact energy pathways helps ensure the flow of impact forces around the brain instead of through it (Benoit *et al.*, 2016, 2017b; Midzuk, 2020), and the fragile pineal nerve and eye being positioned posteriorly to the impact stress pathways would have reduced the risk of damaging these organs (Fig. 2D) (Benoit *et al.*, 2016, 2017b). These adaptations are further complemented by the enclosed braincase of dinocephalians (Fig. 2B), which is atypical compared to many other non-mammalian therapsids, and may have provided additional protection to the central nervous system (Boonstra, 1936, 1968; Barghusen, 1975; Benoit *et al.*, 2016, 2017b; Midzuk, 2020).

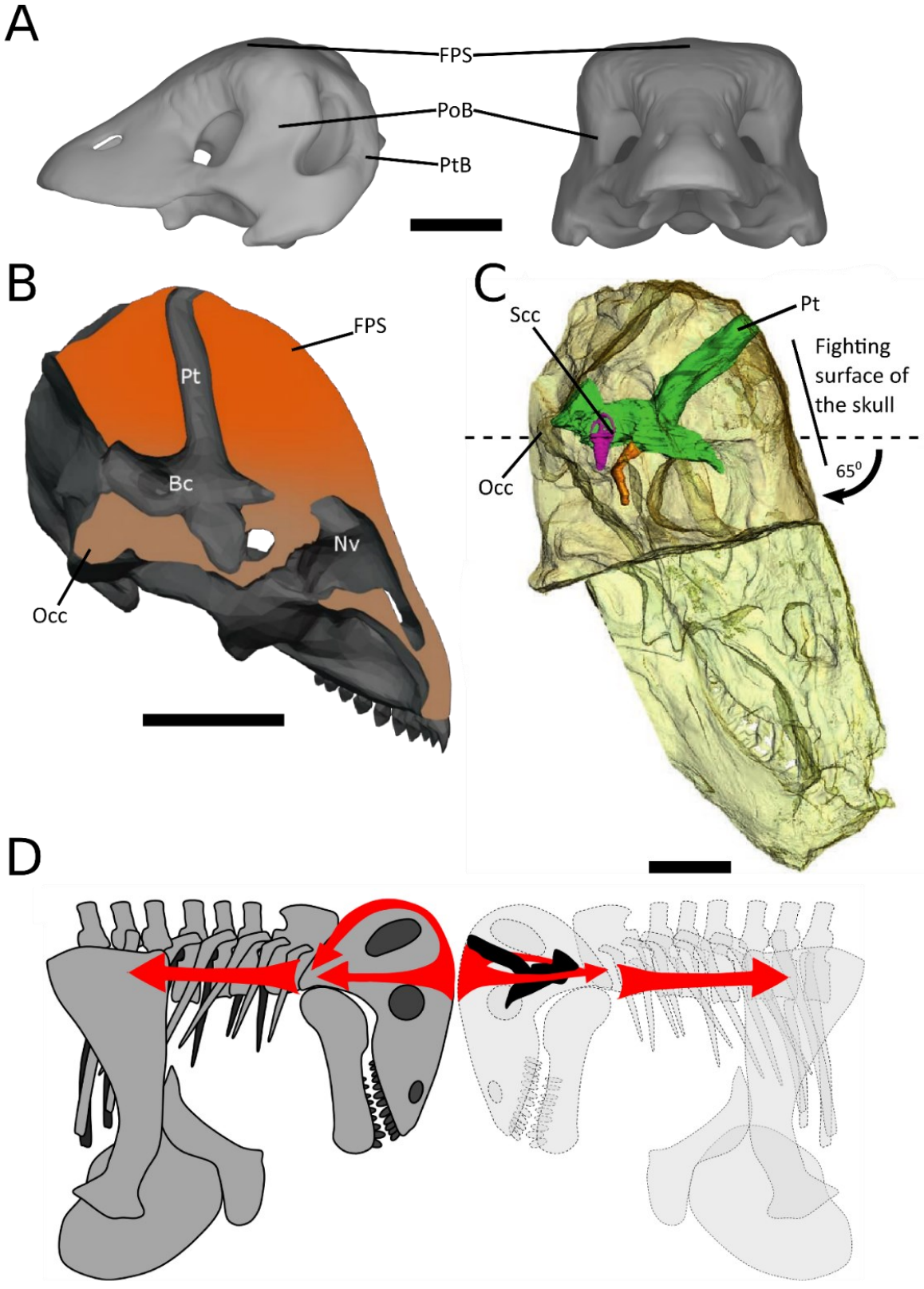

Figure 2: Adaptations for head-butting in the Dinocephalia.

A: Left lateral and anterior view of *Moschops* showing thickened frontoparietal shield, postorbital bar, and post-temporal bar (Models by Adam Midzuk), scale bar = 10 cm, B: Sagittal section of *Moschops* showing the widened pineal tube, enclosed and reoriented braincase, and the thickened frontoparietal shield (from

Midzuk, 2020), scale bar = 10 cm, C: Semi-transparent skull of *Moschognathus whaitsi* Broom, 1914 (AM4950) aligned on the plane of the lateral semicircular canal, with the black arrow depicting the tilting of the long axis of the skull compared to the plane of the lateral semicircular canal (dashed line), this relationship being indicative of the reorientation of the braincase (From Benoit *et al.*, 2021b) scale bar = 5 cm, D: Reconstructed head-butting energy dissipation pathways during head-butting between two *Moschognathus*, showing how the fighting surfaces are aligned in one plane and how energy dissipates throughout the skull and along the length of the vertebral column (from Benoit *et al.,* 2017b), Left: dermatocranium dissipation pathway, right: braincase dissipation pathway. FPS = frontoparietal shield, PoB = postorbital bar, PtB = post-temporal bar, Pt = Pineal tube, Bc= Braincase, Occ = occipital condyles, Nv = nasal vacuity, Scc = semicircular canal.

Barghusen (1975) concludes that a horizontal head posture in tapinocephalids would be unlikely as the occiput would collide with the spinal process of the atlas. Barghusen's theories on head posture would later be justified by the observations of Benoit *et al.* in their work on the CT scans of *Moschognathus whaitsi* (formerly designated as *Moschops capensis*) and *Anteosaurus magnificus* (Benoit *et al.*, 2017b; Neumann, 2019; Midzuk, 2020; Benoit *et al.*, 2021b). Their findings on the orientations of the braincase and lateral semicircular canals indicated that the natural posture of the skull of *Moschognathus* had a distinct downward rotation, to the extent that the snout was angled ventrally at a 60 to 65-degree angle to the horizontal (Fig. 2C) (while the inclination in *Anteosaurus* is reconstructed at 25 degrees), resulting in a FPS that faces anteriorly (Benoit *et al.*, 2017b; Midzuk, 2020; Benoit *et al.*, 2021b).

These findings for *Moschognathus* are very compatible with theories of head-butting, as this would enable a straight-line dissipation of impact loads, circumventing the brain and pineal canal, and into the spine (Fig. 2D) (Barghusen, 1975; Benoit *et al.*, 2017b; Midzuk, 2020; Benoit *et al.*, 2021b). The orientation of the braincase perpendicular to the impact energy pathways would also help ensure the flow of impact forces around the brain instead of through it (Benoit *et al.*, 2016, 2017b; Midzuk, 2020).

The near-vertical head posture of tapinocephalids and reorientation of the braincase is closely replicated in known head-butting bovids (Schaffer and Reed, 1972) and theorised head-butting pachycephalosaurid dinosaurs (Bourke *et al.*, 2014; Benoit *et al.*, 2017b; Midzuk, 2020). Furthermore, the tapinocephalid head and neck posture and adaptations associated with it would have reduced the risk of injuries due to misalignment between the fighting surface and neck, and the blunt FPS of *Moschops* may have had a self-correcting effect during improperly aligned collisions (Barghusen, 1975; Midzuk, 2020; Benoit *et al.*, 2021b).

Soft-tissue adaptations for head-butting can also be inferred from the structures seen in dinocephalian crania, such as a layer of adnexa that likely lined the notably widened pineal tube and is thought to have protected the fragile nerve within (Benoit *et al.*, 2017b). Dinocephalian skulls are also thought to have had their cranial bosses covered by a cornified keratin sheet, because of the rugosity of the FPS and the presence of multiple vascular channels that run through the bones, which may have supplied a keratinous sheath (Benoit *et al.*, 2017b, 2021b).

The morphological divide between tapinocephalids and non-tapinocephalids is illustrated by Benoit *et al*.'s (2021) study, where they compared the braincases and possible adaptations for head-butting in *Moschognathus* and *Anteosaurus*. *Moschognathus*, a typical tapinocephalid, has a considerably pachyostosed skull which forms a frontoparietal shield, and braincase orientation that would permit the energy of impacts encountered during head-butting to be dispersed throughout the vertebral column by aligning the neck, frontoparietal shield, and foramen magnum in a single plane (Barghusen, 1975; Benoit *et al.*, 2017b, 2021b)(Fig. 2D). In contrast, *Anteosaurus*, much like other non-tapinocephalids, seems to have been much more poorly equipped for head-butting, with noticeably less cranial pachyostosis, and a vertically orientated occiput, that would lead to misalignments between the neck and skull roof during head-butting. This could have made injuries to the skull and vertebral column more likely (Barghusen, 1975; Benoit *et al.*, 2021b).

Therefore, it has been hypothesised that *Anteosaurus* and other non-tapinocephalids could not effectively participate in head-butting behaviours, or that they were only capable of low-energy forms of these behaviours, such as flank butting or face-biting (Barghusen, 1975; Benoit *et al.*, 2021b).

Modern ruminants are known to engage in several styles of intraspecific combat (Vander Linden and Dumont, 2019). The observed cranial fighting behaviours of ruminants are divided into four categories by Vander Linden and Dumont (2019). These researchers were able to determine which category of fighting behaviour a ruminant would have been involved in by performing phylogenetic generalised least-squares (PGLS) analyses of quantified linear measurements of their cervical vertebrae (Vander Linden and Dumont, 2019). The four categories of fighting behaviours they delineated were direct cranial collision (ramming), interlocking antlers or horns and shoving an opponent (wrestling),

raising the body upwards and colliding on the descent (fencing), and impaling an adversary's head or body with horn tips (stabbing) (Vander Linden and Dumont, 2019). It is possible that the diverse cranial anatomies of dinocephalians could be the reflection of a similar variety of fighting behaviours. For example, the antler-like horns of *Estemmenosuchus* appear to be suited for wrestling, while the blunt domes of *Moschops* may have been used in fencing, and *Struthiocephalus* may have used their horned skulls in stabbing.

The matter of suitability of skull structures for head-butting is not always readily apparent within dinocephalians, which have all sorts of cranial ornamentations and orientations. For instance, the bizarre antler-like horns of *Estemmenosuchus* do not seem to be obviously advantageous structures for head-butting, rather they are theorised to have been used to control the skull of an adversary in a style that is likely to be similar to the wrestling doctrine of extant ruminants (Barghusen, 1975; Vander Linden and Dumont, 2019). Similarly confusing cranial anatomies can also be found in the tapinocephalids, as shown by *Struthiocephalus*, with its single central boss, which may have been the core for a keratinous horn, and may have been used defensively or in intraspecific combat (Barghusen, 1975). Barghusen (1975), concluded that the post-orbital and middorsal bosses of *Struthiocephalus* would have been more effective in flank-butting than in direct head-to-head combat.

There are some alternative theories, which state that cranial structures of dinocephalians may have had primary functions other than those of combat, such as being used as a stress-sink for jaw abduction, as in the case of *Anteosaurus*, where the post-temporal and post-orbital pachyostosis is thought to have served as attachment sites for robust musculature that permitted bone-crushing bites (Kammerer, 2011; Midzuk, 2020). It is also possible that cranial pachyostosis may have been important for sexual display, and it may indicate sexual dimorphism in certain dinocephalian taxa (Geist, 1966; Kammerer, 2011; Neumann, 2019; Midzuk, 2020).

Limited cranial pachyostosis and large canines may have been the ancestral condition for dinocephalians (Kammerer, 2011; Fraser-King *et al.*, 2019; Benoit *et al.*, 2021b). The Tapinocephalia, particularly the tapinocephalids, then evolved smaller canines, and much larger horns and bosses, further developing a trend of increasing cranial ornamentation while reducing the importance of the canines that started in more basal clades, such as

the Styracocephalidae, Titanosuchidae, and Estemmenosuchidae (Geist, 1971; Angielczyk and Kammerer, 2018; Fraser-King *et al.*, 2019; Benoit *et al.*, 2021b) (Fig. 1B).

This evolutionary transition of shifting the combat apparatus from the mouth (fangs) to the skull (horns and antlers) has been replicated in several clades, such as giraffids and cervids (Geist, 1966; Cabrera and Stankowich, 2020; Benoit *et al.*, 2021b). This evolutionary transition is often correlated with a change from solitary to social behaviour in modern mammals, as intraspecific combat with canines would be more detrimental in herd animals. The damage inflicted by canine-stabbing is far more harmful than by head-butting or ritualised display using enlarged head adornment (Geist, 1961). While this behaviour is not as detrimental in solitary animals, living in herds increases the probability of encounters which would result in injuries and may draw in predators (Cabrera and Stankowich, 2020; Benoit *et al.*, 2021b).

Instead, gregarious genera tend to practice safer and less random combat behaviours with the aid of duller but way larger and more conspicuous cranial structures, like the rounded and blunt skull of tapinocephalids (Geist, 1966; Schaffer and Reed, 1972; Emlen, 2008; Cabrera and Stankowich, 2020; Benoit *et al.*, 2021b). Furthermore, intraspecific combat can indicate other derived behaviours, including dominance hierarchies and territoriality (Geist, 1966; Schaffer and Reed, 1972; Emlen, 2008; Cabrera and Stankowich, 2020; Benoit *et al.*, 2021b), and if these behaviours are found to have existed within the Dinocephalia, then it would make them the oldest known example of sociality (Benoit *et al.*, 2021b). Therefore, evidence of head-butting in the dinocephalians could be indicative of a far more sophisticated behavioural complexity than what is expected to be typical for non-mammalian therapsids in the Palaeozoic. This has been supported by the study of the size of the brain in *Struthiocephalus* and *Moschognathus*, as their encephalisation quotients appear larger than those of other basal therapsids and more closely resemble those of derived non-mammalian therapsids (Benoit *et al.*, 2017a; Midzuk, 2020).

Multiple dinocephalian individuals have been found in close association, for example, Boonstra found three *Jonkeria* skulls next to each other in the same sandstone layer (Boonstra, 1962; Benoit *et al.*, 2023), and in several instances, tapinocephalids have been collected in assemblages of five to twelve animals (Gregory, 1926; Boonstra, 1955; Rubidge *et al.*, 2019; Almond, 2022; Benoit *et al.*, 2023). It is therefore plausible that

tapinocephalids and titanosuchids remained together in small herds, at the minimum for short periods such as during mating seasons (Benoit *et al.*, 2023).

The problem at large is that despite the rich record of likely head-butting adaptations within the dinocephalians, no proper physical testing or comparison of their skull structures and their ability to withstand the stresses and strains associated with head-butting has been undertaken (Barghusen, 1975; Midzuk, 2020; Benoit *et al.*, 2021b). Additionally, despite head-butting behaviour often being observed in living ungulates, no suitable analogues to the structures seen in dinocephalians have been found within extant nor extinct members of the group (Benoit *et al.*, 2017b). The reason for this is that the cranial structures used in combat by ungulates are typically formed from keratin, which rarely preserves in the fossil record, and those that are formed from bone contain air sinuses, rather than the compact bone of dinocephalians (Farke, 2008, 2010; Benoit *et al.*, 2017b, 2021b).

These conundrums prompt the use of Finite Element Analysis (FEA), a computerised methodology that can accurately simulate deformation, stress, and strain by dividing a model of a structure into a multitude of discrete components, all of which are subjected to a well-grounded mathematical analysis (Rayfield, 2007).

FEA has been used to simulate head-butting impacts in ruminants, giraffids and pachycephalosaurid dinosaurs (Farke, 2008; Snively and Cox, 2008; Snively and Theodor, 2011; Wang *et al.*, 2022). Snively and Theodor (2011) found the skull structure of *Stegoceras* performs better in head-butting simulations than known high-energy impact head-butting ungulates. Therefore, by following a similar methodology, the role of the skull structures in dinocephalians could be tested.

Palaeopathologies can also be used to make inferences about the behaviours of extinct animals, and have been used to support theories of intraspecific combat in several genera and clades, such as the well-known *Triceratops* (D'Anastasio *et al.*, 2022), pachycephalosaurids (Peterson and Vittore, 2012; Peterson *et al.*, 2013), and gorgonopsians (Benoit *et al.*, 2021a). No comprehensive palaeopathological studies have been performed on dinocephalians, although a possible predatory bite mark has been found in a limb bone of *Jonkeria* (Shelton *et al.*, 2019). Finding palaeopathologies linked to head-butting in dinocephalians would strongly support that they engaged in this behaviour and will be used here to validate FEA models.

This project seeks to determine if dinocephalians engaged in head-butting behaviours, and if so, which families may have been best adapted for it. This is done through Finite Element Analyses (FEA) of the skulls, and the study of cranial pathologies will be used to validate these analyses.

Aims and Objectives

Aim 1: Determine the capability of dinocephalian skull models to withstand head-butting forces through FEA.

> Objective 1.1: Perform finite element analyses on 3D cranial reconstructions of the selected dinocephalians, as well as the biarmosuchian *Hipposaurus* and the pachycephalosaurid dinosaur *Stegoceras*.
>
> Objective 1.2: Compare FEA results amongst these cranial reconstructions, and then determine whether any of the models involved could withstand the stresses generated during head-butting.

Aim 2: Determine whether the results of the finite element analyses are consistent with observed pathologies.

> Objective 2.1: Examine dinocephalian fossil remains for pathologies that could have been sustained during head- or flank-butting, or face-biting, in the case of dinocephalians with large canines.
>
> Objective 2.2: Compare these pathologies with the results of the FEA to address whether their location is consistent with the high-stress areas on the models.

Hypotheses

1) I hypothesise that FEA will enable biomechanical reconstruction of stresses and strains.

2) I hypothesise that the models will serve as a reasonable approximation for the behaviour of the skulls in life.

3) I hypothesise that it is possible to use *Stegoceras* as an example of a head-butting tetrapod, and *Hipposaurus* as an example of a non-head-butting tetrapod, and that by

comparing their FEA performance with those of the relevant dinocephalian cranial models, the relative fitness of these dinocephalians can be evaluated.

4) I hypothesise that the tapinocephalid dinocephalian models, *Moschops* in particular, will be better suited to withstand head-butting, while the non-tapinocephalid models, including those for *Anteosaurus*, *Jonkeria* and *Estemmenosuchus* will be poorly adapted for head-butting. In particular, I predict that *Jonkeria* will be the worst performer in these analyses.

5) I hypothesise that tapinocephalid adaptations such as the reorientated braincase and pineal canal, conspicuous pachyostosis, and reoriented occiput will greatly benefit their performance in FEAs.

Materials and methods

Sampling of models

The models selected for these FEA have been chosen to broadly represent the clades of dinocephalian phylogeny, and to characterise a wide range of skull morphologies and the various combinations of traits which are thought to have played a role in head-butting in dinocephalians.

The dinocephalian clades (Fig. 1B), and their representative genera (in brackets), were the following: the Anteosauria (*Anteosaurus*), Estemmenosuchidae (*Estemmenosuchus*), Titanosuchidae (*Jonkeria*), and the Tapinocephalidae (*Moschops* and *Struthiocephalus*) (Fraser-King *et al.*, 2019; Benoit *et al.*, 2021b). The FEA performances of these models were compared to those of the basal Biarmosuchian, *Hipposaurus*, which has no known adaptations for head-butting (Benoit *et al.*, 2017a), and the pachycephalosaurid dinosaur, *Stegoceras*, which is considered well-adapted for head-butting (Snively and Theodor, 2011).

Moschops was chosen to represent the dome-headed tapinocephalids, which are thought to be the most likely candidates for head-butting within the Dinocephalia. The skull of *Moschops* is replete with many adaptations which probably facilitated head-butting, such as anteroventrally shifted occiput and occipital condyle, a reoriented braincase, and a thick

and more posteriorly located pineal canal (Barghusen, 1975; Benoit *et al.*, 2017b; Midzuk, 2020).

Struthiocephalus has many of the same cranial adaptations as *Moschops* does, however, the fighting surfaces are very different and take the form of two supra-orbital bosses and a conspicuous middorsal boss (Barghusen, 1975). The skull is also a great deal larger than that of *Moschops*, with a much longer snout (Brink, 1958; Barghusen, 1975; Neumann, 2019). The skull model of *Struthiocephalus* serves as a representative for the long-snouted tapinocephalids, particularly those with middorsal bosses, in order to compare their suitability for head-butting with that of the domed skulls of other tapinocephalids like *Moschops* (Barghusen, 1975; Kammerer, 2009; Neumann, 2019).

Anteosaurus represents a possibly intermediate level of adaptation for head-butting. It has some slight reorientation of the braincase, an enlarged pineal canal, a great deal of pachyostosis, as well as sizeable skull bosses, away from which the pineal canal is posteriorly located by a short distance (Boonstra, 1968; Midzuk, 2020; Benoit *et al.*, 2021b). However, the more horizontal reconstructed head posture and the position of the occiput and occipital condyle may have led to neck injuries due to misalignment (Barghusen, 1975).

Jonkeria is representative of the Titanosuchidae and was chosen as it seemingly has little to no adaptations for head-butting. It has no obvious horns or bosses, a pineal canal that bends anteriorly, instead of posteriorly as in the tapinocephalids, and not nearly as much braincase reorientation as in *Anteosaurus*, however, it does have a similarly hypertrophied pineal canal (Boonstra, 1968; Midzuk, 2020). As such, it was chosen to represent dinocephalians that are less likely to have engaged in head-butting (Barghusen, 1975).

Estemmenosuchus possesses antler-like horns that are not replicated in any other clade of the Dinocephalia (Barghusen, 1975). *Estemmenosuchus* has a slightly reorientated occiput, suggesting frontal combat, but also has large canines (Barghusen, 1975). *Estemmenosuchus*, like *Anteosaurus*, represents a possible intermediate stage of adaptation in a shift from face-biting to head-butting, as has been observed in cervids and giraffids (Geist, 1966; Cabrera and Stankowich, 2020; Benoit *et al.*, 2021b). The uniqueness and uncertain function of the horns of *Estemmenosuchus* also prompted the incorporation of this skull model into these analyses.

Stegoceras was chosen to serve as a high-suitability control for head-butting analyses, due to the promising performance it displayed in Snively and Theodor's (2011) FEA work. It has many of the same adaptations as the dinocephalians, such as the reorientated occiput and occipital condyles, a pachyostosed dome-shaped skull, and a reorientated braincase, and as such, serves as a much closer structural analogue to the skulls of dinocephalians (Snively and Theodor, 2011; Benoit *et al.*, 2017b). The availability of a 3D model from CT scans of the same skull used in these analyses also made *Stegoceras* a prudent addition to these analyses (Snively and Theodor, 2011; Witmer *et al.*, 2018)

Hipposaurus was chosen as a low-suitability control for head-butting, as it possesses none of the likely adaptations for head-butting (Barghusen, 1975), belongs to the biarmosuchians, and existed in the same assemblage zone as many dinocephalians did (Day and Rubidge, 2020). The previous segmentation work of the skull and endocast also made this an attractive choice for inclusion (Benoit *et al.*, 2017a).

As the dinocephalian skull models significantly outperformed both control skulls (see results), enlarged versions of the *Hipposaurus* and *Stegoceras* skulls were used to test the effects of absolute size on FEA performance and see how they compare with the other models. Both control skulls were proportionally enlarged and made to have the same length as that of *Moschops*, which has similar proportions due to its short snout. These will be referred to as the enlarged *Hipposaurus* and enlarged *Stegoceras* models.

Construction of models

With the exception of *Stegoceras*, all the models which were used in this study were created *de novo* using Blender 3D software by an Honours student at the Evolutionary Studies Institute, Adam Midzuk (Midzuk, 2020). He chose this method over the digital acquisition of cranial models due to the scarcity of complete and undeformed dinocephalian skulls, and the deformed and incomplete nature of available reference specimens. Internal cranial anatomy is derived from Boonstra's (1968) work on the sectioned skulls of several dinocephalians, which was then adjusted to match the appropriate external morphology from other papers (Benoit *et al.*, 2016, 2017b; Midzuk, 2020). These models include *Struthiocephalus*, *Moschops, Anteosaurus, Jonkeria*, *Estemmenosuchus*, and *Hipposaurus* (Fig. 3, 4).

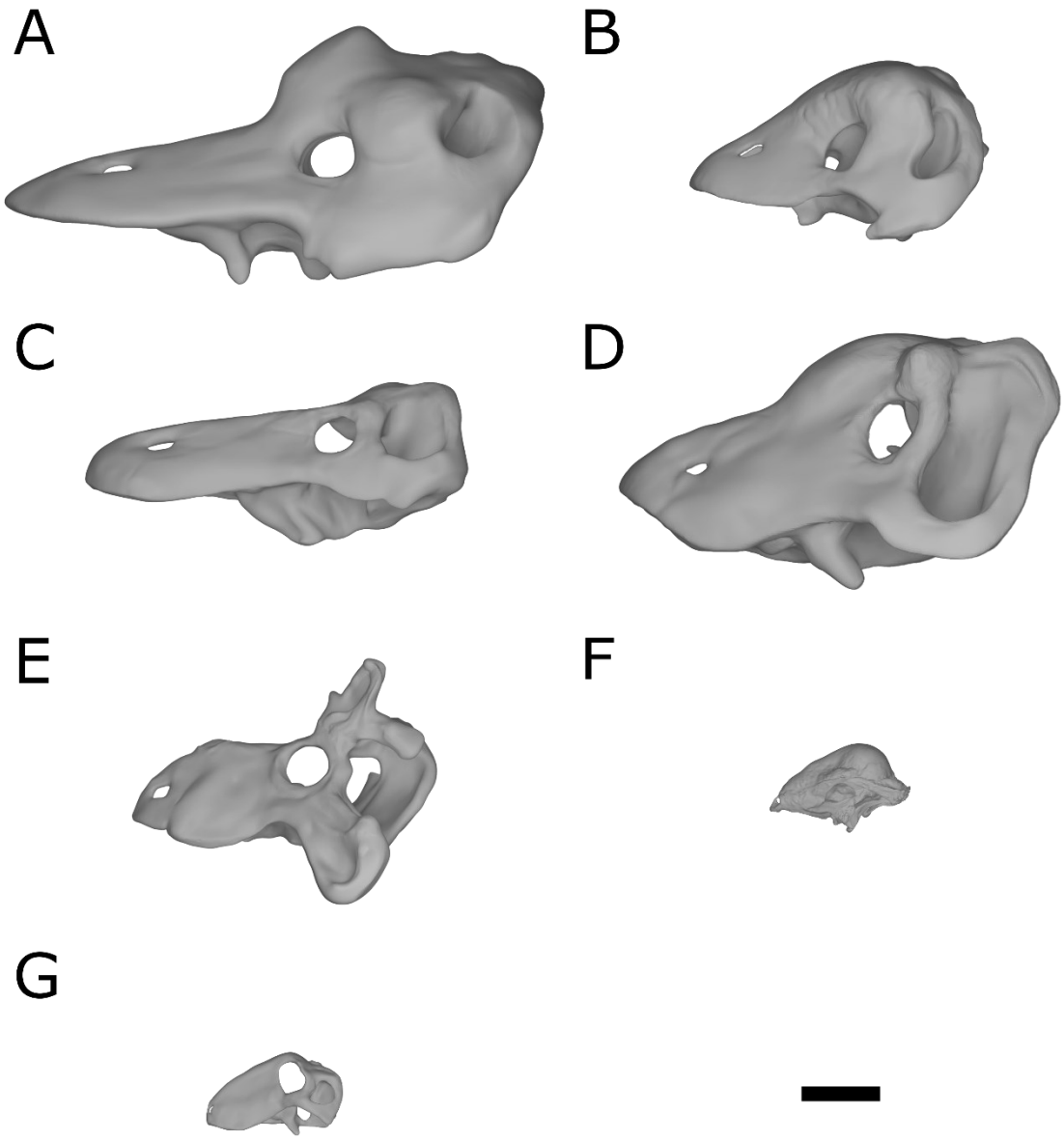

Figure 3: Left Lateral view of the skull models.

A: *Struthiocephalus*, B: *Moschops*, C: *Jonkeria*, D: *Anteosaurus*, E: *Estemmenosuchus*, F: *Stegoceras*, G: *Hipposaurus*. Scale bar = 10 cm.

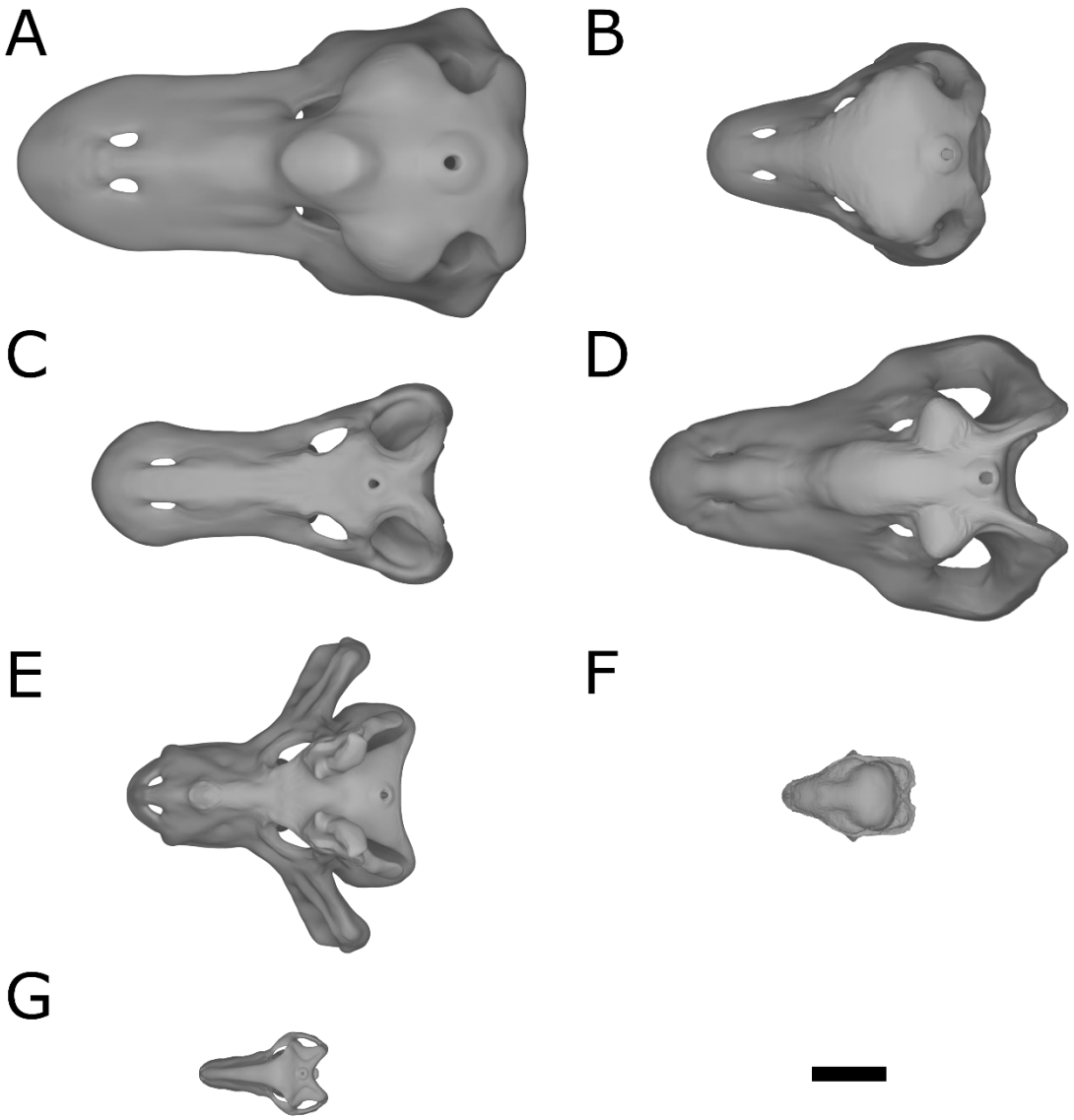

Figure 4: Dorsal view of the skull models.

A: *Struthiocephalus*, B: *Moschops*, C: *Jonkeria*, D: *Anteosaurus*, E: *Estemmenosuchus*, F: *Stegoceras*, G: *Hipposaurus*. Scale bar = 10 cm.

The endocranial cavities were modelled from the reconstructions produced by Boonstra (1968) of the endocranial cavities of *Moschops* (SAM-PK-11972), *Struthiocephalus* (SAM-PK-12049), *Jonkeria* (SAM-PK-11556), and *Anteosaurus* (SAM 12082). Fortunately, all Boonstra's figures were created in both lateral and dorsal aspects, (except *Anteosaurus*) which simplified the process of modelling in 3D. These were lined up with the foramen magnum and pineal foramen of the skull, and adjusted where necessary, using the sections of Boonstra (1968) as a guide (Midzuk, 2020).

The 3D model of the skull of *Stegoceras* was created by Witmer *et al.* (2018) using CT scans downloaded from Morphosource.org. This model was then retrodeformed and simplified by Adam Midzuk in order to make it comparable to the dinocephalian skulls and suitable for FEA (Fig. 5). Specifically, within the object deform modifier, he used a lattice deform modifier with a lattice object to address the bulk of the left-right deformation due to shearing. The detail of the model was reduced using the "detail flood fill function", setting the resolution to 22.9 with the constant detail option. Midzuk further diminished the surface details, shifted areas of minimal distortion, and removed cavities and pinching with grab elastic sculpt, grab, smooth, and inflate brushes. Afterwards, he utilised the symmetrise tool to create a symmetrical model using the least distorted side of the model. A decimate modifier was used to lower the polygon count to 18000 surface triangles.

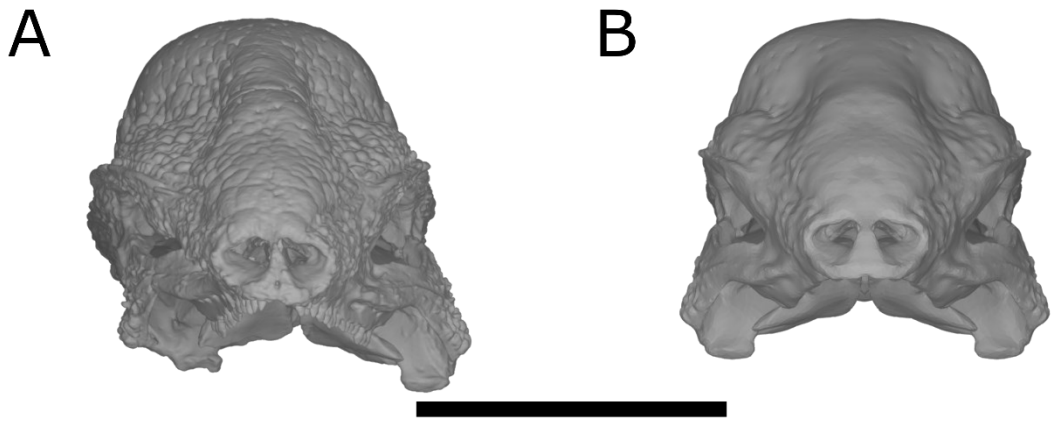

Figure 5: Anterior view of the original and modified *Stegoceras* skull models.

A: Original model, B: Modified version

Moschops was reconstructed based on illustrations of SAM-PK-11985 (Boonstra, 1968), SAM-PK-11582 (Boonstra, 1957; Barghusen, 1975), and internal structures were derived from AMNH 5550, 5552, and 5553 (Boonstra, 1936, 1968; Kammerer, 2009).

The model for *Anteosaurus* was sculpted from SAM-PK-11296 (the holotype specimen for *Anteosaurus abeli*) (Boonstra, 1954; Barghusen, 1975; Kammerer, 2009), SAM-PK-K360 (Kammerer, 2011), SAM-PK-K284 (Kammerer, 2009, 2011), BMNH R3595 (Kammerer, 2011), *Doliosauriscus yanshinovi* (=*Titanophoneus potens*), PIN 157/3 (Kammerer, 2011) and a generalised drawing with the internal anatomy modelled from SAM-PK-12082 (Boonstra, 1968) and SAM-PK-9085 (anterior sagittal section from Boonstra, 1968).

The main source for the *Struthiocephalus* model was BP/1/1575 (Brink, 1958) which is identified as *Struthiocephalus whaitsi* (Boonstra, 1969; Neumann, 2019). Sections of *Struthiocephalus* are derived from SAM-PK-9129, SAM-PK-12049, and SAM-PK-5584 (Boonstra, 1968).

The *Jonkeria* model is derived from TM212 (Kammerer, 2009), and the reconstructions of the skull done by Janensch and Boonstra (Boonstra, 1954, 1963, 1969; Janensch, 1959). Internal structures are based on SAM-PK-11556 and SAM-PK-11574 (Boonstra, 1968).

Hipposaurus is based on SAM-PK-8950 (Haughton, 1929; Sigogneau-Russel, 1989), CG-WB123 (Sigogneau-Russel, 1989; Benoit, 2015), SAM-PK-12252 and SAM-PK-9081 (Sigogneau-Russel, 1989), and a generalised reconstruction by Boonstra (Boonstra, 1969). Internal anatomy was derived from synchrotron scans of CG-WB123 (Benoit *et al.*, 2017a).

The external morphology of *Estemmenosuchus* was sculpted on the basis of drawings of the holotype of *Estemmenosuchus mirabilis*, specimen PIN 1758/6 (Chudinov, 1965; Ivakhnenko, 2008), and a picture of a skull cast of *Estemmenosuchus mirabilis* at the Royal Tyrell Museum in Canada (Tanglao, 2012). The internal structures of the skull model for *Estemmenosuchus* were constructed much in the same way as those of the *Hipposaurus* model were, as boolean operations were used to reconstruct the braincase, pineal tube, and other internal structures based on those of *Jonkeria*.

Finite element analysis

The models were analysed using ANSYS Workbench software. The boundary conditions or constraints, which “fixed” the model in space were applied in order to mimic the effects of ligament attachment. Unlike Snively and Theodor (2011), *Stegoceras* was not constrained at the basal tubera, since the two constraints on the reconstructed sites of ligament attachment and the one constraint on the occipital condyle are deemed to be sufficient, and as these structures are not present in the other skull models.

Finite element mesh was refined and simplified to achieve a state of mesh independence, where the number of mesh elements is as low as possible while still not affecting the outcome of the analysis (Gardiner, 2017). This was done through initial modifications in blender using various operations with the decimate tool and the triangulate and mirror modifiers until the models had as detailed a mesh as possible while still being compatible

with the Ansys Mechanical software and being able to perform FEA operations within a reasonable timeframe and computational expense. Further refinements were done with the mesh sizing tool in Ansys Mechanical, which was applied with various mesh sizes per model to see which sizes yielded acceptably similar results with reference to the maximum and average equivalent stresses.

Four series of FEA tests were applied to the various 3D models. These consisted of two load protocols, each with two load magnitudes. In the first load protocol, the load was applied on the reconstructed force application points on the tops of the skulls to recreate an impact sustained during head-butting. In the other load protocol, the load was applied on reconstructed force application points on the supra-orbital bosses to simulate a flank-butting impact (Geist, 1966). The first load magnitude was 1000 N, which represents a conservative force value, as Snively and Theodor (2011) reconstructed an impact force of 1360 N at a closing speed of 3 m/s for *Stegoceras*, and as Bighorn Sheep are known to collide with impact forces in excess of 3400 N (Farke, 2008). Accordingly, the second load magnitude was set at 3400 N, representing some of the highest known impact forces in Bighorn Sheep (Farke, 2008).

Estemmenosuchus (Figure 7), due to its unique anatomy, required additional investigation to reconstruct the likely force application points. This problem was addressed with the use of 3D printed scale models of Midzuk's reconstructions (Fig. 6) and physical manipulation of the models which indicated likely contact sites for the skull structures, similar to the testing done by Farke with scale models of *Triceratops* (Farke, 2004).

This led to three head-butting force application points: two points on the anterior bases of both dorsal horns, as well as on the nasal boss. In flank-butting protocols, force application points were placed on the apices of both horns on the left side of the skull. The general placement of force application points and fixed constraints can be seen in Figures 7 to 12.



Figure 6: *Estemmenosuchus* 3D printed models used to infer the most likely points of impact.

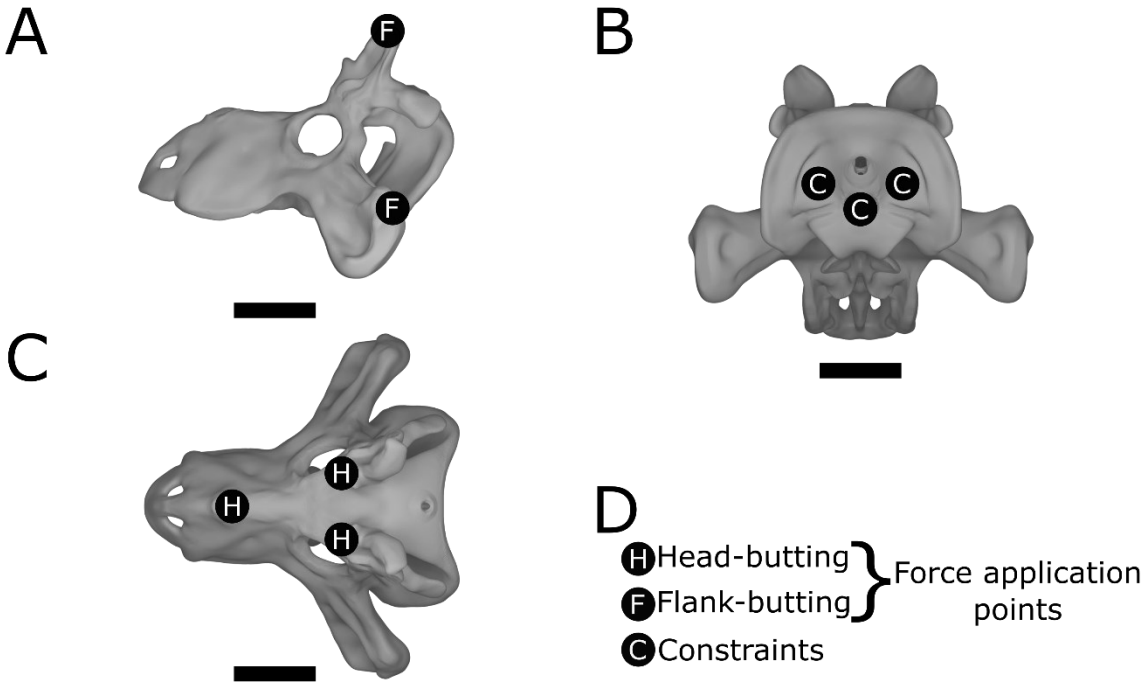

Figure 7: *Estemmenosuchus* skull model with force application points and constraints.

(A) Left lateral view, (B) posterior view of occiput, (C) dorsal view, and (D) legend, Scale bars = 10 cm.

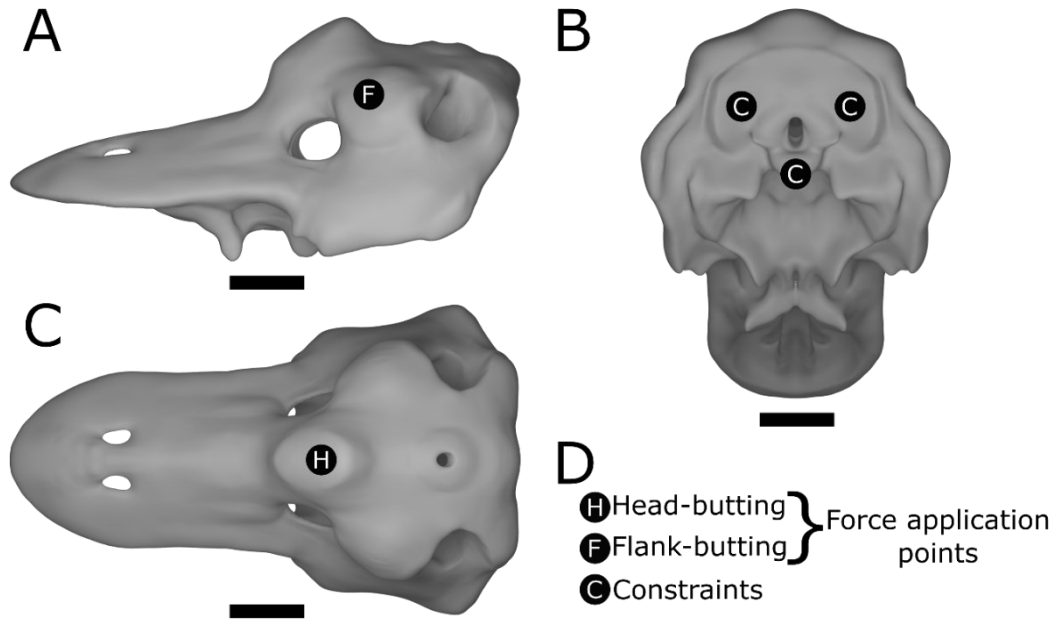

Figure 8: *Struthiocephalus* skull model with force application points and constraints.

(A) Left lateral view, (B) posterior view of occiput, (C) dorsal view, and (D) legend, Scale bars = 10 cm.

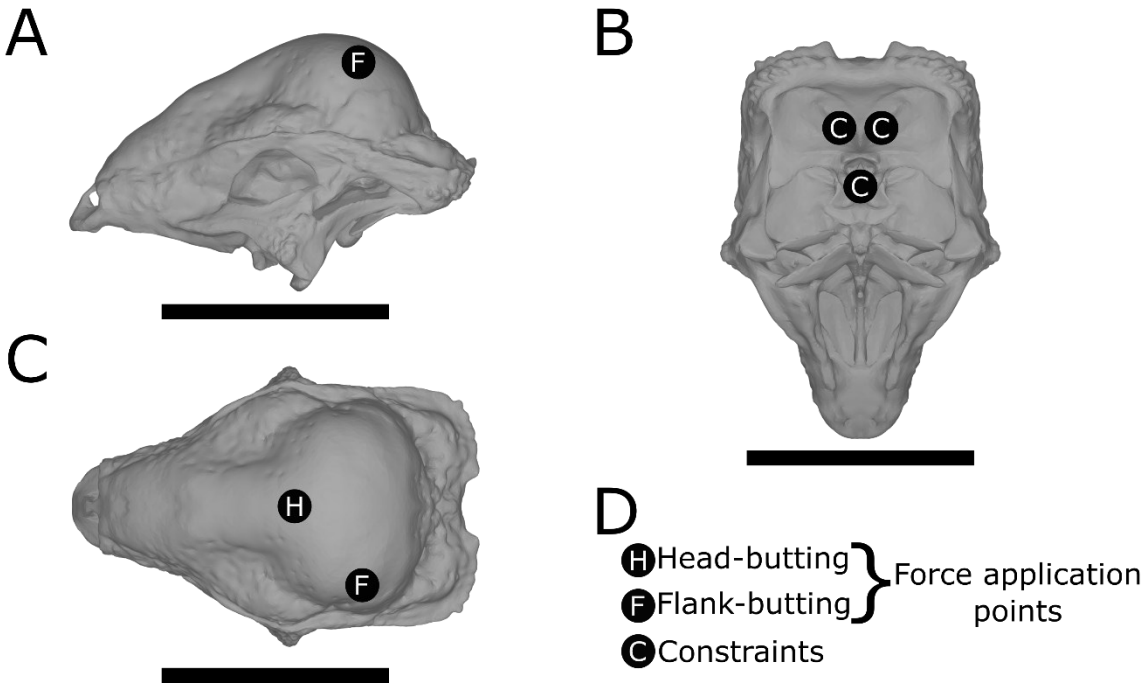

Figure 9: *Stegoceras* skull model with force application points and constraints.

(A) Left lateral view, (B) posterior view of occiput, (C) dorsal view, and (D) legend, Scale bars = 10 cm.

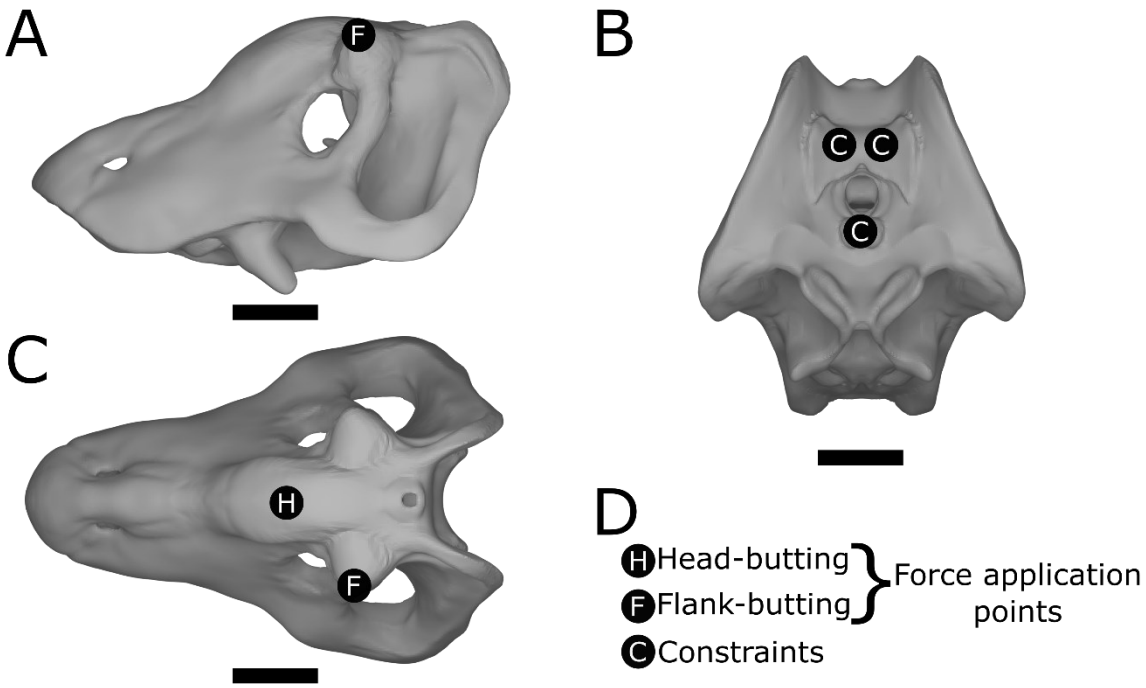

Figure 10: *Anteosaurus* skull model with force application points and constraints.

(A) Left lateral view, (B) posterior view of occiput, (C) dorsal view, and (D) legend, Scale bars = 10 cm.

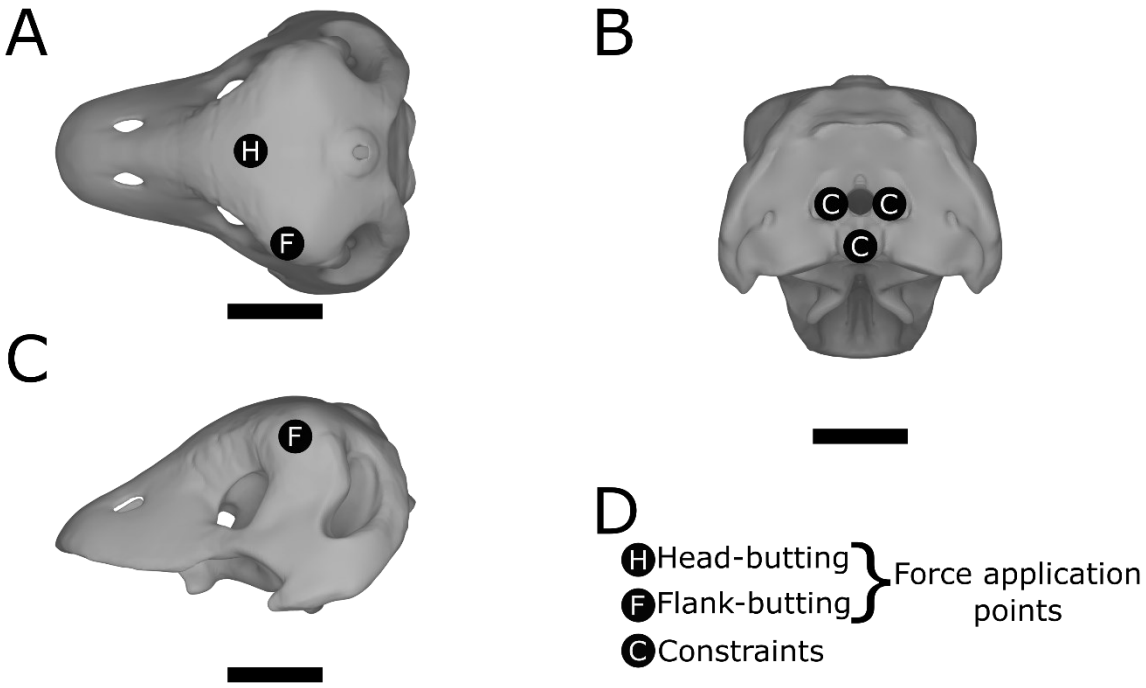

Figure 11: *Moschops* skull model with force application points and constraints.

(A) Left lateral view, (B) posterior view of occiput, (C) dorsal view, and (D) legend, Scale bars = 10 cm.

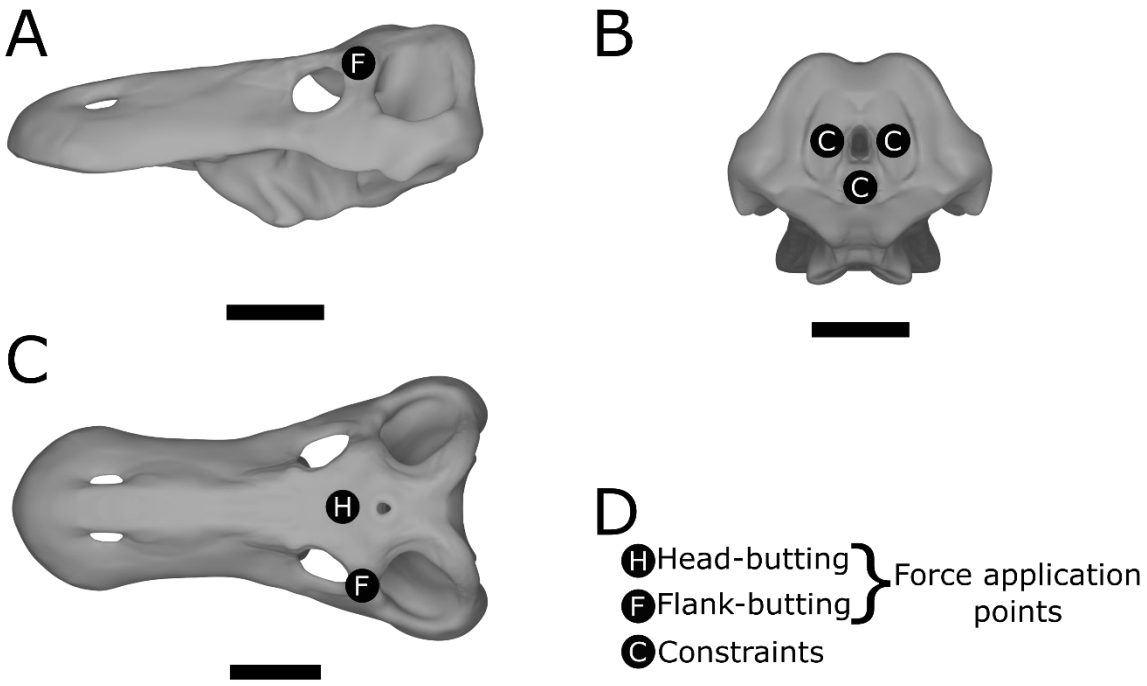

Figure 12: *Jonkeria* skull model with force application points and constraints.

(A) Left lateral view, (B) posterior view of occiput, (C) dorsal view, and (D) legend, Scale bars = 10 cm.

The teeth were not modelled, because small pointy geometries (relative to the size of the body) automatically mesh with smaller mesh elements due to the size of the geometry. If the remainder of the mesh does not use a similar size element (which would be computationally expensive), the finer mesh in these areas creates artificial stress concentrations which inflate the stress values in that area (Benoit and Mangera, Pers. Comm.). Accordingly, teeth were removed from the *Stegoceras* model.

The material properties selected were those used by Snively and Cox (2008), which represent typical values for compact bone. The same material properties were applied isotropically for all models in order to ensure that only the geometry of the skull would affect the results, to take into account the fact that osteohistological data are not available for most of the taxa studied, and to reduce the computation complexity of the analyses. The approach of maintaining the same material properties throughout the skulls of therapsids has been used in published FEA research (Lautenschlager *et al.*, 2020) and is justified here as dinocephalians, unlike ruminants, do not have sinuses in their cranial adornments (Boonstra, 1968; Benoit *et al.*, 2021b).

The Poisson ratio, which measures the amount of contraction of a material, was set to 0.4, the material density was set to 2000 kg/m^3, and the Young's Modulus, which acts as a measure of material stiffness, was set to 20 000 MPa. The tensile and compressive yield Strength was set to 200 MPa according to the correction made by Snively and Theodor (2011), as this represents the ultimate stress of bone in compression. The ultimate stress is value which is typically higher than the yield stress and signifies a material being completely compromised and broken (Snively and Theodor, 2011). Therefore, using the ultimate stress as the yield stress represents a conservative approach.

Only bone structures were examined in these analyses, therefore it is worth noting that cranial models that appear structurally sound by means of the safety factor might still have undergone significant soft tissue trauma. Braincases are modelled as hollow structures, and no keratinous caps are modelled, due to the loss of most available evidence for them in fossils. It is worth noting that the choice of failure theory can affect the factor of safety values that the simulations yield, yet the various theories can still yield the same outcome, such as one of no breakage or failure (Mangera, Pers. Comm.). This approach is also less expensive computationally, and as such was beneficial for these analyses.

One of the values used as an indicator of performance was the maximum equivalent stress surrounding the application point in Megapascals (see Fig. 8). The maximum equivalent stress is the combined and resultant stress value which considers direct and shear stresses, with lower equivalent stress values indicating better performance and stress dissipation (Mangera, Pers. Comm.). This value was chosen as the maximum stresses experienced by the models were in most examples at the constraint artifacts, and as these values typically far exceeded the equivalent stress values elsewhere in the skull. Average equivalent stress values could not be used, as they would be affected constraint artifacts and could be biased towards models with higher polygon counts.

For each model, a safety factor was calculated. This was done to indicate the theoretical load limits that could be endured by the FE models in their various protocols. A safety factor at or below 1 indicates that a material has reached its breaking point (Maria, 2016). Throughout all variations of protocols and models, the factor of safety values seldom approach this value, indicating little to no permanent deformation.

It was not obvious, even concerning material property values from Snively and Cox (2008), and Snively and Theodor (2011), whether the compact bone analogue should be treated

as a brittle or a ductile material. Therefore, failure theories applicable to brittle materials (Mohr-Coulomb failure theory) and ductile materials (Maximum equivalent stress) were applied to each of the models (Kosaraju, 2022).

The Mohr-Coulomb failure criterion is a set of linear equations regarding principal stresses and how they relate to the failure conditions for isotropic materials, ignoring the role of intermediate principal stresses (Labuz and Zang, 2012). The maximum equivalent stress criterion (also known as the von Mises criterion) states that yielding occurs when the elastic energy of distortion matches or surpasses a critical value (Hill, 1950; Francis, 2016). Tables with the results from these failure criteria can be found in Appendix 3 and 4.

As a qualitative measure, the distribution and magnitudes of stresses through the skull were observed and compared between models. This qualitative approach is used in addition to the force application point stresses since factor of safety values seldom approached critical values in the majority of models and protocols. As such, it was decided that using the safety value below one as a failure criterion (Snively and Cox, 2008) would not be the primary tool for comparison.

Stress values observed in the skulls are typically either relatively high or relatively low, and can have a wide range between all the tested skull models and protocols. Therefore, to make visual comparison of stresses between skull models and protocols easier, the stress legend for Figs. 18-21 is non-linear and encompass the range of observed non-constraint artifact related stress values in all models and protocols. The stress legend was adjusted and fine-tuned to be applicable to all skulls and thus facilitate visualising trends in stresses between all the analyses, force magnitudes, and protocols, as linear keys tended to be too broad to be useful. As a result, a decision was made to divide the stress legend into seven ranges of stress values only and, as a visual tool, the stress legend was set up in a manner that helps distinguish the differences in performances between all of the models, particularly those that fall within a relatively similar range of stresses.

The upper limit of the stress legend (200 MPa) is meant to emphasise the maximum stresses observed in, e.g., the *Hipposaurus* model, so that the 6-200 MPa range encompasses most of the stresses observed in the analyses and maximise the visual contrast between the highest and lowest stress values. Minimum stresses could be as low as 0.17 Pa.

Institutional abbreviations

AMNH, American Museum of Natural History, New York, USA; **BPI**, Evolutionary Studies Institute (formerly the Bernard Price Institute) University of the Witwatersrand, Johannesburg, South Africa; **NMQR**, National Museum, Bloemfontein, South Africa; **ROZ**; Roy Oosthuizen collection, currently housed at the Iziko South African Museum, Cape Town, South Africa; **SAM**, Iziko, South African Museum, Cape Town, South Africa; **KNP**, Karoo National Park, Beaufort West, South Africa.

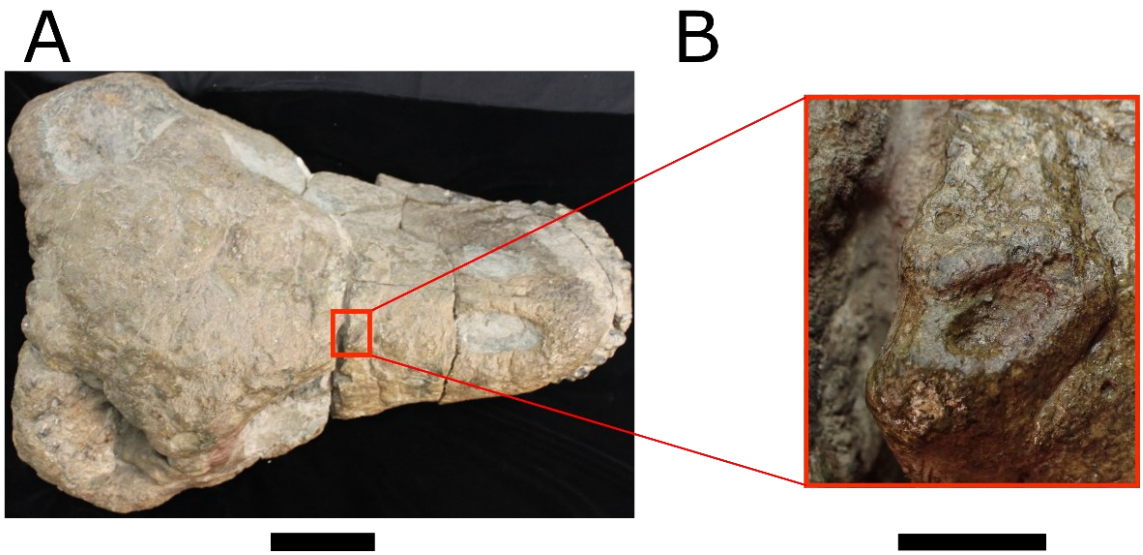

Figure 13: SAM-PK-11693 skull and pathology.

A: SAM-PK-11693 skull with pathology in red box, scale bar = 10 cm, B: Pathology, scale bar = 1 cm.

In the search for these pathologies, I visually examined two hundred and two dinocephalian specimens (listed in Appendix 5) in the collections of the Evolutionary Studies Institute, Iziko South African Museum in Cape Town, National Museum in Bloemfontein, the Albany Museum in Makhanda (Grahamstown), and the Fransie Pienaar Museum in Prince Albert. Synchrotron data for AM4950 was also included from Benoit *et al.* (2017).

Pathological analysis

The FEA work was complemented by a search for palaeopathologies in fossil remains of dinocephalians. These remains were visually inspected for pathologies that could have resulted from head-butting impacts, and in dinocephalians with large canines, by face-biting behaviours, such as healed bite marks similar to the one found in a gorgonopsian snout (Benoit *et al.*, 2021a). Pathologies were identified on the basis of conspicuous differences from the surrounding bone and other skulls in terms of shape, texture, and symmetry (Lovell, 1997; Lingham-Soliar, 2004; Benoit *et al.*, 2021a). Pathologies were distinguished from post-mortem damage by traces of healing, such as the growth of raised and rugose callus bone, which occurs several weeks after an injury is inflicted (Lovell, 1997; Bell and Currie, 2010; Benoit *et al.*, 2021a). SAM-PK-11693 is a good example of a skull with a pathology (Fig. 13).

Results

Finite element analysis

In these FEAs, the dinocephalian skull models performed better than expected. It was thought that *Moschops* and *Struthiocephalus* might fare better than a specialised head-butter like *Stegoceras*, but the results suggest that all dinocephalian models outperform *Stegoceras* (Fig. 14). In both qualitative and quantitative measures, dinocephalian skull models outperformed the low-suitability control of *Hipposaurus*, and the high-suitability control of *Stegoceras* (Figs. 14-21). The extremely high performance of the dinocephalians and low performance of *Hipposaurus* and *Stegoceras* in these analyses surpassed the range of expected outcomes.

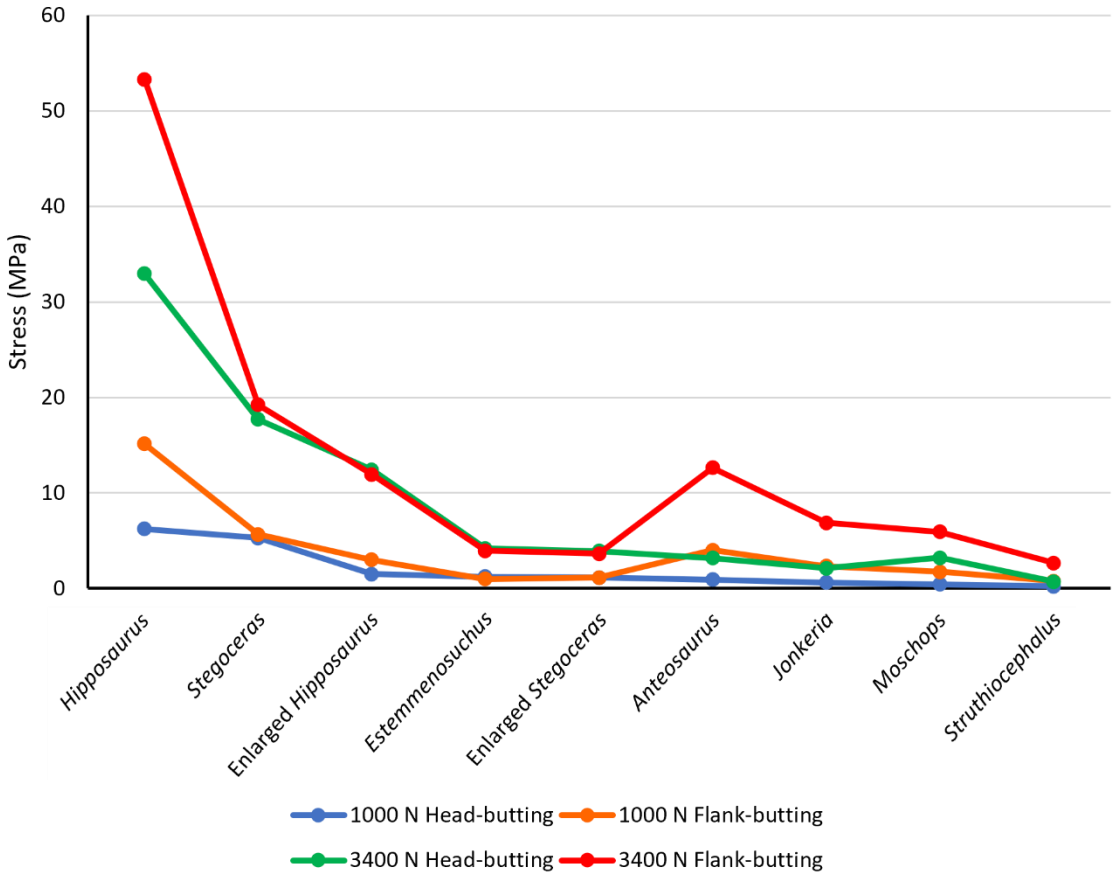

Figure 14: Force application point stresses of selected skull models in all tested load magnitude and force protocols.

The Mohr-Coulomb criterion yields lower factor of safety values than the maximum equivalent stress criterion (Appendix 3,4). It should be noted that Ansys Mechanical only yields safety factor values up to 15, thus limiting the usefulness of these values. *Struthiocephalus* and *Moschops* do not yield any values lower than 15, and several other models yield minimum safety factors of 15, which makes comparison difficult. *Hipposaurus* and its enlarged version are the only models that generate factor of safety values lower than 1, which would indicate failure of the material (Fig. 15, 16).

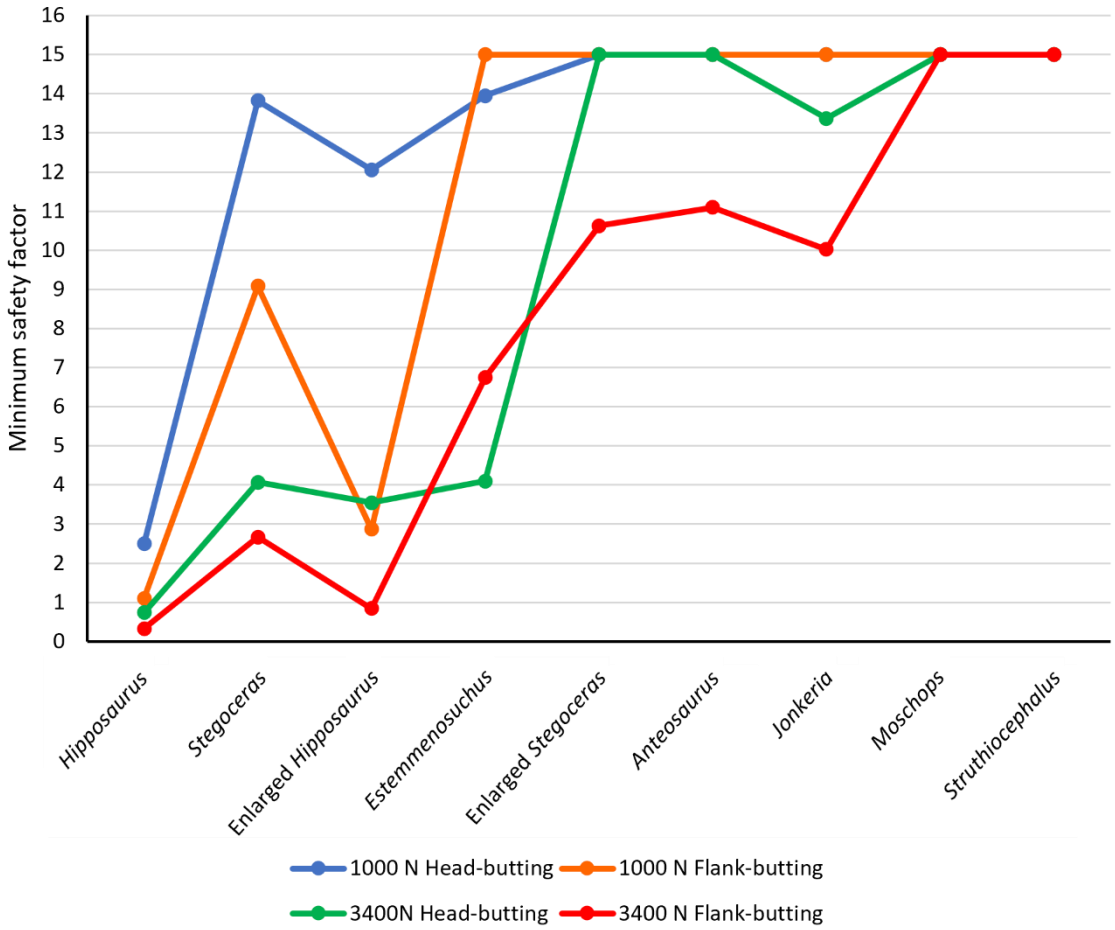

Figure 15: Minimum safety factor values according to the Mohr-Coulomb failure criterion.

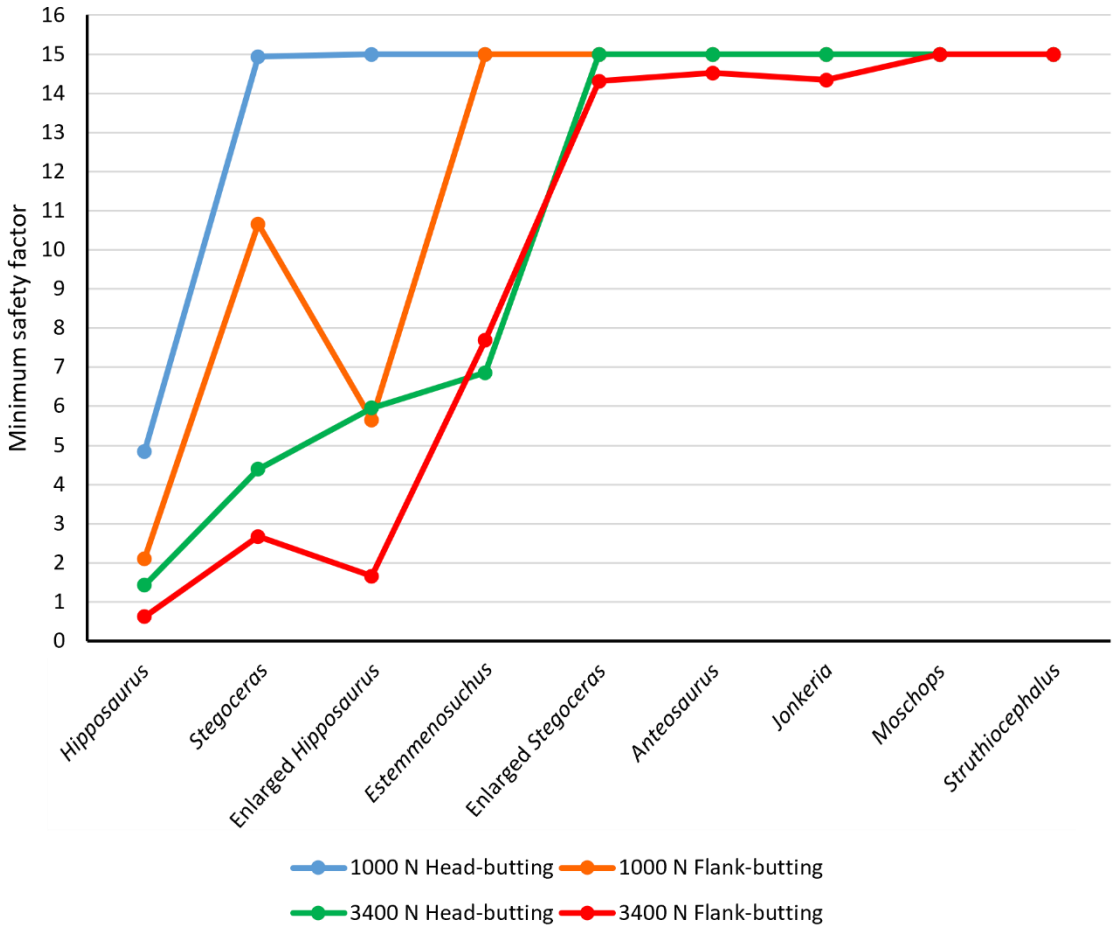

Figure 16: Minimum safety factor values according to the maximum equivalent stress (von Mises) failure criterion.

In Fig. 17, the averages of all minimum safety factor values from all protocols and failure criteria are plotted for each of the tested models. *Struthiocephalus* and *Moschops* yield the same value of 15, which represents the limits of the software. *Anteosaurus*, *Jonkeria* and the enlarged *Stegoceras* model yield average similar safety factor values in the margin between 14 and 15. *Estemmenosuchus* has the next lowest mean safety factor value of 10.5437. This is followed by the values of 7.7880 for *Stegoceras* and 5.9475 for the enlarged *Hipposaurus*. The standard *Hipposaurus* model has the lowest mean safety factor value of 1.7082, being separated from the other means by a wide margin.

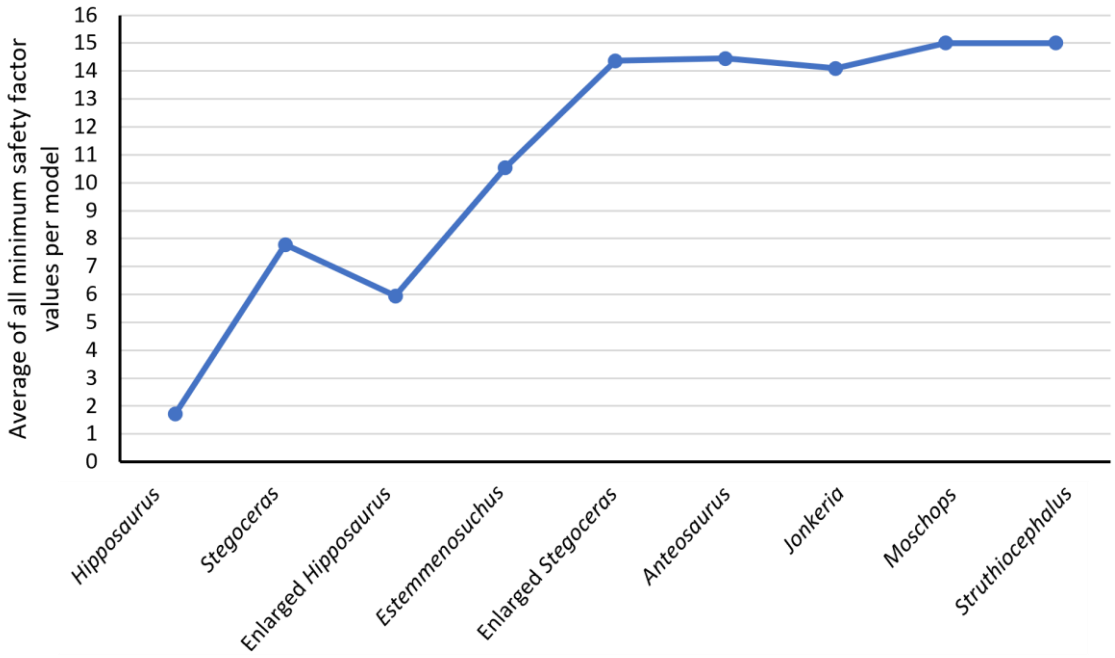

Figure 17: Graph showing the average of all minimum safety factor values per model in protocols and failure criteria.

There appears to be a tendency for larger skull models to perform better than their smaller counterparts. This can be observed in terms of force application point stresses (Fig. 14), minimum safety factor values (Figs. 15-17), and equivalent stress distributions (Figs 18-21). This is illustrated by *Stegoceras* and *Hipposaurus*, in which the standard skull models have much more pervasive and extreme stress distribution, but the enlarged models show much lower stress levels, with similar relative distributions of stress. For example, in the 3400 N head-butting protocol, the peak force application point stress levels in the enlarged models for *Stegoceras* and *Hipposaurus* are reduced to 22.1% and 37.7% of their standard models respectively. These enlarged *Stegoceras* and *Hipposaurus* models have volumes which are respectively 9.52 and 10.50 times those of their standard counterparts. Therefore, these larger skulls provide greater surface areas and volumes to dissipate stress throughout (Appendix 1, 2). This emphasises the importance of absolute cranial size for

high-energy head-butting (see discussion).

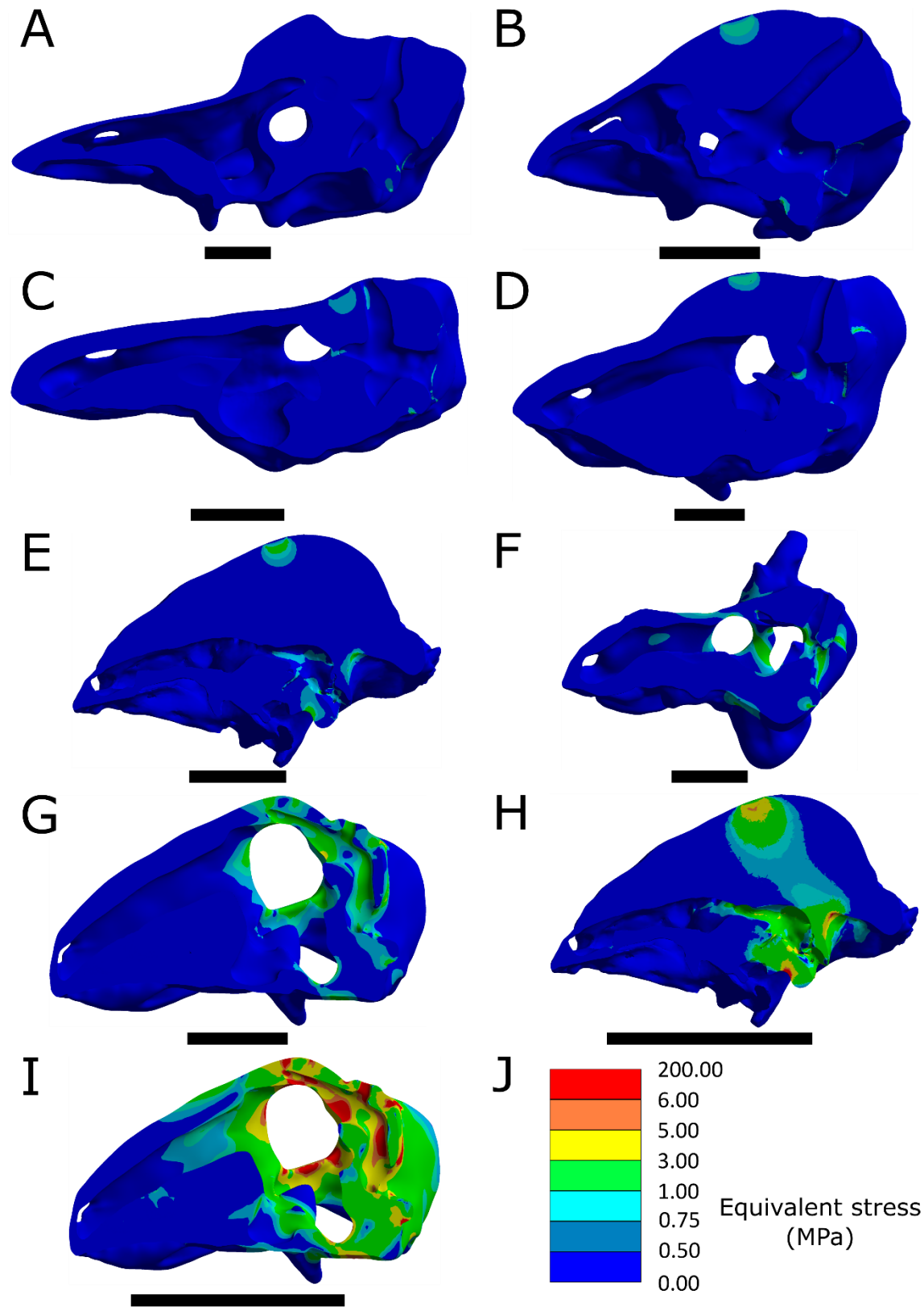

Figure 18: Comparison of sagittal sections of stress distributions in the 1000 N head-butting protocol.

A: *Struthiocephalus*, B: *Moschops*, C: *Jonkeria*, D: *Anteosaurus*, E: *Stegoceras* enlarged, F: *Estemmenosuchus*, G: *Hipposaurus* enlarged, H: *Stegoceras*, I: *Hipposaurus*, J: Legend. Scale bars = 10 cm.

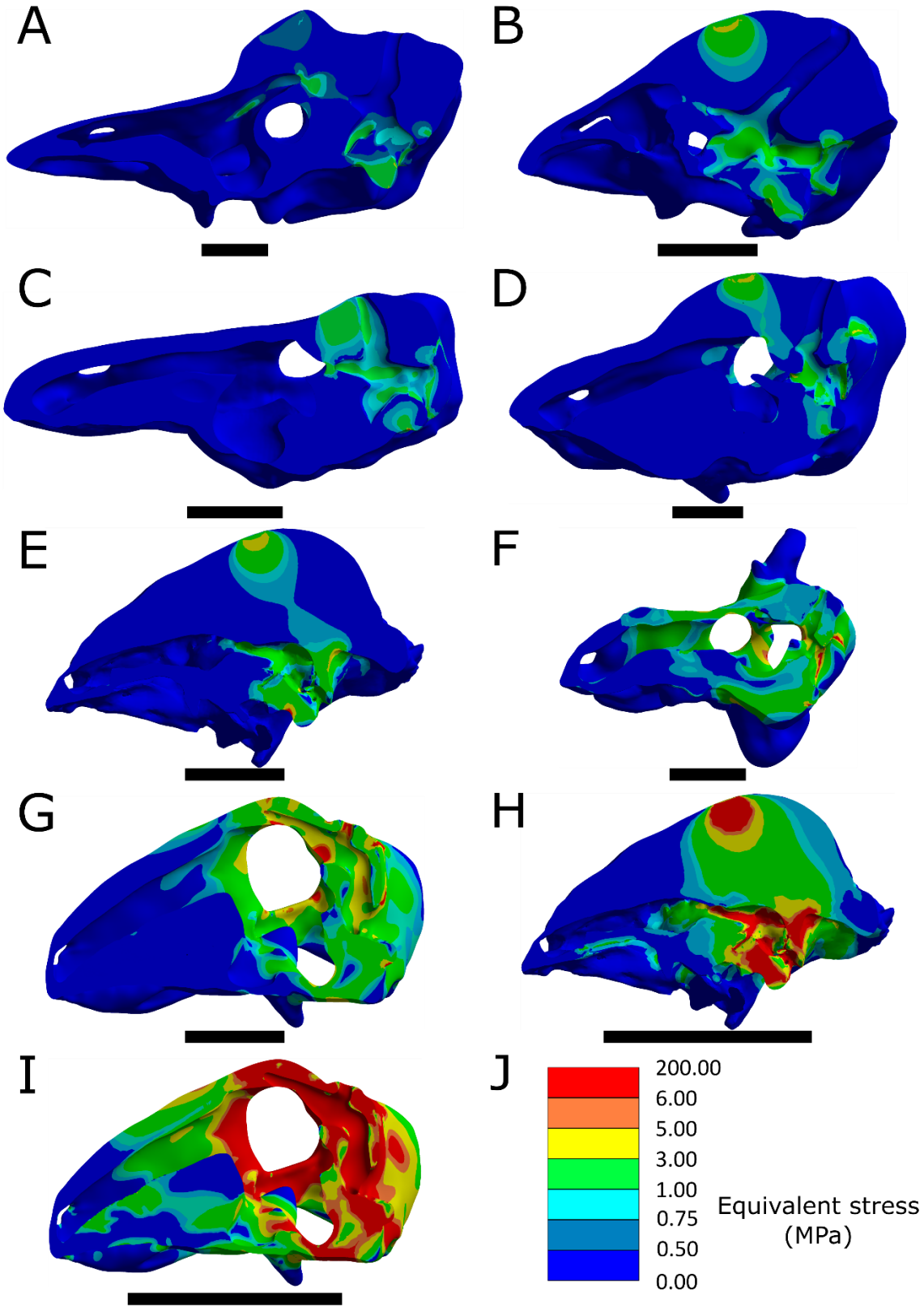

Figure 19: Comparison of sagittal sections of stress distributions in the 3400 N head-butting protocol.

A: *Struthiocephalus*, B: *Moschops*, C: *Jonkeria*, D: *Anteosaurus*, E: *Stegoceras* enlarged, F: *Estemmenosuchus*, G: *Hipposaurus* enlarged, H: *Stegoceras*, I: *Hipposaurus*, J: Legend. Scale bars = 10 cm.

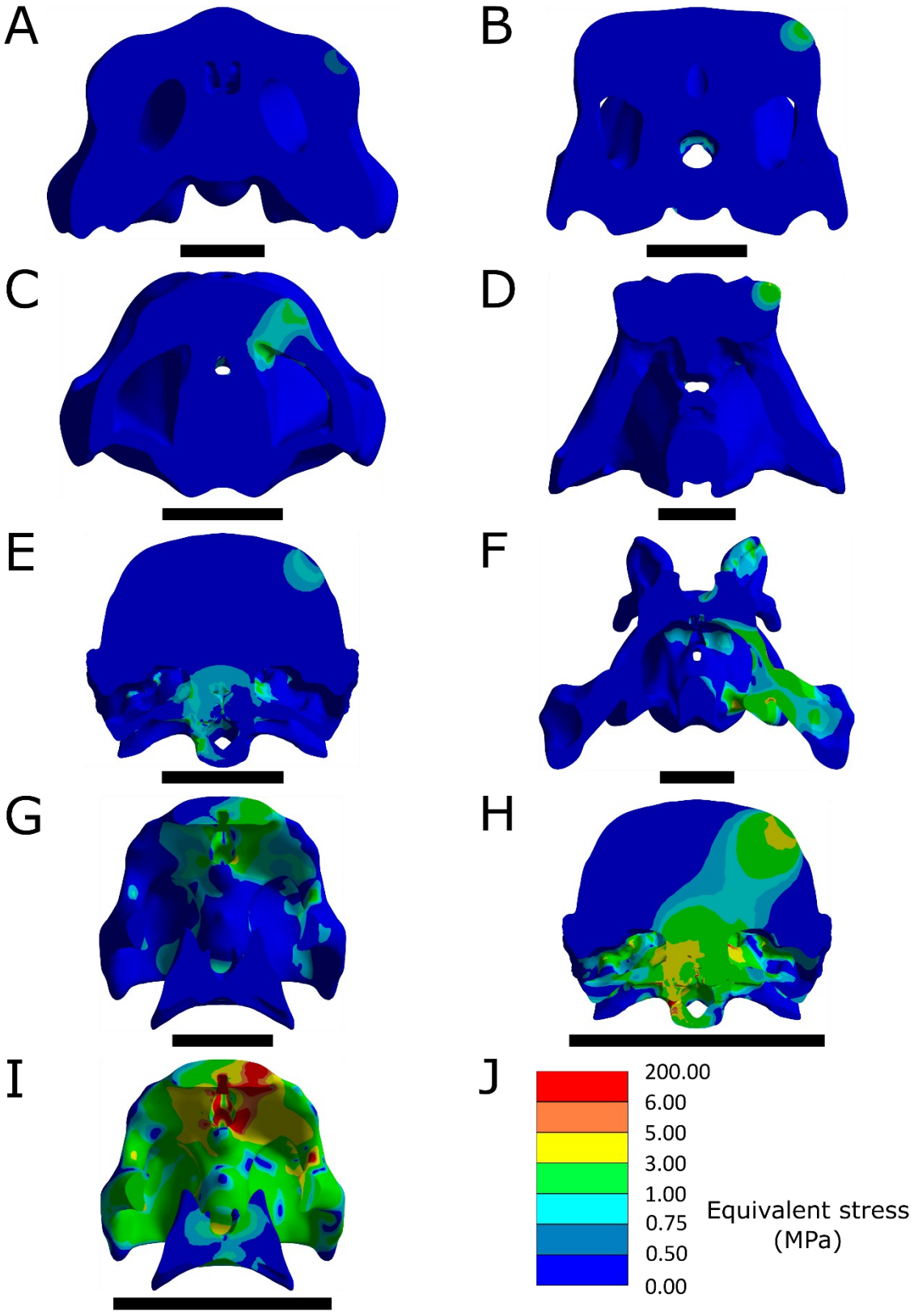

Figure 20: Comparison of transverse sections of stress distributions in the 1000 N flank-butting protocol taken at greatest extent of strain from force application points.

A: *Struthiocephalus*, B: *Moschops*, C: *Jonkeria*, D: *Anteosaurus*, E: *Stegoceras* enlarged, F: *Estemmenosuchus*, G: *Hipposaurus* enlarged, H: *Stegoceras*, I: *Hipposaurus*, J: Legend. Scale bars = 10 cm.

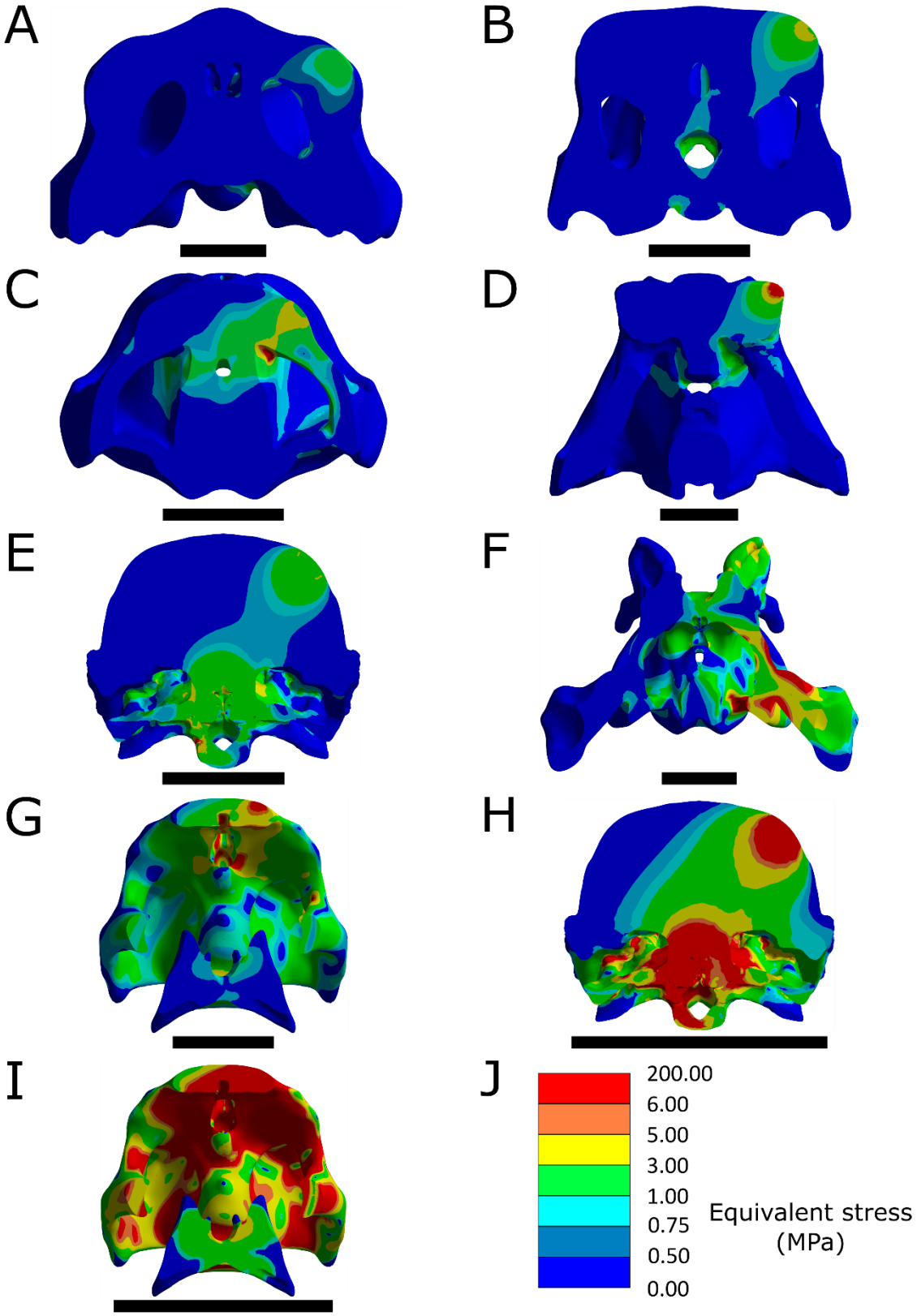

Figure 21: Comparison of transverse sections of stress distributions in the 3400 N flank-butting protocol.

A: *Struthiocephalus*, B: *Moschops*, C: *Jonkeria*, D: *Anteosaurus*, E: *Stegoceras* enlarged, F: *Estemmenosuchus*, G: *Hipposaurus* enlarged, H: *Stegoceras*, I: *Hipposaurus*, J: Legend. Scale bars = 10 cm.

***Hipposaurus*:**

Hipposaurus is the least suited model for cranial combat as expected, yielding the highest stresses of all models (Fig. 14). Additionally, *Hipposaurus*, and its enlarged version, are the only models with safety factor values below one, thus achieving failure according to the Mohr-Coulomb and maximum equivalent stress (von Mises) failure criteria (Figs. 15, 16). Failure by these standards still only occurs in a small region of the squamosal for flank-butting and near the constraints for head-butting protocols. It should also be noted that these failures only occur in the 3400 N head-butting and flank-butting protocols, though safety factor values are still low in the 1000 N protocols. In the 1000 N head-butting protocol, the peak force application point stress is 6.2481 MPa, while in the 1000 N flank-butting protocol, this stress reaches 15.1450 MPa (Appendix 1).

This performance can be related to the relatively small skull size, less robust construction, and the lack of any adaptations for head-butting. Stresses routinely exceed 6 MPa in the post-orbital bar, the pineal foramen, and the regions surrounding the braincase in all protocols, and elevated levels of stress extend to a greater proportion of the volume of the skull than all other models (Figs. 18-21 (I)). In the 3400 N head-butting and flank-butting protocols, stresses greater than 6 MPa almost entirely surround the braincase, pineal canal, and post-orbital bar (Figs. 19,21 (I)). In the 3400 N head-butting protocol, the force application point stresses reach 32.9450 MPa, and they reach 53.2750 MPa in the 3400 N flank-butting protocol.

Enlarged *Hipposaurus*

The enlarged *Hipposaurus* model, much like the enlarged *Stegoceras* model, displayed similar stress distribution patterns to its life-size counterpart, but at diminished magnitudes and extents (Figs 18-21 (G, I)). Stress values greater than 6 MPa only appear in the region of the braincase in the 3400 N load protocols and are not as pervasive as those of the standard *Hipposaurus*. However, stresses in the braincase reach

approximately 1-3 MPa in the braincase, pineal foramen, and postorbital bar in the 1000 N head-and flank-butting protocols.

In the 3400 N head-butting protocol (Fig. 19G), the pineal foramen experiences stresses starting from 3 MPa, with a large region of stress over 6 MPa, and sections of the braincase experience stresses exceeding 6 MPa, peaking at 12.4340 MPa. The majority of the braincase experiences stresses in the 1-5 MPa range. Stresses in the postorbital bar peak at 7.92 MPa. In the 3400 N flank-butting protocol, stress distributions are slightly less severe, with smaller sections of the braincase and pineal foramen receiving stresses above 6 MPa. The stress in the postorbital bar peaks at around 7.30 MPa.

The enlarged *Hipposaurus* model only reaches failure according to the Mohr-Coulomb criterion, in the 3400 N flank-butting protocol, and in a small region of the squamosal (Fig. 15). In terms of stress distribution and force application point stresses, the enlarged *Hipposaurus* model can be said to outperform the standard *Stegoceras*, but it is not as successful as the enlarged *Stegoceras* model, nor that of *Estemmenosuchus*.

In the head-butting protocols for both *Hipposaurus* models, stress distributions are more symmetrical than in flank-butting protocols, and as such, stresses are similar at equidistant points from the sagittal plane. Stresses in the braincase peak in symmetrical regions on the ventral floor of the braincase. In flank-butting protocols, stress distributions are asymmetrical. Stresses in the braincase peak on the dorsal roof, and the left ventral floor. The left postorbital bar receives greater levels of stress than the right bar. The constraint artifacts from the ligament attachment points are more severe, and the constraint artifacts on the occipital condyle shifts to the right. It is difficult to distinguish whether flank-butting or head-butting impacts would be more detrimental.

***Stegoceras*:**

The *Stegoceras* skull model yields greater stresses in these analyses than in head-butting simulations of the *Stegoceras* model used by Snively and Theodor (2011), and different stress distribution patterns.

The closest analogue to the protocol applied by Snively and Theodor is the 1000 N head-butting protocol. In this protocol peak stress at the force application point is approximately

5.28 MPa, this dissipates to approximately 0.5-0.75 MPa in the region dorsal to the braincase. The stress within the braincase is mostly within the 1-5 MPa range, with some portions in the 5-6 MPa range. Stresses in the post-orbital bar are low, not exceeding 0.5 MPa. Meanwhile, in Snively and Theodor's (2011) 1360 N head-butting protocol, peak stress at the force application point reaches 40-50 MPa for concentrated impacts (though these are thought to have been caused by artificial singularities) with stresses descending to 1.5-2 MPa a short distance ventral from these points. Stresses dissipate to approximately 0.6 MPa ventral to the braincase, and they reach approximately 1.2 MPa within the braincase. The stresses within the postorbital bar are not directly stated, but from the figures provided they appear minimal. The skull of *Stegoceras* has no pineal foramen, which appears to be advantageous for the integrity of the skull during impacts.

In the 1000 N flank-butting protocol, stress levels are marginally higher. Peak force application point stress is 5.65 MPa, and larger portions of the braincase experience stresses within the 5-6 MPa range with stresses being greater on the side of the braincase opposite to the force application point. A small section of the post-orbital bar falls within the 0.5-1.0 MPa range, and 1-3 MPa stresses can be found in the postorbital bar.

In the 3400 N head-butting protocol, a peak force application point stress of 17.70 MPa is generated, 1-3 MPa stresses permeate to the dorsal margin of the braincase, and a major portion of the braincase exceeds 6 MPa. In the 3400 N flank-butting protocol, the peak force application point stress generated is 19.23 MPa, and stresses exceed 6 MPa dorsal to the braincase and in a major portion of the braincase. *Stegoceras* performs better in head-butting protocols than in flank-butting protocols.

Stegoceras does not yield safety factor values that are indicative of failure, yet it should be noted that the failure criteria used here show that it comes closest to failure in the 3400 N flank-butting protocol. These values are 2.6707 according to the Mohr-Coulomb criterion, and 2.6745 according to the von Mises criterion. These values occur at the constraints.

Enlarged *Stegoceras*:

As mentioned previously, the standard *Stegoceras* model is vastly outperformed by the dinocephalians by a significant margin (Figs. 14-17). To assess if this was due to the size

disparity, the *Stegoceras* model was enlarged. This enlarged model yields lower stress values than the normal *Stegoceras*. The dissipation pathways taken by stresses in the enlarged *Stegoceras* are similar to the life-sized model, but the stresses are reduced in intensity and extent (Figs. 18-21 (E, H)).

The force application point stresses are typically less than a quarter of those observed in the standard *Stegoceras* model. In the 1000 N head-butting protocol, the peak force application point stress is only 1.14 MPa and stresses dorsal to the braincase do not exceed 0.5 MPa, with a small portion of the braincase receiving stresses in the 0.5-0.75 MPa range (Fig. 18E). The majority of the elements in the model receives stresses below 0.5 MPa. In the 1000 N flank-butting protocol, force application point stress was 1.13 MPa, and stresses of 0.5-1 MPa reach the braincase, while the postorbital bar doesn't receive any stresses above 0.5 MPa.

In the 3400 N head-butting protocol, the force application point stress is 3.91 MPa, the braincase is covered in 1-3 MPa stresses, and the postorbital bar stresses do not exceed 0.5 MPa (Fig. 19E). In the 3400 N flank-butting protocol, the force application point stress is 3.63 MPa, the braincase is completely surrounded by 1-3 MPa stresses, with small patches of stress in the 3-5 MPa range, and a minor portion of the postorbital bar receives stresses in the 0.75-1 MPa range (Fig. 21E).

The 3400 N protocols of the enlarged *Stegoceras* model yield similar stress intensities and distributions to those seen in the 1000 N protocols for the standard *Stegoceras* model. In terms of overall performance, the enlarged *Stegoceras* model performs marginally better than *Estemmenosuchus*, but it fares worse than all of the other dinocephalians (Figs. 18-21 (E)). Much like the standard *Stegoceras* model, the enlarged *Stegoceras* model performs better in head-butting protocols than in flank-butting protocols.

The lowest safety factor value of the enlarged *Stegoceras* model is 0.8437 and occurs in the 3400 N flank-butting protocol according to the Mohr-Coulomb failure criterion (Fig. 15). This is approximately 3.98 times the safety factor value obtained from the standard *Stegoceras* model in the same conditions.

Struthiocephalus:

The *Struthiocephalus* skull model is the top performer in both 1000 N head-butting and flank-butting protocols, (see Appendix 1) yielding the lowest force application point equivalent stresses and the least pervasive distribution of stress.

In the 1000 N head-butting protocol, observed stresses are extremely minor, with the peak force application point stress being only 0.21 MPa (Fig. 18A). The model is devoid of any stresses over 0.5 MPa with the exception of small pockets of stress that reach the 1-3 MPa range in the areas surrounding the constraint artifact and the foramen magnum, and a pocket of 0.5-1 MPa in a region anterior to the olfactory bulb and ventral to the middorsal boss, at the most posterior point of the nasal vacuity (presumably where the frontal and septosphenoid would intersect) (Boonstra, 1968; Midzuk, 2020).

In the 1000 N flank-butting protocol (Fig. 20A), forces applied to the postorbital boss dissipate from 0.79 MPa at the force application point to below 0.5 MPa approximately 2 cm away along the stress distribution pathway. The rest of the model is devoid of stresses greater than 0.5 MPa with the exception of small constraint artifacts and minor sections around the foramen magnum, where stresses reach the 1-3 MPa range.

In the 3400 N head-butting protocol, peak stress at the force application point is approximately 0.70 MPa, which dissipates within the middorsal boss to around 0.5-0.75 MPa (Fig. 19A). Stresses reach 1-3 MPa in and anterior to the olfactory bulb and ventral portions of the braincase. No stresses beyond 0.5 MPa are observed in the postorbital bar, and the highest stresses are observed at the constraints, which yield a small region of ~6 MPa. In the 3400 N flank-butting protocol, peak stresses at the force application points reach 2.68 MPa, and then dissipate to below 0.5 MPa ~7 cm from there within the postorbital boss (Fig. 21A). Stresses are less pervasive around the braincase than the head-butting protocol of the same magnitude, with relatively small regions of 0.5-1 MPa appearing in ventral portions of the braincase.

The minimum safety factor value for *Struthiocephalus* is 15 in all protocols and failure criteria (Figs. 15,16), which suggests that the actual safety factor values may be higher than the software can account for, and this is indicative of negligible material failure.

In all protocols, the braincase of *Struthiocephalus* experiences the least stress of all skull models (Figs. 18-21). Factors that may assist with this excellent performance may include the greater reconstructed force application surface area, due to the flatter broad fronto-

nasal boss, the braincase and pineal canal being located further behind the straight-line path from the fighting surface to the occipital condyles, and the generally large skull volume (Fig. 18A). It should be noted that the angle of the fronto-nasal boss is such that for two *Struthiocephalus* skulls to collide at this location, they may have had to twist their skulls slightly in order to avoid impacting their snouts.

***Moschops*:**

The skull model of *Moschops* comes a close second in terms of overall performance compared to *Struthiocephalus*, as though stress levels are still relatively low throughout the skull, there is still a greater distribution of stress that occurs in the braincase than in *Struthiocephalus* (Figs. 18-21 (B)). This may be due to the braincase and parts of the pineal canal being in the middle of the pathway between the fighting surface and occipital condyle, as well as the reduced surface area of the reconstructed force application point.

In the 1000 N head-butting protocol (Fig. 18B), the peak force application point stress is 0.42 MPa, which descends below 0.5 MPa within 3 cm of propagation. Stresses do not exceed 0.5 MPa anywhere else in the model except at the constraint artifacts and at a minuscule point of 0.5-0.75 MPa within the braincase. In the 1000 N flank-butting protocol (Fig. 20B), the highest stress at the force application point is 1.74 MPa, and this dissipates to 0.5 MPa within 3 cm of propagation. Non-artifact Stresses do not exceed 0.5 MPa in any region other than a small segment of the posterior portion of the braincase which reaches 0.75-1.0 MPa, but this may also be due to constraint artifacts.

In the 3400 N head-butting protocol the peak force application stress is 3.22 MPa, while the braincase exhibits large regions of stress within 1-3 MPa, and a section of the pineal canal receives stresses of 0.5 to 0.75 MPa (Fig. 19B). The postorbital bar stresses do not exceed 0.5 MPa. In the 3400 N flank-butting protocol, peak application point stress is 5.92 MPa, and the stress radiates 11 cm towards the braincase before dissipating to 0.5 MPa. Stresses in the postorbital bar reach the 0.5-1 MPa range in small sections, but they are relatively low throughout. Stresses in the braincase reach 1-3 MPa in posterior regions, 0.5-0.75 MPa in ventral regions, and the anterior wall of the pineal tube receives 0.5-0.75 MPa stresses.

The minimum safety factor value for *Moschops* is 15 in all protocols and failure criteria (Figs. 14, 15), indicating minimal breakage, thus being equivalent to *Struthiocephalus* without access to higher safety factor values.

Compared to flank-butting protocols, the head-butting protocols for *Moschops* yield lower stresses about the force application point, but higher stresses surrounding the braincase (Figs. 18-21 (B)). It should be noted that the skull proportions of the *Moschops* model were based on SAM-PK-11582, and although this skull is relatively complete, it is not as large as other skulls of *Moschops* capensis, such AMNH FR5550 and KNPI, and as such, may still represent an earlier stage in an ontogenetic sequence (Neumann, 2019). It is likely that a model based on a more mature specimen with a thicker and larger skull may yield even better FEA performance.

Anteosaurus:

Though *Anteosaurus* receives higher levels of stress at the force application point in all protocols than *Jonkeria*, it appears in most cases that *Anteosaurus* experiences less stress surrounding the braincase, particularly in flank-butting (Figs. 18-21 (C, D)). This is likely in part due to the larger bosses, and more posteriorly positioned pineal canal and braincase.

In the 1000 N head-butting protocol (Fig. 18D), the peak force application point stress is 0.93 MPa, and this dissipates down to 3 MPa within 3 cm of propagation through the frontal boss. Non-constraint stresses do not exceed 0.5 MPa, except for a region of 0.5-1.0 MPa at an anterior portion of the braincase. In the 1000 N flank-butting protocol, stresses peak at the top of the postfrontal boss at 4.05 MPa and descend to 0.5 MPa within the boss. Much like the head-butting protocol, non-constraint stresses do not exceed 0.5 MPa except in an even smaller section at the anterior of the braincase, where stresses reach 0.5-0.75 MPa.

In the 3400 N head-butting protocol, force application point stress peaks at 3.19 MPa, and transmits almost all the way to the braincase before reducing to 0.5 MPa (Fig. 19D). Braincase stresses are highest at the anterior portion, within 3-5 MPa, while large portions of the braincase experience 1-3 MPa stresses, which permeate anteriorly a short distance into the pineal tube and reduce to 0.5-0.75 MPa just over halfway from the opening. The postorbital bar receives stresses within the 0.5-1 MPa range. In the 3400 N flank-butting

protocol (Fig. 21D), force application point stresses peak at 13.77 MPa and dissipate laterally and ventrally through the postfrontal horn to the quadrate where stresses reduce to 0.5-0.75 MPa. Stresses on the lateral walls of the braincase reach 1-3 MPa stresses in a smaller anterior portion of the braincase, and a larger dorsal region posterior to the pineal canal. A larger portion of the braincase does not exceed 0.5 MPa, while 0.5-1.0 MPa stresses permeate anteriorly further along the pineal tube. Stresses in the postorbital bar only reach 0.5-0.75 MPa.

The only protocol in which *Anteosaurus* shows safety factor values below 15 is the 3400 N flank-butting protocol. These values are 11.093 and 14.522 in the Mohr-Coulomb and von Mises failure criteria respectively (Figs. 15, 16). These values occur in small sections of the postfrontal horn where the flank-butting load was applied. Though these values are indicative of elevated stress levels, they are far from the values required for failure.

***Jonkeria*:**

The stress distribution observed in *Jonkeria* is slightly more extensive than in *Anteosaurus* or *Moschops*, but not as severe as what is observed in *Stegoceras* (Figs. 18-21). This may be due to the deceptively thick construction of the skull, particularly in terms of the structures surrounding the braincase and pineal canal (Fig. 18C). Unlike *Struthiocephalus*, *Moschops*, or *Anteosaurus* the pineal canal is not redirected from the possible fighting surface, and as such it experiences more stress there (Fig. 18 (A-D)). Stresses in *Jonkeria* are more pervasive in flank-butting protocols than in head-butting protocols (Figs. 18-21 (C)).

In the 1000 N head-butting protocol, the peak force application point stress is 0.63 MPa, and this dissipates to 0.5 MPa within 3 cm of propagation (Fig. 18C). Non-constraint stresses do not exceed 0.5 MPa elsewhere in the skull except for a small anterior portion of the braincase (0.5-1 MPa), and a dorsal portion of the pineal canal (0.5-0.75 MPa). In the 1000 N Flank-butting protocol (Fig. 20C), the peak force application point stress is 2.32 MPa, which dissipates to 0.5 MPa before reaching the braincase. Postorbital bar stresses peak at 1-3 MPa and 0.5-0.75 MPa stresses permeate through at least half of the dorsal surface of the bar. However, most of the stress transmits towards the braincase rather than through the post-orbital bar. 0.5-0.75 MPa stresses can be found on the dorsal and

ventral walls of the braincase, with small regions of 0.75-1.0 MPa, and 0.5-0.75 MPa stresses at the anterior region of the braincase. 0.5-0.75 MPa stresses are found in sporadic patches throughout the pineal canal.

In the 3400 N head-butting protocol (Fig. 19C), the peak force application point stress is 2.11 MPa and 1-3 MPa stresses penetrate into the anterior wall of the pineal canal. The majority of the braincase experiences 0.5-1.0 MPa stresses, with large sections in the braincase and pineal canal receiving 1-3 MPa stresses, such as the anterior portion of the braincase. Stresses in the postorbital bar are mostly in the 0-0.5 MPa range, with a small region yielding 0.54 MPa. In the 3400 N flank-butting protocol (Fig. 21C), force application point stress peak at 6.87 MPa, transmitting 1-3 MPa stresses through most of the post-orbital bar (with a small patch of 3-5 MPa) and to the borders of the braincase. 1-3 MPa stresses almost entirely surround the braincase and much of the bone dorsal to it and transmit all the way to the anterior opening of the pineal foramen.

Minimum safety factor values below the software's upper limit of 15 are only observed in 3400 N load magnitudes (Figs. 15, 16). In the 3400 N flank-butting protocol, the minimum safety factor values are 10.021 and 14.522 for the Mohr-Coulomb and von Mises failure criteria respectively at the constraints. In the 3400 N head-butting protocol, a minimum safety factor value of 13.369 is observed at the constraints in the Mohr-Coulomb failure criterion.

***Estemmenosuchus*:**

In the 1000 N head-butting protocol, the peak force application point stress in *Estemmenosuchus* is 1.24 MPa. 1-3 MPa stresses can be found in the pineal canal, braincase, postorbital bar, and the dorsal surface of the skull between the anterior boss and dorsal horns (Fig. 18F). Most of the stresses in the pineal canal do not exceed 0.5 MPa. In the 1000 N flank-butting protocol (Fig. 20F), the peak force application point stress is 1.00 MPa, but stresses exceed 6 MPa at the base of the lateral horn. 1-3 MPa stresses permeate through much of the lateral horn and postorbital bar, with a region of 3-5 MPa stresses being found at the dorsal contact of the lateral horn and the left postorbital bar. The dorsal horn receives much less stress, with stresses observed there being mostly in

the 0.5-1.0 MPa range, with patches of 1-3 MPa. A small region of 0.5-1.0 MPa stress is found in the braincase and extends dorsally into the pineal canal.

In the 3400 N head-butting protocol (Fig. 19F), the peak force application point stress is 4.18 MPa, while much of the dorsal surface of the skull, including the force application points, experience 1-3 MPa stresses. Most of the braincase and pineal canal is subject to stresses of 1-3 MPa, with smaller sections of the skull being subject to stresses in excess of 6 MPa. The postorbital bars are also mostly within the 1-3 MPA range, with regions of stress within the 3-5 MPa range and smaller sections being in excess of 6 MPa. In the 3400 N flank-butting protocol (Fig. 21F), force application point stress peaks at 3.94 MPa, but large regions of the lateral horn experience stresses greater than 6 MPa, particularly at the base of the horn on the dorsal and ventral portions, while 1-5 MPa stresses permeate throughout the lateral horn. The dorsal horn experiences less stress, peaking in the 5-6 MPa range but mostly falling within the 1-3 MPa range. The postorbital bar experiences a large region of stress over 6 MPa extending from the lateral horn and is mostly within the 1-5 MPa range. Stresses in the braincase and pineal tube range from 0.5 to 3.0 MPa, with small sections of the braincase receiving 3-5 MPa stresses.

Estemmenosuchus experiences the highest stress levels of the dinocephalian models, however, the stress distribution is not as pervasive as in *Stegoceras* (Figs. 18-21 (F, H)). The performance of *Estemmenosuchus* in flank butting was unique, owing to its distinctive anatomy. In flank-butting protocols (Figs. 20, 21 (F)), the stress at the force application points on the apices of the horns was relatively low, but the stress at the base of the lateral horn was considerably high, resulting from the increased leverage that this horn provides compared to other impact surfaces.

The lowest safety factor value observed in *Estemmenosuchus* is 4.1025. This value occurs in a region near the constraints in the 3400 N head-butting protocol according to the Mohr-Coulomb failure criterion (Fig. 15). For the same criterion, the minimum safety factor value of 6.7411 occurs at the base of the lateral horn. These values are indicative of elevated stresses, but not failure.

Palaeopathologies

Of the 202 skulls observed, six yielded definite external pathologies (Fig. 22 (A, C)). The skull of AM4950 had the only observed internal pathology. Although the number of specimens observed with palaeopathologies is seemingly low compared to the total number of specimens observed for this project (making up 3.47 % of the total), the reasons for this low rate of occurrence may be related to preservation rather than palaeobiology. The skulls on which pathologies are observed are typically some of the most complete and best-preserved specimens available, as it can be difficult to plausibly conclude that an abnormal structure represents a palaeopathology unless it and the surrounding bone structures are perfectly preserved, skilfully prepared, and relatively undeformed. Most dinocephalian cranial material, unfortunately, does not fulfil these requirements.

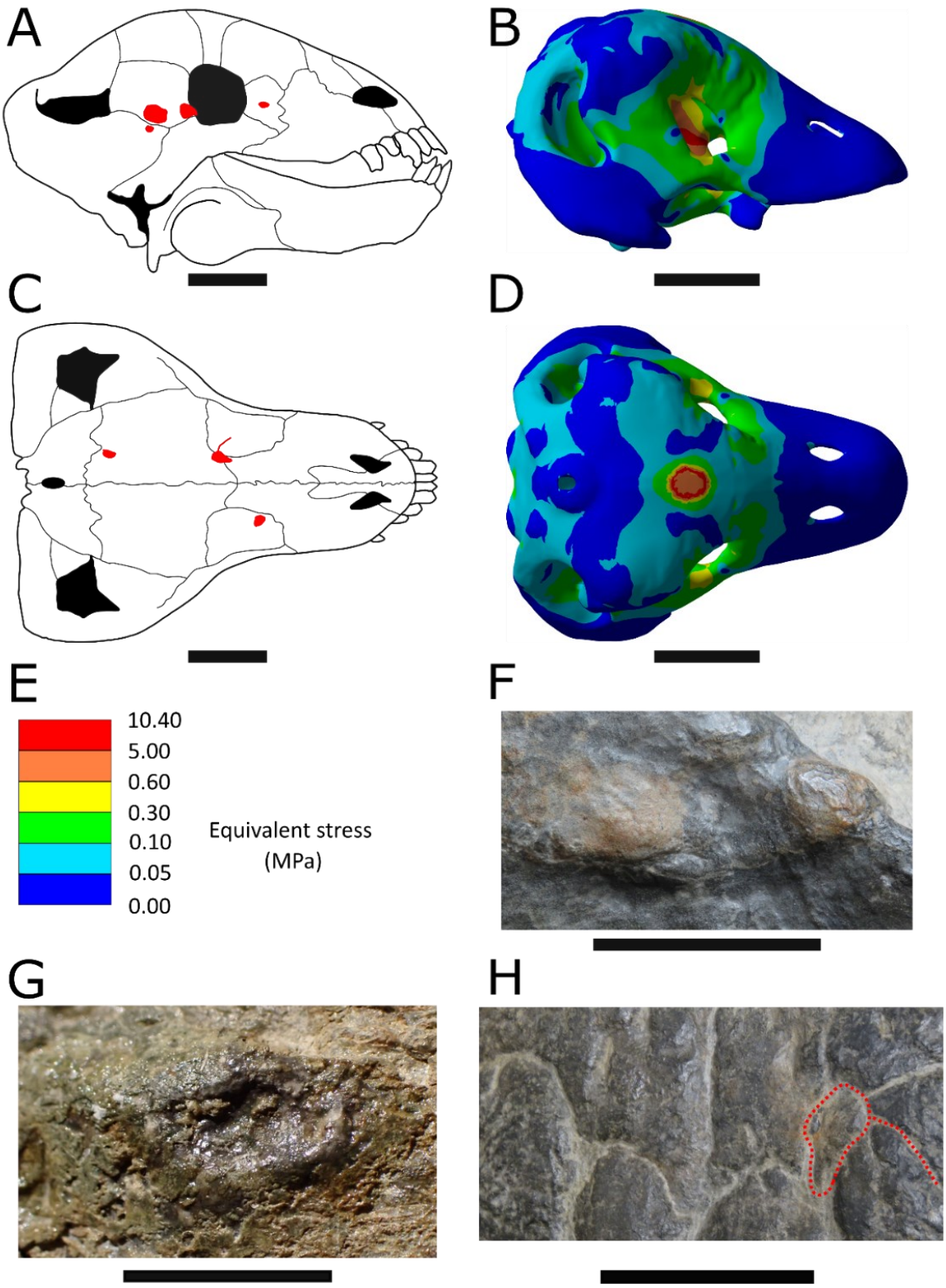

Figure 22: External cranial pathologies and their distributions (A and C adapted from illustrations by Anne Westoby (Rubidge and Day, 2020)).

(A&C) Lateral and Dorsal views respectively of external pathologies (red marks) mapped onto the skull of *Tapinocaninus pamelae*, scale bars = 10 cm (B&D) Lateral and dorsal views of *Moschops* model in the 3400 N head-butting protocol with equivalent stress legend altered to more accurately depict lower stress levels,

scale bars = 10 cm (E) Equivalent stress legend for B and C (F) Pathologies on the right postorbital bar of NMQR 2985, scale bar = 5 cm (G) Pathology on the left maxilla of SAM-PK-11582, scale bar = 1 cm (H) Pathology on dorsal surface of NMQR 2987, pathology shape and connected fracture indicated by red dashed line, scale bar = 5 cm.

More often than not, the bone surface is very eroded, making any conclusion on the nature of a possible pathology impossible or extremely speculative at best. Additionally, all the skulls identified to have palaeopathologies are either mostly or completely prepared, which is not the case for many skulls in collections. Therefore, the rate of pathologies in the Dinocephalia is very likely to be much higher than what the current study suggests. Pathologies are found in specimens of *Moschops capensis* (SAM-PK-11582), *Struthiocephalus whaitsi* (SAM-PK-11693, formerly *S. duplessi*), and four specimens of *Tapinocaninus pamelae* (BP/1/9331, NMQR 2985, NMQR 2987, and ROZ-K95). One internal pathology is found in the skull of *Moschognathus whaitsi* (AM4950). The distribution of these external pathologies can be seen in Fig. 22 A and C.

As shown in Figure 22, the skull anatomy of *Tapinocaninus pamelae* was chosen for the mapping of external pathologies as four of the six skulls with external pathologies were members of the genus *Tapinocaninus*, and therefore most of the pathologies could be accurately mapped. Additionally, *Tapinocaninus* has a similar skull morphology to *Moschops*.

The external pathologies found here have been identified as bony calluses, which form 2-9 weeks after injury in mammals, and are later remodelled (Lovell, 1997; Lingham-Soliar, 2004; Benoit *et al.*, 2021a). Some of these calluses have drainage canals, which would have been conduits for pus, and are signs of infection (Benoit *et al.*, 2021a). The presence of these calluses indicates that the specimens in question died at or around the 2-9 week timeframe after injury (Lovell, 1997; Lingham-Soliar, 2004; Benoit *et al.*, 2021a).

Specimen SAM-PK-11582 was described by Boonstra as *Moschops koupensis* (Boonstra, 1957), and was later identified as *Moschops capensis* (Kammerer, 2009; Neumann, 2019). The skull was found on the farm Die Krans in Prince Albert in the *Tapinocephalus* zone (Boonstra, 1957). An asymmetrical bony callus is located on the suture joining the lacrimal and the maxilla on the left side of the skull (Fig. 22G). This has a large central drainage channel and an additional smaller drainage channel located within the raised margin of the callused bone. The callus is darker in colour than the surrounding bone. The presence

of the callus and the raised margin indicates healing via bone growth, and thus precludes a post-mortem origin for the structure (Benoit *et al.*, 2021a). The infection, indicated by the drainage canals, was still ongoing at the death of the animal. The fact that the callus protrudes from a flat surface of surrounding bone that is well preserved and prepared also indicates that the structure is not derived from post-depositional changes or damage during preparation.

Specimen SAM-PK-11693, which has been tentatively identified as *Struthiocephalus whaitsi* (Kammerer, 2009; Neumann, 2019) has an asymmetrical callus (Fig. 13B) on the right dorsal surface of the skull, anterior to the orbit, and within the posterior region of the maxilla (Boonstra, 1952a). The callus is raised above the surface of the surrounding bone, indicating healing, and is approximately 1.8 cm wide at the rim. The lesion contains a large central drainage canal, and an additional canal approximately 1.4 mm in diameter on the raised margin, as well as a circular patch on the surface that is white and approximately 2.5mm wide. The slopes surrounding the callus are steep except on the left margin, where it tapers gradually down to the surface of the surrounding bone. The semi-rugose texture of the bone may indicate partial remodelling of the bone (Arbour *et al.*, 2022). The animal would have died before the bone could be fully consolidated and remodelled, but the infection that resulted in the drainage canals was still ongoing (Lovell, 1997; Benoit *et al.*, 2021a). The asymmetry of the callus, conspicuous elevation above the surrounding bone, and the absence of any similar structures on the right dorsal surface of the skull are all indicative of a pathological origin for the structure. The specimen was found on the farm Dikbome in the Laingsburg district (Boonstra, 1952b).

NMQR 2987 (holotype specimen for *Tapinocaninus pamelae*) was found alongside NMQR 2985 and 2986, in the same sandstone unit on the farm Modderdrift in Prince Albert. It exhibits a small pathology which resembles a bony callus on the left dorsal surface of the skull (Fig. 22H). It is located on an asymmetrical suture intersection between the prefontal, frontal, and nasal bones. The callus is slightly raised and rounded, is lighter in colour than the surrounding bone, rugose in texture and a small fracture extends anteriorly from the callus. The asymmetry that this structure creates in the well-preserved skull sutures, as well as the fracture that spreads from it supports its identification as a pathology.

NMQR 2985 (*Tapinocaninus pamelae*), as mentioned previously was found in close proximity to two other *Tapinocaninus* specimens, NMQR 2986 and NMQR 2987. The skull

exhibits pathologies in the form of two roughly circular raised and discoloured growths on the right postorbital bar (Fig. 22F). The growths are lighter in colour than the surrounding bones, and the largest one is 2.95 cm wide, while the other bump is 2.65 cm wide. Both growths are located on the post-orbital bar and contact the sutures to the jugal and the squamosal. The anterior bump protrudes far into the orbit, much more than any nearby structures do, and it has a spotty colouration with a foliated, rugose texture. The distinct colour disparity between these structures and the surrounding bone, their unusual heights, the deep intrusion of the one structure into the orbit, and distinct morphologies that are not replicated elsewhere in the skull are all indicative features of a pathological origin. These growths are identified as bony calluses, and as such, indicate that the specimen died 2-9 weeks after the injury was sustained (Lovell, 1997; Lingham-Soliar, 2004; Benoit *et al.*, 2021a).

BP/1/9331 (*Tapinocaninus pamelae*) exhibits a raised and rugose callus with a drainage canal. This is located at the posterior portion of the left frontal bone, near the suture with the parietal bone. The drainage canal and raised morphology act as evidence of infection (Benoit *et al.*, 2021a). This specimen was found in 2023 near the town of Prince Albert Road within the *Eodicynodon* assemblage zone (Rubidge and Day, 2020).

AM4950, which has been identified as *Moschognathus whaitsi* (Kammerer, 2009; Neumann, 2019), exhibits the only observed internal pathology (Fig. 23). It is located within the left frontal bone at the suture with the orbitosphenoid. This comes in the form of an asymmetrical cavity approximately 10.7 mm wide within the frontal bone with a closed rim. A mass of remodelled bone exists ventral to the cavity. Such a cavity is not typically found in the frontal bone. The asymmetry of the cavity suggests that it is pathological. The closed rim and remodelled bone ventral to the cavity indicate that the wound had healed at the time of death. The pathology also continues in the frontal sinus, and a pus canal is also visible that would have drained the pus into the orbit. The cavity and the remodelled bone are dorsal to the orbitosphenoid, and it is presumed that the pathology was caused by the orbitosphenoid penetrating the frontal bone during compression of the braincase (i.e. head butting). This skull was found on the farm Grant 39 in Makhanda (Grahamstown) (Neumann, 2019).

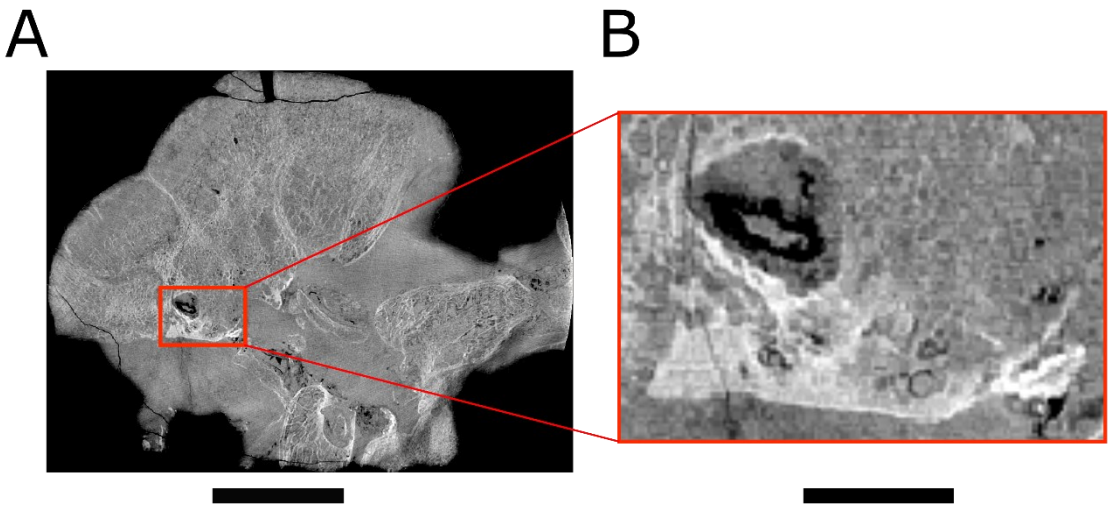

Figure 23: Internal pathology in the skull of *Moshognathus whaitsi* (AM4950).

(A) Skull scan with pathological bone in the red box, scale bar = 5 cm, (B) Pathological bone, scale bar = 1 cm.

General remarks on pathologies:

These pathologies are interpreted to have originated from head-butting impacts rather than predator bites. The pathologies are concentrated around the orbit and the braincase, whereas bites from predators would probably be concentrated around more fragile and easily accessible areas like the snout or lower jaw. The pathology on AM4950 is located internally and deep within a thick region of bone. This location is far out of the reach of predatory bites. The pathology is located at the suture between the orbitosphenoid and the frontal, suggesting that the orbitosphenoid punctured the frontal during a head-butting impact.

The observed pathologies are concentrated around the orbit and braincase, which are predicted to be higher stress areas in the FEAs, while no pathologies appear in low-stress regions such as the snout. Therefore, the predicted regions of high stress from the FEAs and the distributions of pathologies match. It appears that most of the observed pathologies occur relatively close to or at suture lines of the skull. It is possible that these sutures acted as planes of weakness. Noticeably, no definitive bite marks were found in dinocephalians with large canines, such as the anteosaurs and titanosuchids. No *Estemmenosuchus* specimens could be observed.

Discussion

FEA validation

The distribution of pathologies observed in dinocephalian skulls appears to validate the accuracy of the FEA methodology used here, as shown in Fig. 20. The pathologies are mainly found in regions surrounding the orbit and braincase, which are predicted to be high-stress regions in these analyses. Additionally, no pathologies have been found on the snouts of the observed skulls, which supports FEA results of the snout being a region of minimal stress. It appears that most of the observed pathologies occur relatively close to or at the suture lines of the skull. It is possible that these sutures acted as planes of weakness.

The prevalence of pathologies in the circumorbital region is consistent with results from the FEAs, which predict relatively high levels of stress to occur here. It is also possible that pathologies here could have been caused by impacts to the side of the skull from misaligned or chaotic fighting. The high levels of stress there may be attributed to the bone structures around the orbit representing a thinner conduit for forces to flow through compared to the thick dorsal skull shields.

No bite marks have been identified as of yet, and no pathologies of any kind are observed in dinocephalians with large canines such as *Jonkeria* and *Anteosaurus*.

When compared to the *Stegoceras* model used by Snively and Theodor (2011), the FEA of the *Stegoceras* skull model performed here produced greater stress levels and the reconstructed stresses formed different patterns of distribution. There are several methodological differences which may account for this. Firstly, the model has been smoothed to match the dinocephalian models. Secondly, for the sake of comparison with dinocephalians, the location of the force application point for the head-butting protocol was placed more anteriorly than the location chosen by Snively and Theodor (2011).

The force application point used in this study generates lower stress values and less extensive stress distributions than the one placed at a similar location as in Snively and Theodor's FEA. It may be a more optimal point for applying forces, and this may represent a more likely impact point in life. It should be noted that I tested the original placement of the force, and the more posterior force application point yields similar stress distribution patterns to those produced by Snively and Theodor (2011), but higher stress intensities.

Unlike in this study, Snively and Theodor (2011) applied constraints on the basal tubera of *Stegoceras*, which was found to cause stress artifacts in ventral portions of the skull, but these constraints had no effect on stresses within the dome. These constraints were not applied, as the dinocephalians being tested do not have basal tubera.

The skulls in this study are modelled isotropically out of dense, compact bone, while Snively and Theodor modelled different regions of varying bone types, such as cancellous bone, which may be able to absorb stress better.

Additionally, the model used by Snively and Theodor was slightly deformed and asymmetrical, while the model used in this research has been retrodeformed and made symmetrical. Snively and Theodor (2011) applied a load of 1360 N in their tests on *Stegoceras*, as this was one of the impact forces reconstructed by Snively and Cox (2008) for a comparably large pachycephalosaur, *Homolocephale colathoceros*, colliding at a velocity of 3 m/s. The lowest load magnitude applied in the current work was 1000 N, which represents a more conservative magnitude than the one applied by Snively and Theodor (2011).

Despite these differences, the fact that Theodor and Snively's results were reproduced while mimicking their protocol supports that the approach taken here is valid. In conclusion, the above suggests that my results can be considered a reliable enough reflection of the reality of dinocephalian head-butting biology.

FEA performances

The dinocephalian skulls outperformed the expectations set out at the start of this project as they almost all yielded lower equivalent stresses and less pervasive stress distributions in most protocols than the *Stegoceras* and *Hipposaurus* models (Fig. 14, Figs. 18-21). The tapinocephalid dinocephalians (*Moschops* and *Struthiocephalus*) outperformed the non-tapinocephalids (*Jonkeria*, *Anteosaurus*, *Estemmenosuchus*). Therefore, tapinocephalids were better adapted to head butting than their non-tapinocephalid counterparts, as predicted by Barghusen (1975).

Struthiocephalus performs remarkably well and even outperforms *Moschops*, which was initially thought to be the prime candidate for head-butting (Barghusen, 1975). This could be linked to the position of the braincase and pineal canal, which are even further

removed from the plane between the fighting surface and the occipital condyle (Fig. 18A).

Estemmenosuchus yields the weakest FEA performance of the dinocephalians but still outperforms the standard *Stegoceras* model and the enlarged and standard *Hipposaurus* models (Fig. 14). *Estemmenosuchus*, compared to the other dinocephalian models, displays high force application point stresses, relatively pervasive distributions of elevated stresses, and higher levels of stress surrounding the braincase and pineal canal (Figs. 18-21 F)

In head-butting protocols, the non-constraint regions with the highest stresses are the force application points, braincase, and postorbital bars (Figs. 18, 19 (F)) In flank-butting protocols, these regions are the left-postorbital bar, the dorsal surface of the left lateral horn, and the ventral base of the left lateral horn (Figs. 20, 21 (F)).

Stress levels and distributions reach relatively similar levels between head-butting and flank-butting protocols, but the distribution pathways are quite different. Stresses in the braincase and pineal canal are slightly higher and have more pervasive distributions in head-butting than in flank-butting (figs 18-21 (F)). Contrastingly, in flank-butting protocols, a large proportion of the left lateral horn receives elevated stress levels, and higher stresses are seen in a large portion of the left postorbital bar (Figs. 20-21 (F)). In head-butting protocols, the lowest safety factor value is located at the constraints (Figs. 18,19 (F), while in flank-butting protocols it is located at the base of the left lateral horn (Figs. 20, 21 (F).

The results seem to indicate that *Estemmenosuchus* would be marginally better suited to the forces involved in flank-butting than in head-butting, mainly by virtue of the stress levels in the braincase and pineal canal (Figs. 18-21F). Nonetheless, this claim may require further investigation, as due to a lack of information regarding the anatomy of the braincase and pineal canal of *Estemmenosuchus*, these structures were modelled after those of *Jonkeria*, and they may not accurately reconstruct the anatomy present in *Estemmenosuchus*.

Estemmenosuchus skulls of similar size vary in terms of skull ornamentation, coming in the form of tubercles in some specimens, and in the form of large branching horns in others (Ivakhnenko, 2008). It has been hypothesised that these differences represent

sexual dimorphism, with adult males having large horns, and that they played a role in sexual selection (Ivakhnenko, 2008). This suggests that *Estemmenosuchus'* horns were involved in sexual display or at least a low-energy form of cranial combat. Perhaps, this may be in the form of locking antlers and shoving, as seen in modern deer, or flank-butting like in giraffes (Vander Linden and Dumont, 2019; Wang *et al.*, 2022). The results here support that an even higher energy form of combat could have been practised. The potential presence of pathologies in *Estemmenosuchus* could not be investigated during this project. The FEA model predicts high-stress areas in locations such as the bases of the antler-like horns or on the postorbital bar. Pathologies found at or next to these areas may confirm the accuracy of the simulations. A search for pathologies that could have arisen from face-biting would also be required.

The slight disparity between the FEA results of tapinocephalid skull models and non-tapinocephalid skull models does not support Barghusen's (1975) theory that the non-tapinocephalids did not practice head-butting, or that they were restricted to low-energy forms of these behaviours, such as flank-butting.

It should be noted that although *Jonkeria* and *Anteosaurus* yield slightly higher stresses around the braincase, they both perform very well under the same FEA conditions as the tapinocephalids and *Stegoceras*. *Jonkeria* performs surprisingly well in these analyses (Fig. 14, Figs. 18-21 (C)) despite the lack of any obvious horns or bosses, and the only previously known adaptation for head-butting being the widened pineal canal.

The skull orientation of *Jonkeria* and *Anteosaurus* relative to their neck may make them less suitable for head-butting combat behaviour (Barghusen, 1975; Benoit *et al.*, 2021b). As such, though these analyses show that dinocephalian skulls performed comparatively well in FEAs, their performance and behaviour in life may have been limited by the articulation of their cervical vertebrae, which could lead to misalignment between the fighting surfaces, the occipital condyle, and the vertebral column. This could be addressed in the future by incorporating models of the neck vertebrae into FEA protocols, as has been done with *Discokeryx xiezhi* (Wang *et al.*, 2022).

Overall, though they are not as well adapted to head-butting, the skulls of *Anteosaurus* and *Jonkeria*, are capable of withstanding the forces involved. This may be due to the relatively massive size of their skulls (see discussion below on the effect of absolute cranial size).

In summary, all dinocephalians studied here seem to have skulls that would competently handle the forces involved in head- and flank-butting, but future research could more precisely investigate their relative FEA performance with the addition of cervical vertebrae and more accurate cranial anatomy.

Pachyostosis and biting force in *Anteosaurus*

The morphology of the postcanine teeth in anteosaurs is compared to the incrassate teeth of tyrannosaurs, which are theorised to have had a bone-crunching function (Hurum and Currie, 2000; Schubert and Ungar, 2005; Holtz, 2008; Kammerer, 2011). Therefore, bone-crunching may have been a critical capability for the diet of anteosaurs (Kammerer, 2011). Furthermore, the skull morphology of *Anteosaurus* is theorised to have acted as a stress sink for biting forces, with the post-orbital and post-temporal pachyostosis acting as muscle attachment sites for strengthened jaw musculature (Kammerer, 2011; Kruger *et al.*, 2018; Midzuk, 2020). This may very well have been the case, but the performance of *Anteosaurus* in these analyses and the large pachyostotic bosses suggests that the necessity to withstand impacts during combat may have been of equal or greater importance. The performance of these structures as a stress sink and the bite force capabilities of *Anteosaurus* will have to be tested with different FEA approaches.

Effect of absolute cranial size

Absolute skull size seems to be a very important factor according to the FEA results presented here. *Stegoceras* and *Hippposaurus* are nowhere within the size range of dinocephalians and are the least resistant to head and flank butting. For example, the skull volume of *Moschops* is 12.49 times that of *Stegoceras* and is 2.19 times longer.

Proportionally increasing the sizes of the skull models of *Hippposaurus* and *Stegoceras* led to greatly improved FEA performances, and greatly diminished stresses and stress distributions along the same pathways as the life-size models. Safety factor values are also higher in the enlarged models, and force application point stresses are lower (Figs. 14-16). For example, the enlarged *Stegoceras* has a volume 9.52 times that of the standard *Stegoceras*, which results in the peak force application point stress in the 3400N head-butting protocol being reduced to 22.1% of the value observed in the

standard model (Fig. 14; Appendix 1, 2). Similarly, the enlarged *Hipposaurus* has a skull volume 10.50 times that of the standard *Hipposaurus* model, and it yields a peak force application point stress which amounts to only 37.7% of the value observed in the standard model in the same protocol (Fig. 14; Appendix 1, 2).

It must be acknowledged that scaling up the *Hipposaurus* and *Stegoceras* skull models to the same length as that of *Moschops* may not have been an appropriate method for accounting for the effects of skull size. Instead, it may have been preferable to have scaled them up to the same volume as a dinocephalian skull model, for example, *Moschops*. The enlarged *Hipposaurus* model is still the third smallest model by volume (2.92 dm^3), and it is approximately 65.8 % the volume of the smallest dinocephalian model, which is *Estemmenosuchus* (4.51 dm^3) (Appendix 2). The enlarged *Stegoceras* model (4.89 dm^3) is slightly larger than the *Estemmenosuchus* model and has almost exactly the same volume as the *Jonkeria* model (4.90 dm^3) and is therefore within the size range of a dinocephalian skull (Appendix 2). The enlarged *Stegoceras* model is still only approximately 76.3 % the volume of the *Moschops* model (6.41 dm^3) and 30.6 % the volume of the *Struthiocephalus* model (15.97 dm^3) (Appendix 2). Therefore, the enlarged *Hipposaurus* model is a reasonably, though not perfectly appropriate control in terms of volume. Future FEA research will have to use standardised force to volume ratio for all the models, as suggested by previous authors (Dumont *et al.*, 2009).

None of the mature dinocephalian skulls observed in this study fall within the size range of the standard models of *Stegoceras* and *Hipposaurus*. In general, the smallest dinocephalian skulls discovered so far belong to early taxa with little pachyostosis and reduced or no bosses, such as *Sinophoneus* and *Australosyodon* (Kammerer, 2011; Neumann, 2019).

This suggests that large absolute skull size is a prerequisite for being engaged in head-butting. As stress is equal to force over area, smaller surface or cross-sectional areas will experience greater stresses for the same given force. As observed here, larger skulls typically have more robust constructions, to support the increased weight, in following with the square-cube law (Pratt, 2024). As such, these more robust morphologies provide larger cross-sectional areas for stresses to transmit through, leading to lower stress values.

Accordingly, a larger skull in dinocephalians seems to be an adaptation to head butting. Dinocephalians are noted for their disproportionately large skull size compared to body size, as is the case for *Jonkeria*, which is reconstructed with a skull length more than a sixth of its total body length (Broom, 1929).

Dinocephalians are not the only non-mammalian therapsids with large skulls and bodies, for example, the kannemeyeriiform and rhaciocephalid dicynodonts would later reach similar sizes to the dinocephalians (Kammerer, 2009). Further work needs to be done to see how their skull volume compares to their total body size, and to the ratios seen in dinocephalians. Furthermore, certain dicynodonts such as *Aulacephalodon* also have bosses. In the case of *Aulacephalodon*, much like *Estemmenosuchus*, it is theorised that these bosses are sexually dimorphic and that they may have been used by the males in intraspecific combat (Tollman *et al.*, 1980; Ivakhnenko, 2008). Kammerer (2011) also states that the carnivorous anteosaurs and herbivorous dinocephalians may have co-evolved their large body size in a predator-prey relationship.

Dinocephalians are also typically very large animals and are some of the largest terrestrial organisms from the Permian (Angielczyk and Kammerer, 2018). *Tapinocaninus* is a good example of this, as Romano and Rubidge (2021) reconstructed it to have had an average body mass of 892.63 Kg. Syodontines are an exception to this hypothesis as they are relatively small with minimal pachyostosis throughout their entire lineage (Kammerer, 2011). The absence of pachyostosis in syodontines would still be consistent with the hypothesis that an enlarged head is an adaptation to head butting.

Only the enlarged *Stegoceras* model manages to yield better FEA performance than a dinocephalian (*Estemmenosuchus*), and the braincase of the enlarged *Hipposaurus* model still undergoes a great deal of stress. So much stress close to vital organs such as the central nervous system presumably would have been lethal. This suggests that although increasing the size of a skull improves the ability to withstand impact stresses, adaptations of the geometry of the skull (e.g. position of the pineal organ, pachyostosis, structural layout) remain important.

It must be acknowledged that the same load magnitudes were applied to the models irrespective of size, which may not be appropriate for testing the suitability of skull shapes for head-butting, since impact forces of head-butting taxa can vary due to body mass and velocity (Snively and Theodor, 2011), but also because this does not control for the effects

of size on FEA Performance, which may be necessary so that the effect of shape can be properly investigated (Dumont *et al.*, 2009; Marcé-Nogué *et al.*, 2013). For example, Dumont *et al.* (2009) propose that in order to accurately evaluate solely the impact of the shape of a model on the strength of a structure, the effect of size must be controlled for by adjusting the force to keep the force to surface area ratio constant, or by resizing all models such that they all have the same surface area. Additionally, to compare the work efficiency of models without the effects of size, the force to volume ratio must remain constant, similarly, this can be done by adjusting the forces applied to maintain this ratio, or by applying the same forces and adjusting the volume (Dumont *et al.*, 2009). Another method exists which uses a series of formulas to determine what precise values of force should be applied across various two-dimensional models to account for differences in size in plane elasticity FEAs, namely the quasi-homothetic transformation, and it may be possible to adapt this methodology for use with three-dimensional models (Marcé-Nogué *et al.*, 2013).

In future research, more appropriately sized controls may need to be used. For example, *Pachycephalosaurus* could be used as a head-butting control (Snively and Cox, 2008), while large skulled therapsids such as *Cynognathus* (Hancox *et al.*, 2020) could be used as a non-head-butting control. Additionally, the ratio of force to surface area or volume could kept constant across all models to properly isolate and test the strength of skull structures without the effect of size (Dumont *et al.*, 2009; Marcé-Nogué *et al.*, 2013).

Implications for social behaviour

The overall performance of the dinocephalian skull models in these FEAs as well as the occurrence of cranial pathologies strongly suggests that at the very least some dinocephalians, mainly the tapinocephalids, were involved in head-butting behaviours, and therefore, represent extremely early examples of complex social behaviour in tetrapods. Evidence for social behaviour is reinforced by the tendency of dinocephalian remains to be found in close accumulations of multiple individuals (Benoit *et al.*, 2023).

The tapinocephalid dinocephalians performed excellently in these analyses. The fact that they did so is not surprising, considering the extreme levels of pachyostosis and highly reorientated braincase and pineal canal (Benoit *et al.*, 2017b). Nevertheless, what is

surprising here is the extent to which they outperformed the head-butting control of *Stegoceras*.

Though *Moschops* was not the top performer as predicted, the fact that it managed to come a close second to *Struthiocephalus* is noteworthy considering that the skull model used was just over half the length of the *Struthiocephalus* and *Anteosaurus* skull models. It is worth noting that the size of the skull model for *Moschops* was based on SAM-PK-11582. Neumann (2019) states that this skull is not the largest known *Moschops* skull, and as such, this may not represent a fully grown individual. FEA performance still supports an exceptionally resilient skull morphology despite this, but a skull model with the size and proportions of a more fully-grown *Moschops* may yield even better FEA performance.

There is very little doubt from these results that *Struthiocephalus* and *Moschops* could have used their skulls as weapons in intraspecific combat, presumably for head-butting. *Anteosaurus*, *Jonkeria*, and *Estemmenosuchus* may have also done so, but with varying and lesser magnitudes of forces involved in the impacts. In Figure 24, characters relevant to evidence for head-butting are mapped onto a simplified dinocephalian phylogeny.

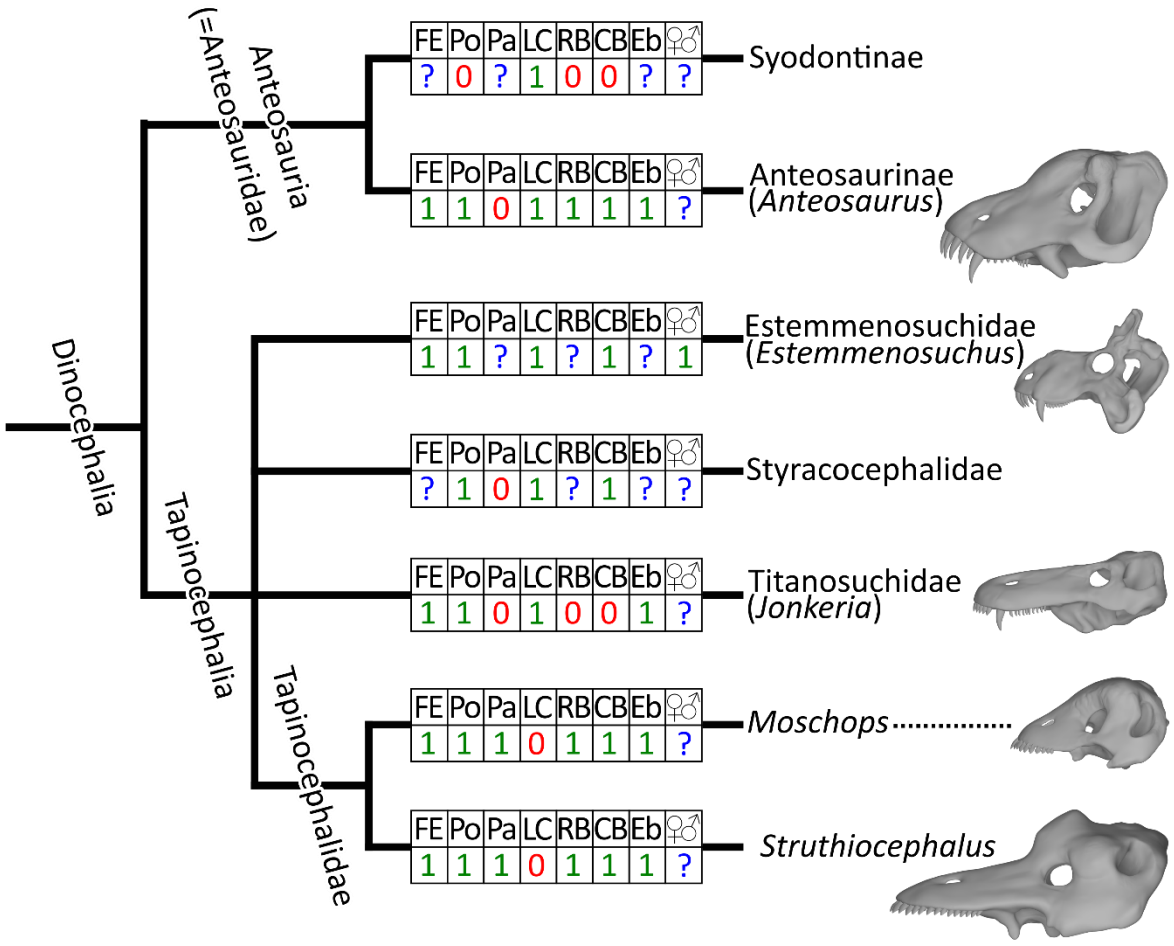

Figure 24*:* Observed evidence for head-butting mapped onto Benoit *et al.'s* (2021a) phylogeny.

FE = good FEA Performance, Po = pachyostosis, Pa = pathologies, LC = large canines, RB = reorientated braincase and pineal canal, Eb = enclosed braincase, ♀♂ = sexual dimorphism. 1 = Present, 0 = Absent, ? = indeterminate.

Tapinocaninus specimens yield the bulk of the external pathologies observed (Fig. 22; Appendix 5), potentially due to the excellent preservation of many of the skulls (Neumann, 2019). Pathologies were only found in tapinocephalids, with other examples being found in *Struthiocephalus whaitsi*, *Moschognathus whaitsi*, and *Moschops capensis*. Cranial pathologies are yet to be observed in *Jonkeria*, *Styracocephalus* or *Anteosaurus*. *Estemmenosuchus* skulls (along with other dinocephalians from Russia such as *Ulemosaurus* and various syodontines) were not accessed during this project.

Tapinocaninus also shares many of the adaptations for head-butting that *Struthiocephalus* and *Moschops* have. These include a dome-shaped skull, a considerable degree of pachyostosis, a wider pineal foramen (which suggests a wide pineal tube), and an

anteroventrally sloping occiput (Rubidge, 1991; Neumann, 2019). As *Tapinocaninus* is a basal tapinocephalid (Neumann, 2019), it may suggest that adaptations for head-butting are plesiomorphic traits for Tapinocephalidae. The dimensions of the braincase and pineal canal in *Tapinocaninus* are not as well-known as other dinocephalian genera and require further investigation.

Large canines are only absent in the tapinocephalid dinocephalians, although they are present yet reduced in basal taxa such as *Tapinocaninus* and *Ulemnosaurus* (Neumann, 2019). Tapinocephalids are otherwise more adapted for head-butting, which may show the decreasing importance of these canines in intraspecific combat. Furthermore, the tapinocephalids appear to be the most adapted for head-butting. The tapinocephalids are also the only dinocephalian clade in which cranial pathologies have been observed yet.

Reorientated braincases and pineal canals are observed in the tapinocephalids and in *Anteosaurus*, but not in *Jonkeria*, or the Syodontinae, and this data is unavailable for the estemmenosuchids and styracocephalids (Boonstra, 1968; Benoit *et al.*, 2021b). This, along with the orientation of the lateral semicircular canals was used to reconstruct the natural postures of the skulls of *Anteosaurus* and *Moschognathus*, with their snouts being angled ventrally at 25 degrees and 60-65 degrees respectively (Benoit *et al.*, 2017b, 2021b; Midzuk, 2020).

The reorientation of the braincase typical of tapinocephalids has also been observed in head-butting bovids (Schaffer and Reed, 1972) as well as pachycephalosaurid dinosaurs, (Bourke *et al.*, 2014; Benoit *et al.*, 2017b; Midzuk, 2020). The forward rotation of the occiput is observed in many dinocephalians, with the rotation being more extreme in the Tapinocephalia, particularly the tapinocephalids, whereas the occiput is vertical in *Anteosaurus*, *Syodon* and *Sinophoneus* (Fraser-King *et al.*, 2019; Benoit *et al.*, 2021b). These adaptations of the head and neck posture are most developed in the tapinocephalids, and would have decreased the risk of injuries from misalignment of the fighting surfaces to the neck (Barghusen, 1975; Midzuk, 2020; Benoit *et al.*, 2021b).

Enclosed (ossified) braincases are interpreted as useful adaptations for head-butting in the Tapinocephalidae (Benoit *et al.*, 2016, 2017b, 2021b). Boonstra's (1968) serial sectioning of an array of dinocephalians and CT scan studies of *Moschognathus* (Benoit *et al.*, 2016, 2017b, 2021b) revealed that the braincase walls consist of thick trabecular bone which entirely surrounds and supports the brain. Contrastingly, anteosaurids and titanosuchids

have braincases with relatively narrower bone layers which only partially surround the braincase ventrally and laterally, with some unossified cavities (Benoit *et al.*, 2016, 2017b).

Jonkeria represents an outlier in the Tapinocephalia, as it possesses fewer of the characters that are associated with head-butting (Barghusen, 1975), and has no observed cranial pathologies. It still performs well in head-butting analyses, perhaps because of its relatively large and robust skull. Face-biting cannot currently be ruled out as a possible behaviour in *Jonkeria* and *Anteosaurus*, as their conspicuously large canines make them seemingly well-suited for this (Barghusen, 1975; Benoit *et al.*, 2016, 2021b; Jirah, 2022).

Cranial bosses are present in all dinocephalians except the Titanosuchidae and Syodontinae. Compared to the Titanosuchidae, the Syodontinae possess fewer of the characters associated with head-butting, and with their smaller skull sizes and lack of pachyostosis, they are even less likely to have been involved in these behaviours (Kammerer, 2011).

The plausibility of head-butting in *Estemmenosuchus* is bolstered by evidence of sexual dimorphism (Ivakhnenko, 2008). Sexual dimorphism is offered as an explanation for why SAM-PK-11693 (formerly *Struthiocephalus duplessisi*) can be tentatively identified as *Struthiocephalus whaitsi*, even though it lacks the prominent horns and bosses of other members of the species (Kammerer, 2009; Neumann, 2019). Although, the presence of a distinct pathology on the skull of this specimen (Fig. 30) may be evidence that this individual represents an immature male, rather than an adult female.

Sexual dimorphism is proposed to account for morphological differences, particularly in terms of the extent of cranial pachyostosis between similarly sized individuals within the Anteosauridae, Tapinocephalidae, and the Titanosuchidae (Kammerer, 2011; Neumann, 2019; Jirah, 2022) but sample sizes are still too small to confirm sexual dimorphism in most dinocephalians (Kammerer, 2011; Neumann, 2019; Jirah, 2022). A more robust investigation with the aid of additional specimens from the same horizons and localities, and ontogenetic data will be required to outright prove the existence of cranial dimorphism in these clades, as has been done in dicynodonts e.g. *Diictodon* and *Aulacephalodon* (Tollman *et al.*, 1980; Sullivan *et al.*, 2003; Kammerer, 2011; Neumann, 2019; Jirah, 2022).

It is worth noting that the presence or absence of horns and bosses resulting from sexual dimorphism is not outright evidence for intraspecific combat, as shown by the African buffalo (Prins, 1996). Male African buffalo use their horns in combat, and the females still possess horns, though they do not grow as large as those of the males (Prins, 1996)

A parallel to the cranial weaponry of *Estemmenosuchus* can be drawn from muntjac deer (*Muntiacus muntjak*) (Barrette, 1977). Muntjacs have skulls with antlers and large canines, while *Estemmenosuchus* has antler-like horns and large canines (Barrette, 1977; Ivakhnenko, 2008). Muntjacs have been observed using both their canines and their antlers in intraspecific sparring and fighting (Barrette, 1977). This shows that possessing large canines does not invalidate the possibility of head-butting in a species, and that both canines and horns can be used intraspecific combat for a species (Barrette, 1977).

Furthermore, if *Estemmenosuchus* practised a combination of head-butting and face-biting during combat in a similar style to the muntjac, it might explain some of its cranial morphology. Theoretically, the lateral outgrowths of the dorsal horns may have aided in blocking a bite from above, acting like the cross-guard of a sword (Fig. 25), and the orientation of the dorsal horns may have been useful in catching an opponent's throat from such a downward blow (Barette, 1977). Additionally, the lateral horns of *Estemmenosuchus* may have also been used to defend against bites to the sides of the neck (Barette, 1977).

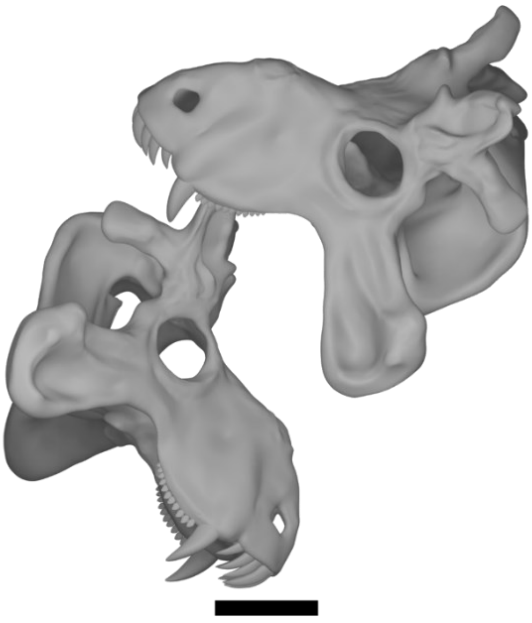

Figure 25*:* Hypothetical combat interaction between two *Estemmenosuchus.*

The figure depicts a possible interaction, where a male *Estemmenosuchus* is attempting a bite from above, while the male below attempts to block the bite with their horns. Drawn from observations of muntjac deer by Barrete (1977).

In this case, the cranial variation of the Tapinocephalia may also be explained by differences in combat styles. It should be noted that the tapinocephalids gain pachyostosis to the detriment of their biting force, further developing a trend of shifting the combat apparatus from the mouth to horns or bosses, as seen in cervids and giraffids (Geist, 1966; Cabrera and Stankowich, 2020; Benoit *et al.*, 2021b).

This is exemplified in the ontogenetic sequence of *Moschops capensis* (Neumann, 2019). The species shows thickening of the zygoma, postorbital bar, and intertemporal width with age, as well as a decrease in the size of the temporal fenestra and orbit, and an anteroventral shift of the occipital plate which moves the jaw joint forward (Neumann, 2019).

The ontogenetic sequences of anteosaurs such as *Sinophoneus yumenensis*, *Titanophoneus potens*, and *Anteosaurus magnificus* also show increased cranial pachyostosis within larger individuals, with *Anteosaurus magnificus* adults developing an enormous frontal bone that radically alters the dorsal profile of the skull (Orlov, 1958; Kammerer, 2011; Liu, 2013; Kruger *et al.*, 2018). The height and degree of pachyostosis of the pineal boss also increases with age in *Anteosaurus* (Kruger *et al.*, 2018).

The size of the temporal fenestrae in *Anteosaurus* and *Sinophoneus* increases with positive allometry compared to the size of the skull, and longer and laterally broader temporal fenestra are seen in adult *Titanophoneus* skulls (Orlov, 1958; Kammerer, 2011; Liu, 2013; Kruger *et al.*, 2018). The expansion of these fenestrae is presumably linked to the augmentation of the adductor mandibulae externus muscle in adults, indicating an increased importance of jaw strength (Barghusen, 1973, 1975; Liu, 2013; Kruger *et al.*, 2018). *Anteosaurus magnificus* in particular shows positive allometry of sub- and post-orbital bars, with a consequent decrease in the proportional size of the orbit in adults (Kruger *et al.*, 2018).

The skull anatomy of juvenile *Anteosaurus* is very similar to that of *Syodon* (Kruger *et al.*, 2018). The ontogenetic changes of the Anteosauria show the increased importance of cranial pachyostosis in derived genera. However, this was not to the detriment of their

biting force, as unlike *Moschops* and other tapinocephalids, the temporal fenestrae developed with positive allometry at the same time (Kruger *et al.*, 2018; Benoit *et al.*, 2021b).

From all of the above information, it appears that the primitive condition of the Dinocephalia was similar to that of the Syodontinae and basal anteosaurs, with very few adaptations for head-butting, large canines, and the possible employment of face-biting combat (Barghusen, 1975; Kammerer, 2011; Liu, 2013; Neumann, 2019; Benoit *et al.*, 2021b). It appears more parsimonious that the Anteosauria and Tapinocephalia convergently evolved head-butting behaviours, and that both clades presumably underwent transitional phases when moving from face-biting to head-butting, and in the case of the tapinocephalids, shifted fully towards head-butting (Geist, 1966; Cabrera and Stankowich, 2020; Benoit *et al.*, 2021b). In the aforementioned transitional phase, it is possible that both face-biting and head-butting were practised, particularly in genera such as *Estemmenosuchus*, *Anteosaurus, Styracocephalus*, and *Jonkeria* (Barrete, 1977). The prevalence of face-biting in the Dinocephalia is yet to be determined, particularly with respect to dinocephalians with both cranial adornments and large canines. Direct evidence of face-biting has so far been found in one gorgonopsian and a few specimens of therocephalians only (Benoit et al 2021; Benoit et al 2023).

Head-butting in the dinocephalians is indicative of derived behaviours such as dominance hierarchies and territoriality (Geist, 1966; Schaffer and Reed, 1972; Emlen, 2008; Cabrera and Stankowich, 2020; Benoit *et al.*, 2021b). Furthermore, it is a behaviour more typical of gregarious genera, suggesting that head-butting dinocephalians such as the tapinocephalids may have lived in herds or small groups, at least during the mating season (Geist, 1966; Schaffer and Reed, 1972; Emlen, 2008; Cabrera and Stankowich, 2020; Benoit *et al.*, 2021b). The occurrence of an internal pathology, plausibly originating from head-butting, in a specimen of *Moschognathus whaitsi* (AM4950) which may not be fully mature could indicate that the injury was caused during a play-fighting incident, and may serve as evidence of even more complex social behaviours, such as the signalling of intent for play, and the repeated practice of ritualised behaviour (Pellis and Pellis, 1998, 2017; Norton *et al.*, 2009; Benoit *et al.*, 2024).

Further support for this interpretation can be found in the relatively high encephalisation quotients of *Moschognathus* and *Struthiocephalus* compared to other more basal

therapsids, with these quotients being more typical of derived non-mammalian therapsids (Benoit *et al.*, 2017a; Midzuk, 2020).

Remarks on hypotheses

1) The hypothesis that FEA will enable biomechanical reconstructions is supported.

2) The hypothesis that the models will serve as a reasonable approximation for the behaviour of the skulls in life is supported. The distribution of palaeopathologies matches up with the FEA inferred distributions of stress.

3) The hypothesis that it is possible to use *Stegoceras* as an example of a head-butting tetrapod, and *Hipposaurus* as an example of a non-head-butting tetrapod, and that by comparing their FEA performance with those of the relevant dinocephalian cranial models, the relative fitness of these dinocephalians can be evaluated, is supported, but with some conditions. Though certainly *Hipposaurus* is unlikely to have been engaged in head-butting (Barghusen, 1975), *Stegoceras*, which was expected to be the best head-butting animal, proved to have a less efficient cranial geometry than the dinocephalians in that respect. This means that future work will have to find better comparison taxa. The scaling issue pointed out earlier, thought relevant here, is attenuated be the fact that the scaled up model of *Stegoceras* was comparable in volume to the dinocephalians but still performed worse than all dinocephalians except Estemmenosuchus.

4) The hypothesis that the tapinocephalid dinocephalian models will be better suited to withstand head-butting than the non-tapinocephalid models is partly verified. Though the tapinocephalid models were still the best performers, *Anteosaurus* and *Jonkeria* were found to be intermediately capable of head-butting, with *Anteosaurus* performing slightly better than *Jonkeria*. *Jonkeria* performed much better than expected despite lacking many obvious adaptations for head-butting. *Estemmenosuchus* had the poorest FEA performance of all the dinocephalian models instead of *Jonkeria*. All dinocephalian models still outperformed the low- and high-suitability controls of *Hipposaurus* and *Stegoceras* respectively. Although these controls were enlarged proportionally to the same length as that of the *Moschops* model, only the enlarged *Stegoceras* model managed to outperform *Estemmenosuchus*.

5) With regards to the hypothesis that tapinocephalid adaptations such as the reorientated braincase and pineal canal, conspicuous pachyostosis, and reoriented occiput will greatly benefit their performance in FEAs, this appears to have been the case. *Moschops* and *Struthiocephalus*, which are the tapinocephalid representatives were the best performing models in all load magnitudes and protocols. Furthermore, models which had less of these traits, or where these were less developed, such as the non-tapinocephalid dinocephalians (*Anteosaurus*, *Jonkeria*, *Estemmenosuchus*), tended to fare more poorly. In general, the more fully these traits were developed, the more successful the model was in the analyses.

Conclusion

In conclusion, FEA results and palaeopathology distribution indicate that most dinocephalian taxa were capable of head-butting and flank-butting combat, with tapinocephalids like *Struthiocephalus* and *Moschops* being the most capable, *Anteosaurus* and *Jonkeria* being intermediately capable, and *Estemmenosuchus* being the least capable. Observed palaeopathologies are identified to have originated from head-butting impacts, and their distributions validate the accuracy of predictions from FEAs. The tendency of dinocephalians to be preserved in small groups, their capability for head-butting, and pathologies derived from head-butting indicate that dinocephalians were social animals.

In future research, I intend to examine the cervical vertebrae of dinocephalians in search of pathologies and to determine possible fighting styles using the method set forward by Vander Linden and Dumont (2019). Additionally, I intend to perform scans of dinocephalian crania (and cervical vertebrae if possible). In doing so, I plan to reconstruct more accurate material properties through their opacity values in sections and reconstruct the differing densities of bone throughout the skull (Boonstra, 1968; Snively and Theodor, 2011). Furthermore, I intend to scan skulls with potential pathologies in order to more accurately identify them and their provenances. I also plan to observe dinocephalian specimens in collections outside of South Africa for pathologies.

Lastly, I intend to add articulated cervical vertebrae into the framework of these analyses in order to investigate the role played by the neck in dissipating impact forces, following the procedures applied to these skeletal elements in *Discokeryx* (Wang *et al.*, 2022).

Acknowledgements

I would like to thank Dr. Julien Benoit and Taahirah Mangera for supervising this project, Adam Midzuk for his skilful creation of models, the University of the Witwatersrand for its facilities, the various museums I visited for allowing me to access the collections, GENUS, and PAST for funding this project, and Tristen Lafferty for finding potentially the first observed internal cranial pathology in a dinocephalian.

References

Almond, J.E., 2022. Proposed Jessa M, Jessa S and Jessa Z wind energy facilities (WEFs) & associated infrastructure, Beaufort West Municipality, Western Cape Province. *SAHRA*, February 2022 (2): 1–96.

Angielczyk, K.D. and Kammerer, C.F., 2018. 5. Non-Mammalian synapsids: the deep roots of the mammalian family tree. *In*: *5. Non-Mammalian synapsids: the deep roots of the mammalian family tree*. De Gruyter, 117–198.

Arbour, V.M., Zanno, L.E., and Evans, D.C., 2022. Palaeopathological evidence for intraspecific combat in ankylosaurid dinosaurs. *Biology Letters*, 18 (12): 20220404. https://doi.org/10.1098/rsbl.2022.0404.

Barghusen, H.R., 1973. The Adductor Jaw Musculature of Dimetrodon (Reptilia, Pelycosauria). *Journal of Paleontology*, 47 (5): 823–834.

Barghusen, H.R., 1975. A review of fighting adaptations in dinocephalians (Reptilia, Therapsida). *Paleobiology*, 1 (3): 295–311. https://doi.org/10.1017/S0094837300002542.

Barrette, C., 1977. Fighting Behavior of Muntjac and the Evolution of Antlers. *Evolution*, 31 (1): 169–176. https://doi.org/10.2307/2407555.

Bell, P.R. and Currie, P.J., 2010. A tyrannosaur jaw bitten by a confamilial: scavenging or fatal agonism? *Lethaia*, 43 (2): 278–281. https://doi.org/10.1111/j.1502-3931.2009.00195.x.

Benoit, J., 2015. Objects: WB123 [online]. *SAHRIS*. Available from: https://sahris.sahra.org.za/objects/wb123 [Accessed 5 Dec 2023].

Benoit, J., Araujo, R., Lund, E.S., Bolton, A.D., Lafferty, T., Macungo, Z., and Fernandez, V., 2024. Early synapsids neurosensory diversity revealed by CT and synchrotron scanning. *The Anatomical Record*, https://doi.org/10.1002/ar.25445.

Benoit, J., Browning, C., and Norton, L.A., 2021a. The First Healed Bite Mark and Embedded Tooth in the Snout of a Middle Permian Gorgonopsian (Synapsida: Therapsida). *Frontiers in Ecology and Evolution*, 9:.

Benoit, J., Fernandez, V., Manger, P., and Rubidge, B., 2017a. Endocranial Casts of Pre-Mammalian Therapsids Reveal an Unexpected Neurological Diversity at the Deep Evolutionary Root of Mammals. *Brain Behavior and Evolution*, 90: https://doi.org/10.1159/000481525.

Benoit, J., Kruger, A., Jirah, S., Fernandez, V., Rubidge, B., Kruger, J., Jirah, A., and Fernandez, S., 2021b. Palaeoneurology and palaeobiology of the dinocephalian therapsid *Anteosaurus magnificus*. *Acta Palaeontologica Polonica*, 66: 2021. https://doi.org/10.4202/app.00800.2020.

Benoit, J., Manger, P.R., Fernandez, V., and Rubidge, B.S., 2016. Cranial Bosses of *Choerosaurus dejageri* (Therapsida, Therocephalia): Earliest Evidence of Cranial Display Structures in Eutheriodonts. *PLOS ONE*, 11 (8): e0161457. https://doi.org/10.1371/journal.pone.0161457.

Benoit, J., Manger, P.R., Norton, L., Fernandez, V., and Rubidge, B.S., 2017b. Synchrotron scanning reveals the palaeoneurology of the head-butting *Moschops capensis* (Therapsida, Dinocephalia). *PeerJ*, 5: e3496. https://doi.org/10.7717/peerj.3496.

Benoit, J., Norton, L.A., and Jirah, S., 2023. The maxillary canal of the titanosuchid *Jonkeria* (Synapsida, Dinocephalia). *The Science of Nature*, 110 (4): 27. https://doi.org/10.1007/s00114-023-01853-w.

Boonstra, L.D., 1936. Some Features of the Cranial Morphology of the Tapinocephalid Deinocephalians. *Bulletin of the American Museum of Natural History*, 72: 75–98.

Boonstra, L.D., 1952a. LVII.—On a new tapinocephalid deinocephalian. *Annals and Magazine of Natural History*, 5 (53): 509–511. https://doi.org/10.1080/00222935208654321.
Boonstra, L.D., 1952b. *Struthiocephaloides*: 'n nuwe genus van mormosauride tapinocephaliërs. *Tydskrif vir Wetenskap en Kuns*, 12: 237–241.
Boonstra, L.D., 1954. The Cranial Structure of the Titanosuchian: *Anteosaurus*. *Annals of the South African Museum*, 42: 108–148.
Boonstra, L.D., 1955. The girdles and limbs of the South African Deinocephalia. *Annals of the South African Museum. Annale van die Suid-Afrikaanse Museum*, 42: 185–326.
Boonstra, L.D., 1957. The Moschopid skulls in the South African Museum. *Annals of the South African Museum. Annale van die Suid-Afrikaanse Museum*, 44: 15–38.
Boonstra, L.D., 1962. The dentition of the titanosuchian dinocephalians. *Annals of the South African Museum. Annale van die Suid-Afrikaanse Museum*, 46: 57–112.
Boonstra, L.D., 1963. Diversity within the South African Dinocephalia. *South African Journal of Science*, 59 (5): 196–206. https://doi.org/10.10520/AJA00382353_2352.
Boonstra, L.D., 1968. The braincase, basicranial axis and median septum in the Dinocephalia. *Annals of the South African Museum*, v.50 (10): 195–273.
Boonstra, L.D., 1969. The fauna of the *Tapinocephalus* zone (Beaufort beds of the Karoo). *Annals of the South African Museum*, 56: 1–73.
Bourke, J.M., Ruger Porter, Wm., Ridgely, R.C., Lyson, T.R., Schachner, E.R., Bell, P.R., and Witmer, L.M., 2014. Breathing Life Into Dinosaurs: Tackling Challenges of Soft-Tissue Restoration and Nasal Airflow in Extinct Species. *The Anatomical Record*, 297 (11): 2148–2186. https://doi.org/10.1002/ar.23046.
Brink, A.S., 1958. *Struthiocephalus kitchingi* sp. nov. *Palaeontologia Africana*, 5: 39–56.
Broom, R., 1929. On the carnivorous mammal-like reptiles of the family Titanosuchidae. *Annals of the Transvaal Museum*, 13 (1): 9–36. https://doi.org/10.10520/AJA00411752_683.
Cabrera, D. and Stankowich, T., 2020. Stabbing Slinkers: Tusk Evolution Among Artiodactyls. *Journal of Mammalian Evolution*, 27 (2): 265–272. https://doi.org/10.1007/s10914-018-9453-x.
Chudinov, P.K., 1965. New Facts about the Fauna of the Upper Permian of the U.S.S.R. *The Journal of Geology*, 73 (1): 117–130.
D'Anastasio, R., Cilli, J., Bacchia, F., Fanti, F., Gobbo, G., and Capasso, L., 2022. Histological and chemical diagnosis of a combat lesion in *Triceratops*. *Scientific Reports*, 12 (1): 3941. https://doi.org/10.1038/s41598-022-08033-2.
Day, M.O. and Rubidge, B.S., 2020. Biostratigraphy of the *Tapinocephalus* Assemblage Zone (Beaufort Group, Karoo Supergroup), South Africa. *South African Journal of Geology*, 123 (2): 149–164. https://doi.org/10.25131/sajg.123.0012.
Dumont, E.R., Grosse, I.R., and Slater, G.J., 2009. Requirements for comparing the performance of finite element models of biological structures. *Journal of Theoretical Biology*, 256 (1): 96–103. https://doi.org/10.1016/j.jtbi.2008.08.017.
Emlen, D.J., 2008. The Evolution of Animal Weapons. *Annual Review of Ecology, Evolution, and Systematics*, 39 (1): 387–413. https://doi.org/10.1146/annurev.ecolsys.39.110707.173502.
Farke, A.A., 2004. Horn Use in *Triceratops* (Dinosauria: Ceratopsidae): Testing Behavioral Hypotheses Using Scale Models. *Palaeontologia Electronica*, 7 (1): 1–10.
Farke, A.A., 2008. Frontal sinuses and head-butting in goats: a finite element analysis. *Journal of Experimental Biology*, 211 (19): 3085–3094. https://doi.org/10.1242/jeb.019042.

Farke, A.A., 2010. Evolution and functional morphology of the frontal sinuses in Bovidae (Mammalia: Artiodactyla), and implications for the evolution of cranial pneumaticity. *Zoological Journal of the Linnean Society*, 159 (4): 988–1014. https://doi.org/10.1111/j.1096-3642.2009.00586.x.
Francis, L.F., 2016. Chapter 4 - Solid Processes. *In*: L.F. Francis, ed. *Materials Processing*. Boston: Academic Press, 251–342.
Fraser-King, S.W., Day, M.O., and Rubidge, B.S., 2019. Cranial morphology and phylogenetic relationship of the enigmatic dinocephalian Styracocephalus platyrhynchus from the Karoo Supergroup, South Africa. *Palaeontologia Africana*, 54: 14–29.
Gardiner, J., 2017. Finite Element Analysis Convergence and Mesh Independence. *XCEED Engineering*.
Geist, V., 1966. The Evolution of Horn-Like Organs. *Behaviour*, 27 (1–2): 175–214. https://doi.org/10.1163/156853966X00155.
Geist, V., 1971. An Ecological and Behavioural Explanation of Mammalian Characteristics, and their Implication to Therapsid Evolution. *Zeitschrift für Säugetierkunde : im Auftrage der Deutschen Gesellschaft für Säugetierkunde e.V*, 37: 1–15.
Gregory, W.K., 1926. The skeleton of *Moschops capensis* Broom, a dinocephalian reptile from the Permian of South Africa. Bulletin of the AMNH ; v. 56, article 3., 56: 179–251.
Hancox, P.J., Neveling, J., and Rubidge, B.S., 2020. Biostratigraphy of the Cynognathus Assemblage Zone (Beaufort Group, Karoo Supergroup), South Africa. *South African Journal of Geology*, 123 (2): 217–238. https://doi.org/10.25131/sajg.123.0016.
Haughton, S.H., 1929. On some New Therapsid Genera. *Annals of the South African Museum*, 28: 55–78.
Hill, R., 1950. *"The Mathematical Theory of Plasticity*. 1st ed. London: Oxford University Press.
Holtz, T., 2008. A critical reappraisal of the obligate scavenging hypothesis for Tyrannosaurus rex and other tyrant dinosaurs. *Tyrannosaurus rex the Tyrant King*, 371–396.
Hurum, J.H. and Currie, P.J., 2000. The Crushing Bite of Tyrannosaurids. *Journal of Vertebrate Paleontology*, 20 (3): 619–621.
Ivakhnenko, M.F., 2008. Cranial morphology and evolution of Permian Dinomorpha (Eotherapsida) of eastern Europe. *Paleontological Journal*, 42 (9): 859–995. https://doi.org/10.1134/S0031030108090013.
Janensch, W., 1959. Eine *Jonkeria* aus der Karru-Formation des Kaplandes. *Paläontologische Zeitschrift*, 33 (1): 22–49. https://doi.org/10.1007/BF02988978.
Jirah, S., 2022. Middle Permian diversity of large herbivores: taxonomic revision of the Titanosuchidae (therapsida, dinocephalia) of the Karoo basin, South Africa. University of the Witwatersrand, Johannesburg.
Kammerer, C.F., 2009. Cranial disparity in the non-mammalian synapsida. Ph.D. The University of Chicago, United States -- Illinois.
Kammerer, C.F., 2011. Systematics of the Anteosauria (Therapsida: Dinocephalia). *Journal of Systematic Palaeontology*, 9 (2): 261–304. https://doi.org/10.1080/14772019.2010.492645.
Kemp, T.S., 2005. *The Origin and Evolution of Mammals*. Oxford University Press.
Kosaraju, S., 2022. Brittle And Ductile Failure Theories In FEA - Which Ones Should We Choose? [online]. *Fidelis*. Available from: https://www.fidelisfea.com/post/brittle-and-ductile-failure-theories-in-fea-which-ones-should-we-choose [Accessed 16 Feb 2024].
Kruger, A., Rubidge, B.S., and Abdala, F., 2018. A juvenile specimen of *Anteosaurus magnificus* Watson, 1921 (Therapsida: Dinocephalia) from the South African Karoo, and

its implications for understanding dinocephalian ontogeny. *Journal of Systematic Palaeontology*, 16 (2): 139–158. https://doi.org/10.1080/14772019.2016.1276106.
Labuz, J.F. and Zang, A., 2012. Mohr–Coulomb Failure Criterion. *Rock Mechanics and Rock Engineering*, 45 (6): 975–979. https://doi.org/10.1007/s00603-012-0281-7.
Lautenschlager, S., Figueirido, B., Cashmore, D.D., Bendel, E.-M., and Stubbs, T.L., 2020. Morphological convergence obscures functional diversity in sabre-toothed carnivores. *Proceedings of the Royal Society B: Biological Sciences*, 287 (1935): 20201818. https://doi.org/10.1098/rspb.2020.1818.
Lingham-Soliar, T., 2004. Palaeopathology and injury in the extinct mosasaurs (Lepidosauromorpha, Squamata) and implications for modern reptiles. *Lethaia*, 37 (3): 255–262. https://doi.org/10.1080/00241160410006519.
Liu, J., 2013. Osteology, ontogeny, and phylogenetic position of *Sinophoneus yumenensis* (Therapsida, Dinocephalia) from the Middle Permian Dashankou Fauna of China. *Journal of Vertebrate Paleontology*, 33 (6): 1394–1407. https://doi.org/10.1080/02724634.2013.781505.
Lovell, N.C., 1997. Trauma analysis in paleopathology. *American Journal of Physical Anthropology*, 104 (S25): 139–170. https://doi.org/10.1002/(SICI)1096-8644(1997)25+<139::AID-AJPA6>3.0.CO;2-#.
Marcé-Nogué, J., DeMiguel, D., Fortuny, J., de Esteban-Trivigno, S., and Gil, L., 2013. Quasi-homothetic transformation for comparing the mechanical performance of planar models in biological research. *Palaeontologia Electronica*, 16 (3): 1–15. https://doi.org/10.26879/365.
Maria, R., 2016. *Summary of Safety Criteria in Design*.
Midzuk, A.J., 2020. The 3D Reconstruction of the Skulls of some Dinocephalia (Therapsida) for usage in Finite Element Study. Honours Research Project. University of the Witwatersrand.
Neumann, S., 2019. Taxonomic revision of the short-snouted tapinocephalid dinocephalia (Amniota-Therapsida): the key to understanding middle Permian Tetrapod biodiversity. University of the Witwatersrand.
Neumann, S., Rubidge, B., and Abdala, F., 2009. Taxonomic re-evaluation of tapinocephalid dinocephalians. *Palaeontologia Africana*, 44: 83–87. https://doi.org/10.13140/RG.2.1.3932.6482.
Norton, L.A., Tafforeau, P., Rubidge, B.S., and De Klerk, W.J., 2009. Use of synchrotron microtomography to examine tooth replacement patterns in a tapinocephalid dinocephalian. *Journal of Vertebrate Paleontology*, 29: 156A.
Orlov, J.A., 1958. Predatory Dinocephalians from the Isheevo Fauna (Titanosuchians). *Trudy Paleontologicheskogo Instituta Akademiya Nauk SSSR*, 72: 1–114.
Pellis, S.M. and Pellis, V.C., 1998. Structure-function interface in the analysis of play fighting. *In*: J.A. Byers and M. Bekoff, eds. *Animal Play: Evolutionary, Comparative and Ecological Perspectives*. Cambridge: Cambridge University Press, 115–140.
Pellis, S.M. and Pellis, V.C., 2017. What is play fighting and what is it good for? *Learning & Behavior*, 45 (4): 355–366. https://doi.org/10.3758/s13420-017-0264-3.
Peterson, J.E., Dischler, C., and Longrich, N.R., 2013. Distributions of Cranial Pathologies Provide Evidence for Head-Butting in Dome-Headed Dinosaurs (Pachycephalosauridae). *PLOS ONE*, 8 (7): e68620. https://doi.org/10.1371/journal.pone.0068620.
Peterson, J.E. and Vittore, C.P., 2012. Cranial Pathologies in a Specimen of *Pachycephalosaurus*. *PLOS ONE*, 7 (4): e36227. https://doi.org/10.1371/journal.pone.0036227.

Pratt, F., 2024. The Square Cube Law [online]. *Mathematical Fiction*. Available from: https://kasmana.people.cofc.edu/MATHFICT/mfview.php?callnumber=mf1401 [Accessed 8 Jan 2024].
Prins, H.H.T., 1996. *Ecology and Behaviour of the African Buffalo*. Dordrecht: Springer Netherlands.
Rayfield, E.J., 2007. Finite Element Analysis and Understanding the Biomechanics and Evolution of Living and Fossil Organisms. *Annual Review of Earth and Planetary Sciences*, 35 (1): 541–576. https://doi.org/10.1146/annurev.earth.35.031306.140104.
Romano, M. and Rubidge, B.S., 2021. First 3D reconstruction and volumetric body mass estimate of the tapinocephalid dinocephalian *Tapinocaninus pamelae* (Synapsida: Therapsida). *Historical Biology*, 33 (4): 498–505. https://doi.org/10.1080/08912963.2019.1640219.
Rubidge, B.S., 1991. A new primitive dinocephalian mammal-like reptile from the Permian of southern Africa. *Palaeontology*, 34 (3): 547–559.
Rubidge, B.S. and Day, M.O., 2020. Biostratigraphy of the Eodicynodon Assemblage Zone (Beaufort Group, Karoo Supergroup), South Africa. *South African Journal of Geology*, 123 (2): 141–148. https://doi.org/10.25131/sajg.123.0010.
Rubidge, B.S., Govender, R., and Romano, M., 2019. The postcranial skeleton of the basal tapinocephalid dinocephalian Tapinocaninus pamelae (Synapsida: Therapsida) from the South African Karoo Supergroup. *Journal of Systematic Palaeontology*, 17 (20): 1767–1789. https://doi.org/10.1080/14772019.2018.1559244.
Rubidge, B.S. and Sidor, C.A., 2001. Evolutionary Patterns Among Permo-Triassic Therapsids. *Annual Review of Ecology and Systematics*, 32 (1): 449–480. https://doi.org/10.1146/annurev.ecolsys.32.081501.114113.
Schaffer, W.M. and Reed, C.A., 1972. The co-evolution of social behavior and cranial morphology in sheep and goats (Bovidae, caprini). *Fieldiana Zoology*, 61 (1): 1–88.
Schubert, B.W. and Ungar, P.S., 2005. Wear facets and enamel spalling in tyrannosaurid dinosaurs. *Acta Palaeontologica Polonica*, 93–99.
Shelton, C.D., Chinsamy, A., and Rothschild, B.M., 2019. Osteomyelitis in a 265-million-year-old titanosuchid (Dinocephalia, Therapsida). *Historical Biology*, 31 (8): 1093–1096. https://doi.org/10.1080/08912963.2017.1419348.
Sigogneau-Russel, D., 1989. Theriodonta I. *Handbuch der Paläoherpetologie, Teil 17B/1*, 20–21.
Snively, E. and Cox, A., 2008. Structural Mechanics of Pachycephalosaur Crania Permitted Head-Butting Behavior. *Palaeontologia Electronica*, 11 (1): 1–17.
Snively, E. and Theodor, J.M., 2011. Common Functional Correlates of Head-Strike Behavior in the Pachycephalosaur *Stegoceras validum* (Ornithischia, Dinosauria) and Combative Artiodactyls. *PLOS ONE*, 6 (6): e21422. https://doi.org/10.1371/journal.pone.0021422.
Sullivan, C., Reisz, R.R., and Smith, R.M.H., 2003. The Permian Mammal-like Herbivore *Diictodon*, the Oldest Known Example of Sexually Dimorphic Armament. *Proceedings: Biological Sciences*, 270 (1511): 173–178.
Tanglao, R., 2012. *Estemmenosuchus* Tyrrell [online]. *Wikimedia Commons*. Available from: https://en.m.wikipedia.org/wiki/File:Estemmenosuchus_Tyrrell.jpg.
Tollman, S.M., Grine, F.E., and Hahn, B.D., 1980. Ontogeny and sexual dimorphism in Aulacephalodon (Reptilia, Anomodontia). *Annals of the South African Museum. Annale van die Suid-Afrikaanse Museum*, 81: 159–186.
Vander Linden, A. and Dumont, E.R., 2019. Intraspecific male combat behaviour predicts morphology of cervical vertebrae in ruminant mammals. *Proceedings of the Royal*

Society B: Biological Sciences, 286 (1915): 20192199. https://doi.org/10.1098/rspb.2019.2199.
Wang, S.-Q., Ye, J., Meng, J., Li, C., Costeur, L., Mennecart, B., Zhang, C., Zhang, J., Aiglstorfer, M., Wang, Y., Wu, Y., Wu, W.-Y., and Deng, T., 2022. Sexual selection promotes giraffoid head-neck evolution and ecological adaptation. *Science*, 376 (6597): eabl8316. https://doi.org/10.1126/science.abl8316.
Witmer, L.M., Bourke, J., Porter, R., Nassif, J., and Ridgely, R., 2018. The Visible Interactive Pachycephalosaur – part of the Visible Interactive Anatomy series at WitmerLab at Ohio University [online]. *Morphosource*. Available from: https://www.morphosource.org/projects/00000C286?locale=en.

Appendix 1:

Table of force application point stresses (MPa) in tested skull models

Model	Protocol			
	1000 N Head-butting	3400 N Head-butting	1000 N Flank-butting	3400 N Flank-butting
Struthiocephalus	0.21397	0.70437	0.7867	2.6767
Moschops	0.42702	3.2200	1.7423	5.9237
Jonkeria	0.62858	2.1144	2.3277	6.8676
Anteosaurus	0.93849	3.1911	4.0507	13.7720
Enlarged *Stegoceras*	1.1400	3.9120	1.1325	3.6304
Estemmenosuchus	1.2374	4.1801	0.99904	3.9408
Enlarged *Hipposaurus*	1.5097	12.4340	2.9940	11.9230
Stegoceras	5.2826	17.7030	5.6555	19.2290
Hipposaurus	6.2481	32.9450	15.1450	53.2750

Appendix 2:

Table of volume (dm^3) and reconstructed skull mass (kg) in tested skull models

Model	Volume (dm^3)	Reconstructed Skull mass (kg)
Struthiocephalus	15.96705	31.93409
Moschops	6.409779	12.81956
Jonkeria	4.903708	9.807416
Anteosaurus	10.6713	21.3426
Enlarged *Stegoceras*	4.889623	9.779247
Estemmenosuchus	4.512674	9.025348
Enlarged *Hipposaurus*	2.922265	5.84453
Stegoceras	0.513178	1.026355
Hipposaurus	0.278219	0.556439

Appendix 3:

Table of minimum safety factor values obtained from tested skull models through the Mohr-Coulomb failure criterion

Model	Protocol			
	1000 N Head-butting	3400 N Head-butting	1000 N Flank-butting	3400 N Flank-butting
Struthiocephalus	15	15	15	15
Moschops	15	15	15	15
Jonkeria	15	13.369	15	10.021
Anteosaurus	15	15	15	11.093
Enlarged *Stegoceras*	15	15	15	10.623
Estemmenosuchus	13.948	4.1025	15	6.7411
Enlarged *Hipposaurus*	12.054	3.5452	2.8684	0.84365
Stegoceras	13.823	4.0657	9.0805	2.6707
Hipposaurus	2.501	0.7356	1.1065	0.3254

Appendix 4:

Table of minimum safety factor values obtained from tested skull models through the maximum equivalent stress failure criterion

Model	Protocol			
	1000 N Head-butting	3400 N Head-butting	1000 N Flank-butting	3400 N Flank-butting
Struthiocephalus	15	15	15	15
Moschops	15	15	15	15
Jonkeria	15	15	15	14.34
Anteosaurus	15	15	15	14.522
Enlarged *Stegoceras*	15	15	15	14.311
Estemmenosuchus	15	6.8632	15	7.6948
Enlarged *Hipposaurus*	15	5.6516	5.6516	1.6622
Stegoceras	14.934	4.3922	10.663	2.6745
Hipposaurus	4.8468	1.4255	2.1054	0.61294

Appendix 5:

List of dinocephalian specimens observed in this study

Specimen number	Collection	Identification	Pathology present (Y/N)
AM4950	Albany Museum	*Moschognathus whaitsi*	Y
BP/1/9331	Evolutionary Studies Institute	*Tapinocaninus pamelae*	Y
NMQR 2985	National Museum, Bloemfontein	*Tapinocaninus pamelae*	Y
NMQR 2987	National Museum, Bloemfontein	*Tapinocaninus pamelae*	Y
ROZ-K95	Iziko South African Museum	*Tapinocaninus pamelae*	Y
SAM-PK-011582	Iziko South African Museum	*Moschops capensis*	Y
SAM-PK-011693	Iziko South African Museum	*Struthiocephalus whaitsi*	Y
BP/1/1041	Evolutionary Studies Institute	Titanosuchidae indet.	N
BP/1/1263	Evolutionary Studies Institute	Indet. Dinocephalian	N
BP/1/1369	Evolutionary Studies Institute	*Anteosaurus abeli*	N
BP/1/1370	Evolutionary Studies Institute	*Anteosaurus* sp.	N
BP/1/1575	Evolutionary Studies Institute	*Struthiocephalus kitchingi* (sp. nov.)	N
BP/1/1576	Evolutionary Studies Institute	cf. *Criocephalosaurus*	N
BP/1/1579	Evolutionary Studies Institute	cf. Titanosuchidae	N
BP/1/1581	Evolutionary Studies Institute	*Mormosaurus* or *Struthiocephalus*	N
BP/1/1582	Evolutionary Studies Institute	*Criocephalosaurus* sp.	N
BP/1/4849	Evolutionary Studies Institute	Titanosuchid indet	N
BP/1/4851	Evolutionary Studies Institute	cf. *Anteosaurus*	N
BP/1/4856	Evolutionary Studies Institute	Indet. Dinocephalian	N
BP/1/4858	Evolutionary Studies Institute	cf. *Anteosaurus*	N
BP/1/5386	Evolutionary Studies Institute	Indet. Dinocephalian	N
BP/1/5390	Evolutionary Studies Institute	Indet. Dinocephalian	N

BP/1/5393	Evolutionary Studies Institute	cf. *Titanosuchus*	N
BP/1/5409	Evolutionary Studies Institute	Titanosuchidae indet.	N
BP/1/5416	Evolutionary Studies Institute	Indet. Tapinocephalid	N
BP/1/5417	Evolutionary Studies Institute	Indet. Dinocephalian	N
BP/1/5428	Evolutionary Studies Institute	*Styracocephalus*	N
BP/1/5431	Evolutionary Studies Institute	Indet. Dinocephalian	N
BP/1/5432	Evolutionary Studies Institute	Indet. Dinocephalian	N
BP/1/5433	Evolutionary Studies Institute	*Styracocephalus*	N
BP/1/5445	Evolutionary Studies Institute	*Criocephalosaurus*	N
BP/1/5487	Evolutionary Studies Institute	Indet. Tapinocephalid	N
BP/1/5488	Evolutionary Studies Institute	Indet. Dinocephalian	N
BP/1/5495	Evolutionary Studies Institute	Indet. Dinocephalian	N
BP/1/5595	Evolutionary Studies Institute	Indet. Dinocephalian	N
BP/1/5636	Evolutionary Studies Institute	Indet. Dinocephalian	N
BP/1/5637	Evolutionary Studies Institute	Tapinocephalid indet.	N
BP/1/5638	Evolutionary Studies Institute	Tapinocephalid	N
BP/1/5693	Evolutionary Studies Institute	Tapinocephalid	N
BP/1/5694	Evolutionary Studies Institute	Indet. Dinocephalian	N
BP/1/5696	Evolutionary Studies Institute	Tapinocephalidae	N
BP/1/5709	Evolutionary Studies Institute	Indet. Dinocephalian	N
BP/1/5712	Evolutionary Studies Institute	Tapinocephalidae	N
BP/1/6672	Evolutionary Studies Institute	Dinocephalia, Tapinocephalidae	N
BP/1/6854	Evolutionary Studies Institute	Titanosuchid indet.	N
BP/1/6855	Evolutionary Studies Institute	Tentative dinocephalian	N

BP/1/6856	Evolutionary Studies Institute	*Mormosaurus*	N
BP/1/6858	Evolutionary Studies Institute	*Struthiocephalus*	N
BP/1/6859	Evolutionary Studies Institute	cf. *Jonkeria*	N
BP/1/6860	Evolutionary Studies Institute	Titanosuchid indet.	N
BP/1/6867	Evolutionary Studies Institute	Tapinocephalid indet.	N
BP/1/6873	Evolutionary Studies Institute	Dinocephalian?	N
BP/1/6882	Evolutionary Studies Institute	Tapinocephalid	N
BP/1/6883	Evolutionary Studies Institute	Tapinocephalid (cf. *Styracocephalus*)	N
BP/1/6884	Evolutionary Studies Institute	Titanosuchid indet.	N
BP/1/6985	Evolutionary Studies Institute	*Anteosaurus*	N
BP/1/6986	Evolutionary Studies Institute	*Moschops*	N
BP/1/6993	Evolutionary Studies Institute	*Moschops*	N
BP/1/6995	Evolutionary Studies Institute	cf. *Anteosaurus*	N
BP/1/6999	Evolutionary Studies Institute	Anteosauridae or Titanosuchidae	N
BP/1/7002	Evolutionary Studies Institute	Tapinocephalid indet	N
BP/1/7004	Evolutionary Studies Institute	Tapinocephalid indet.	N
BP/1/7023	Evolutionary Studies Institute	Tapinocephalid indet	N
BP/1/7033	Evolutionary Studies Institute	*Anteosaurus* sp.	N
BP/1/7061	Evolutionary Studies Institute	Anteosauridae	N
BP/1/7071	Evolutionary Studies Institute	cf. Mormosaurus	N
BP/1/7072	Evolutionary Studies Institute	Dinocephalia indet	N
BP/1/7074	Evolutionary Studies Institute	*Anteosaurus*	N
BP/1/7075	Evolutionary Studies Institute	Tapinocephalid indet	N
BP/1/7081	Evolutionary Studies Institute	Dinocephalia indet	N

BP/1/7085	Evolutionary Studies Institute	cf. Anteosauridae	N
BP/1/7094	Evolutionary Studies Institute	Dinocephalia indet.	N
BP/1/7139	Evolutionary Studies Institute	*Styracocephalus*	N
BP/1/7140	Evolutionary Studies Institute	Tapinocephalidae c.f *Moschops*/*Delphinognathus*	N
BP/1/7141	Evolutionary Studies Institute	*Styracocephalus*	N
BP/1/7142	Evolutionary Studies Institute	*Struthiocephalus*?	N
BP/1/7168	Evolutionary Studies Institute	Titanosuchid indet	N
BP/1/7173	Evolutionary Studies Institute	Dinocephalia	N
BP/1/7174	Evolutionary Studies Institute	*Moschops*	N
BP/1/7183	Evolutionary Studies Institute	Tapinocephalid indet	N
BP/1/7185	Evolutionary Studies Institute	Tapinocephalid indet	N
BP/1/7186	Evolutionary Studies Institute	Tapinocephalid indet	N
BP/1/7214	Evolutionary Studies Institute	*Criocephalosaurus*?	N
BP/1/7243	Evolutionary Studies Institute	Titanosuchid indet	N
BP/1/7244	Evolutionary Studies Institute	*Anteosaurus*	N
BP/1/7245	Evolutionary Studies Institute	Dinocephalian indet	N
BP/1/7246	Evolutionary Studies Institute	cf. Tapinocephalia	N
BP/1/7249	Evolutionary Studies Institute	*Anteosaurus*	N
BP/1/7261	Evolutionary Studies Institute	Tapinocephalid indet.	N
BP/1/7287	Evolutionary Studies Institute	Tapinocephalid indet.	N
BP/1/7380	Evolutionary Studies Institute	Titanosuchid dinocephalian	N
BP/1/7457	Evolutionary Studies Institute	Struthiocephalidae?	N
BP/1/7475	Evolutionary Studies Institute	*Moschops*	N
BP/1/7476	Evolutionary Studies Institute	*Moschops*	N

BP/1/7698	Evolutionary Studies Institute	Dinocephalian	N
BP/1/7843	Evolutionary Studies Institute	Anteosaurid	N
BP/1/7887	Evolutionary Studies Institute	Tapinocephalid dinocephalian	N
BP/1/7954	Evolutionary Studies Institute	Tapinocephalid indet	N
BP/1/7955	Evolutionary Studies Institute	Struthiocephalinae?	N
BP/1/7956	Evolutionary Studies Institute	Struthiocephalinae?	N
BP/1/7957	Evolutionary Studies Institute	Struthiocephalinae?	N
BP/1/8002	Evolutionary Studies Institute	Anteosaurid	N
BP/1/8005	Evolutionary Studies Institute	Tapinocephalid	N
BP/1/8007	Evolutionary Studies Institute	Tapinocephalid	N
BP/1/8009	Evolutionary Studies Institute	*Styracocephalus*	N
BP/1/8027	Evolutionary Studies Institute	Tapinocephalid	N
BP/1/8031	Evolutionary Studies Institute	*Jonkeria*	N
BP/1/8031	Evolutionary Studies Institute	*Jonkeria*	N
BP/1/8035	Evolutionary Studies Institute	Tapinocephalid	N
BP/1/8037	Evolutionary Studies Institute	c.f. *Anteosaurus*	N
BP/1/8047	Evolutionary Studies Institute	Dinocephalian indet	N
BP/1/8049	Evolutionary Studies Institute	*Criocephalosaurus*	N
BP/1/8071	Evolutionary Studies Institute	Anteosaurid?	N
BP/1/8072	Evolutionary Studies Institute	Dinocephalian indet	N
BP/1/8125	Evolutionary Studies Institute	*Struthiocephalus*?	N
BP/1/8143	Evolutionary Studies Institute	Tapinocephalid dinocephalian	N
BP/1/8162	Evolutionary Studies Institute	Tapinocephalid	N
BP/1/8163	Evolutionary Studies Institute	Dinocephalian	N

BP/1/8168	Evolutionary Studies Institute	Dinocephalian	N
BP/1/8169	Evolutionary Studies Institute	Tapinocephalid dinocephalian	N
BP/1/8188	Evolutionary Studies Institute	Anteosaurid?/ Titanosuchid?	N
NMQR 2986	National Museum, Bloemfontein	*Tapinocaninus pamelae*	N
ROZ-B96	Iziko South African Museum	*Jonkeria truculenta*	N
SAM-PK-000586	Iziko South African Museum	*Titanosuchus* sp.	N
SAM-PK-000587	Iziko South African Museum	Titanosuchid	N
SAM-PK-000713	Iziko South African Museum	*Delphinognathus conocephalus*	N
SAM-PK-000731	Iziko South African Museum	*Titanosuchus cloetei*	N
SAM-PK-000750	Iziko South African Museum	*Tapinocephalus atherstonei*	N
SAM-PK-000754	Iziko South African Museum	*Titanosuchus ferox*	N
SAM-PK-000769	Iziko South African Museum	*Scapanodon duplessisi*	N
SAM-PK-000915	Iziko South African Museum	*Eccasaurus priscus*	N
SAM-PK-000916	Iziko South African Museum	*Archaeosuchus cairncrossi*	N
SAM-PK-000918	Iziko South African Museum	*Pelosuchus priscus*	N
SAM-PK-002752	Iziko South African Museum	*Anteosaurus* sp.	N
SAM-PK-002753	Iziko South African Museum	Tapinocephalid	N
SAM-PK-002759	Iziko South African Museum	*Titanosuchus dubius*	N
SAM-PK-003012	Iziko South African Museum	*Struthiocephalus whaitsi*	N
SAM-PK-003015	Iziko South African Museum	*Moschosaurus longiceps*	N
SAM-PK-003400	Iziko South African Museum	*Riebeeckosaurus longirostris*	N
SAM-PK-003719	Iziko South African Museum	*Struthiocephalus akraalensis*	N
SAM-PK-004323	Iziko South African Museum	*Micranteosaurus parvus*	N
SAM-PK-004343	Iziko South African Museum	*Dinosphageus haughtoni*	N

SAM-PK-005006	Iziko South African Museum	*Struthiocephalellus parvus*	N
SAM-PK-005010	Iziko South African Museum	*Moschops capensis*	N
SAM-PK-005017	Iziko South African Museum	*Jonkeria* sp.	N
SAM-PK-005584	Iziko South African Museum	Dinocephalian	N
SAM-PK-005607	Iziko South African Museum	*Struthiocephaloides cavifrons*	N
SAM-PK-005614	Iziko South African Museum	*Anteosaurus* sp.	N
SAM-PK-005621	Iziko South African Museum	*Anteosaurus abeli*	N
SAM-PK-008936	Iziko South African Museum	*Styracocephalus platyrhynchus*	N
SAM-PK-009078	Iziko South African Museum	Dinocephalian	N
SAM-PK-009079	Iziko South African Museum	*Jonkeria* sp.	N
SAM-PK-009080	Iziko South African Museum	*Delphinognathus* sp.	N
SAM-PK-009082	Iziko South African Museum	*Mormosaurus seeleyi*	N
SAM-PK-009086	Iziko South African Museum	Titanosuchid	N
SAM-PK-009103	Iziko South African Museum	*Phocosaurus megischion*	N
SAM-PK-009123	Iziko South African Museum	*Anteosaurus abeli*	N
SAM-PK-009127	Iziko South African Museum	*Parascapanodon avifontis*	N
SAM-PK-009162	Iziko South African Museum	Titanosuchus sp.	N
SAM-PK-009166	Iziko South African Museum	*Avenantia kruisvleiensis*	N
SAM-PK-009329	Iziko South African Museum	*Anteosaurus abeli*	N
SAM-PK-011291	Iziko South African Museum	Tapinocephalid	N
SAM-PK-011293	Iziko South African Museum	*Anteosaurus abeli*	N
SAM-PK-011302	Iziko South African Museum	*Anteosaurus abeli*	N
SAM-PK-011485	Iziko South African Museum	*Anteosaurus abeli*	N
SAM-PK-011492	Iziko South African Museum	*Anteosaurus levops*	N

SAM-PK-011493	Iziko South African Museum	*Struthiocephalus whaitsi*	N
SAM-PK-011573	Iziko South African Museum	*Jonkeria ingens*	N
SAM-PK-011576	Iziko South African Museum	*Anteosaurus magnificus*	N
SAM-PK-011577	Iziko South African Museum	*Anteosaurus magnificus*	N
SAM-PK-011591	Iziko South African Museum	*Struthiocephalus whaitsi*	N
SAM-PK-011592	Iziko South African Museum	*Anteosaurus abeli*	N
SAM-PK-011593	Iziko South African Museum	*Tapinocephalus* sp.	N
SAM-PK-011594	Iziko South African Museum	*Struthiocephalus* sp.	N
SAM-PK-011694	Iziko South African Museum	*Anteosaurus cruentus*	N
SAM-PK-011832	Iziko South African Museum	*Agnosaurus pienaari*	N
SAM-PK-011929	Iziko South African Museum	*Anteosaurus abeli*	N
SAM-PK-011932	Iziko South African Museum	*Mormosaurus* sp.	N
SAM-PK-011946	Iziko South African Museum	*Anteosaurus crassifrons*	N
SAM-PK-011947	Iziko South African Museum	*Struthionops intermedius*	N
SAM-PK-011973	Iziko South African Museum	Tapinocephalid	N
SAM-PK-011974	Iziko South African Museum	*Moschops capensis*	N
SAM-PK-011980	Iziko South African Museum	Titanosuchid	N
SAM-PK-011985	Iziko South African Museum	*Tapinocephalus* sp.	N
SAM-PK-011997	Iziko South African Museum	Tapinocephalid	N
SAM-PK-011998	Iziko South African Museum	Tapinocephalus sp.	N
SAM-PK-011999	Iziko South African Museum	Tapinocephalid	N
SAM-PK-012062	Iziko South African Museum	*Struthiocephalus* sp.	N
SAM-PK-11296	Iziko South African Museum	*Anteosaurus abeli*	N
SAM-PK-2344	Iziko South African Museum	*Tapinocephalus atherstonei*	N

SAM-PK-K00272	Iziko South African Museum	*Struthiocephalus kitchingi*	N
SAM-PK-K00284	Iziko South African Museum	*Anteosaurus* sp.	N
SAM-PK-K00287	Iziko South African Museum	Titanosuchian	N
SAM-PK-K00319	Iziko South African Museum	*Criocephalosaurus* sp.	N
SAM-PK-K00365	Iziko South African Museum	Titanosuchian	N
SAM-PK-K01683	Iziko South African Museum	*Anteosaurus* sp.	N
SAM-PK-K08669	Fransie Pienaar Museum	*Tapinocephalus*?	N
SAM-PK-K10895	Iziko South African Museum	Dinocephalian	N
SAM-PK-K10896	Iziko South African Museum	Tapinocephalid	N
SAM-PK-K10897	Iziko South African Museum	Tapinocephalid	N
SAM-PK-K10897	Iziko South African Museum	Tapinocephalid	N
SAM-PK-K11214	Iziko South African Museum	*Mormosaurus seeleyi*	N